



April 8, 2005

Letter No. 99008-05-002

ATTN: Document Control Desk
Director, Spent Fuel Project Office
Office of Nuclear Material Safety and Safeguards
U.S. Nuclear Regulatory Commission
Washington, DC 20555-0001

SUBJECT: Supplemental Information Submittal, Mixed Oxide Fresh Fuel Package (MFFP) Application, Docket No. 71-9295, TAC No. L23747

References: 1. PacTec Letter, 99008-05-001, dated February 4, 2005
2. NRC Letter, "Mixed Oxide Fresh Fuel Package Review Telephone Call," dated March 11, 2005

Dear Sirs:

Packaging Technology, Inc. hereby submits supplemental information to our Reference 1 RAI response submittal. This supplemental information was requested during the March 10, 2005, telephone call documented in your Reference 2 letter. Our response is comprised of two primary submittals. First, each request made in the referenced letter is provided, along with our response. Second, revised pages and drawings are provided, representing Revision 2 to the MFFP Safety Analysis Report.

Included within this application are the following documents:

- Responses to the three information requests in Reference 2, including an addendum to RAI 2-11 concerning computed accelerations.
- Ten paper copies of the revised pages for the Safety Analysis Report (SAR).
- Ten electronic copies of the SAR in PDF format.

The electronic copies are contained on ten CDs in an envelope labeled, "MFFP Docket 71-9295 Electronic Copy of Documents". Included with the revised SAR pages are detailed instructions for replacing pages from the Revision 1 SAR with new pages for this Revision 2.

In addition to providing the requested information, we have made minor corrections to two of the General Arrangement Drawings as a result of inconsistencies noted during the revision process. These corrections affected General Arrangement Drawings 99008-10 and 99008-20, which incorrectly listed a tightening torque, and spacing of the impact limiter attachment lugs, respectively. All changed information is annotated with a vertical bar in the right margin for text pages, or by bubbles on the General Arrangement Drawings.

If you have any questions or comments regarding this submittal, please contact me at 678-362-7110 or at clindner@pactec-tn.com.

PACKAGING TECHNOLOGY, INC.

1102 Broadway Plaza, Suite 300, Tacoma, WA 98402-3526 – USA – Tel: 1 253.383.9000 – Fax: 1 253.383.9002

NMSSO/

U.S. Nuclear Regulatory Commission
Letter No. 99008-05-002
April 8, 2005
Page 2 of 2

Sincerely,

 FOR CURT LINDNER

Curt Lindner, Project Manager
Packaging Technology, Inc.

Enclosure: As Noted

cc: M. Rahimi, NRC/SFPO (letter only)
J. Field (letter only)
R. Clark, DCS (1 copy of all enclosures)
M. Klimas, DOE (2 copies of all enclosures)

Project File 99008

Attachment A
Contents of Electronic Media

This submission is composed of both paper copies and an electronic copy. The electronic copies are contained within an envelope labeled, "MFFP Docket 71-9295 Electronic Copy of Documents". The envelope contains ten discs of the following:

Title	Media Type:	Contents
MOX Fresh Fuel Package Safety Analysis Report	CD-ROM	One file of the complete text of the submittal: MFFP Safety Analysis Report, Rev 2.pdf (24,556 kb) (567 pages)

Delete/Insert Instructions
Revision 2 to MFFP Safety Analysis Report
(10 Copies)

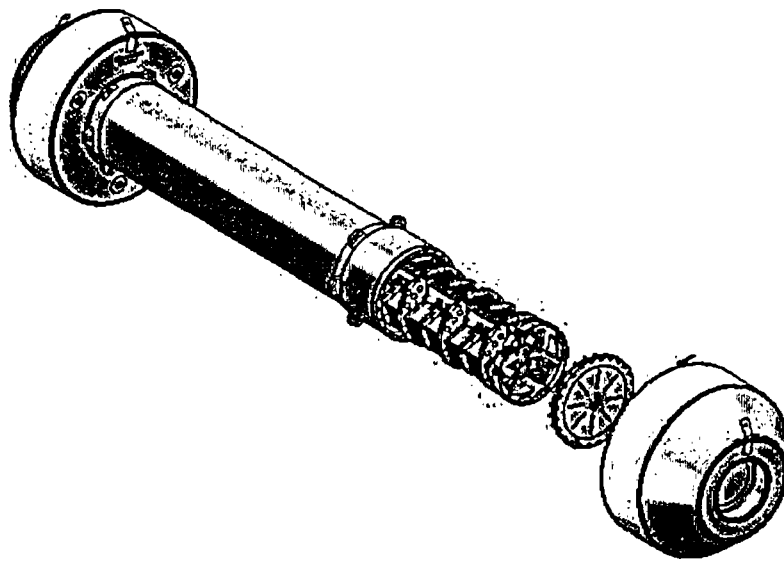
Please incorporate the attached Revision 2 SAR pages as follows:

SAR Section	Delete	Insert
Cover & Spine	Revision 1	Revision 2
Title Page	Revision 1	Revision 2
Table of Contents	Revision 1	Revision 2
1.0	<ul style="list-style-type: none"> • 1.2-5 thru 1.2-10, Rev. 0/1 • N/A • 1.4.2-1 thru 1.4.2-2, Rev. 1 	<ul style="list-style-type: none"> • 1.2-5 thru 1.2-10, Rev. 2 • 1.2-15 thru 1.2-16, Rev. 2 • 1.4.2-1 thru 1.4.2-2, Rev. 2
1.4.2	<ul style="list-style-type: none"> • Dwg 99008-10, Rev. 1 • Dwg 99008-20, Rev. 1 	<ul style="list-style-type: none"> • Dwg 99008-10, Rev. 2 • Dwg 99008-20, Rev. 2
2.0	<ul style="list-style-type: none"> • 2.7-1 thru 2.7-16, Rev. 0/1 	<ul style="list-style-type: none"> • 2.7-1 thru 2.7-16, Rev. 2
2.12	2.12-1 thru 2.12-2, Rev. 0	2.12-1 thru 2.12-2, Rev. 2
2.12.8	N/A	2.12.8-1 thru 2.12.8-10, Rev. 2
6.0	<ul style="list-style-type: none"> • 6.1-1 thru 6.1-2, Rev. 0 • 6.3-1 thru 6.3-6, Rev. 1 • 6.4-1 thru 6.4-10, Rev. 0/1 • 6.6-1 thru 6.6-6, Rev. 0/1 • 6.8-1 thru 6.8-8, Rev. 1 • 6.9.1-1 thru 6.9.1-12, Rev. 0 	<ul style="list-style-type: none"> • 6.1-1 thru 6.1-2, Rev. 2 • 6.3-1 thru 6.3-6, Rev. 2 • 6.4-1 thru 6.4-16, Rev. 2 • 6.6-1 thru 6.6-8, Rev. 2 • 6.8-1 thru 6.8-8, Rev. 2 • 6.9.1-1 thru 6.9.1-10, Rev. 2



DOCKET 71-9295

Mixed Oxide Fresh Fuel Package



Safety Analysis Report

Revision 2
April 2005

TABLE OF CONTENTS

1.0 GENERAL INFORMATION.....	1.1-1
1.1 Introduction	1.1-1
1.2 Package Description	1.2-1
1.2.1 Packaging	1.2-1
1.2.1.1 Body	1.2-1
1.2.1.2 Strongback	1.2-2
1.2.1.3 Impact Limiters	1.2-3
1.2.1.4 Gross Weight	1.2-4
1.2.1.5 Neutron Moderation and Absorption.....	1.2-4
1.2.1.6 Receptacles, Valves, Testing and Sample Ports	1.2-4
1.2.1.7 Heat Dissipation.....	1.2-4
1.2.1.8 Coolants	1.2-4
1.2.1.9 Protrusions	1.2-4
1.2.1.10 Lifting and Tie-down Devices	1.2-5
1.2.1.11 Pressure Relief Systems.....	1.2-5
1.2.1.12 Shielding	1.2-5
1.2.2 Containment System.....	1.2-5
1.2.3 Contents of Packaging.....	1.2-5
1.2.3.1 Radionuclide Inventory.....	1.2-6
1.2.3.2 Maximum Payload Weight	1.2-6
1.2.3.3 Maximum Decay Heat	1.2-6
1.2.3.4 Maximum Pressure Buildup	1.2-6
1.2.4 Operational Features.....	1.2-6
1.3 General Requirements for All Packages	1.3-1
1.3.1 Minimum Package Size.....	1.3-1
1.3.2 Tamper-Indicating Feature	1.3-1
1.3.3 Positive Closure.....	1.3-1
1.3.4 Chemical and Galvanic Reactions.....	1.3-1
1.3.5 Valves.....	1.3-1
1.3.6 Package Design	1.3-1
1.3.7 External Temperatures	1.3-2
1.3.8 Venting	1.3-2
1.4 Appendices	1.4-1
1.4.1 Nomenclature	1.4.1-1
1.4.2 Packaging General Arrangement Drawings.....	1.4.2-1

2.0	STRUCTURAL EVALUATION.....	2.1-1
2.1	Structural Design.....	2.1-1
2.1.1	Discussion	2.1-1
2.1.2	Design Criteria	2.1-1
2.1.2.1	Analytic Design Criteria (Allowable Stresses).....	2.1-2
2.1.2.2	Miscellaneous Structural Failure Modes	2.1-3
2.1.3	Weights and Center of Gravity.....	2.1-6
2.2	Materials.....	2.2-1
2.2.1	Material Properties and Specifications.....	2.2-1
2.2.2	Chemical and Galvanic Reactions.....	2.2-2
2.2.3	Effects of Radiation on Material	2.2-2
2.3	Fabrication and Examination.....	2.3-1
2.3.1	Fabrication.....	2.3-1
2.3.2	Examination.....	2.3-1
2.4	Lifting and Tie-down Standards for All Packages.....	2.4-1
2.4.1	Lifting Devices.....	2.4-1
2.4.2	Tie-down Devices.....	2.4-1
2.4.2.1	Doubler Plate Weld Stress	2.4-1
2.4.2.2	Doubler Plate Bearing Stress	2.4-2
2.4.2.3	Tie-down Device Overload Condition.....	2.4-2
2.4.2.4	Summary	2.4-3
2.5	General Considerations	2.5-1
2.5.1	Evaluation by Test.....	2.5-1
2.5.2	Evaluation by Analysis.....	2.5-1
2.6	Normal Conditions of Transport	2.6-1
2.6.1	Heat	2.6-1
2.6.1.1	Summary of Pressures and Temperatures.....	2.6-1
2.6.1.2	Differential Thermal Expansion	2.6-2
2.6.1.3	Stress Calculations.....	2.6-2
2.6.2	Cold	2.6-8
2.6.3	Reduced External Pressure.....	2.6-9
2.6.4	Increased External Pressure	2.6-10
2.6.5	Vibration and Shock.....	2.6-10
2.6.6	Water Spray	2.6-12
2.6.7	Free Drop.....	2.6-12
2.6.8	Corner Drop.....	2.6-12

2.6.9	Compression.....	2.6-12
2.6.10	Penetration.....	2.6-12
2.7	Hypothetical Accident Conditions	2.7-1
2.7.1	Free Drop.....	2.7-1
2.7.1.1	Technical Basis for the Free Drop Tests.....	2.7-2
2.7.1.2	Summary of Results from the Free Drop Testing	2.7-3
2.7.2	Crush	2.7-7
2.7.3	Puncture.....	2.7-7
2.7.3.1	Technical Basis for the Puncture Drop Tests.....	2.7-7
2.7.3.2	Summary of Results from the Puncture Drop Tests	2.7-8
2.7.4	Thermal	2.7-8
2.7.4.1	Summary of Pressures and Temperatures.....	2.7-8
2.7.4.2	Differential Thermal Expansion	2.7-9
2.7.4.3	Stress Calculations	2.7-9
2.7.5	Immersion – Fissile Material.....	2.7-10
2.7.6	Immersion – All Packages.....	2.7-11
2.7.7	Deep Water Immersion Test (for Type B Packages Containing More than 10^5 A ₂).....	2.7-11
2.7.8	Summary of Damage.....	2.7-12
2.8	Accident Conditions for Air Transport of Plutonium	2.8-1
2.9	Accident Conditions for Fissile Material Packages for Air Transport	2.9-1
2.10	Special Form	2.10-1
2.11	Fuel Rods.....	2.11-1
2.12	Appendices	2.12-1
2.12.1	Impact Limiter Evaluation.....	2.12.1-1
2.12.1.1	Material Properties.....	2.12.1-1
2.12.1.2	Force-Deflection Relations	2.12.1-3
2.12.1.3	Force-Deflection Curves.....	2.12.1-4
2.12.1.4	Impact Analysis Method	2.12.1-4
2.12.1.5	Impact Analysis at Cold Temperature	2.12.1-5
2.12.1.6	Impact Analysis at Hot Temperature	2.12.1-6
2.12.1.7	Worst-Case Slapdown Angle.....	2.12.1-6
2.12.2	Certification Test Plan.....	2.12.2-1
2.12.2.1	Initial Test Conditions	2.12.2-1
2.12.2.2	Certification Test Unit (CTU).....	2.12.2-2
2.12.2.3	Identification of Worst-Case Drop Tests	2.12.2-3

2.12.2.4	Summary of Selected Certification Drop Tests	2.12.2-6
2.12.2.5	Acceptance Criteria.....	2.12.2-8
2.12.3	Certification Test Results	2.12.3-1
2.12.3.1	Introduction.....	2.12.3-1
2.12.3.2	Summary	2.12.3-1
2.12.3.3	Test Facilities.....	2.12.3-2
2.12.3.4	Instrumentation	2.12.3-2
2.12.3.5	Initial Test Conditions	2.12.3-2
2.12.3.6	Test Unit Description.....	2.12.3-3
2.12.3.7	CTU Payloads	2.12.3-5
2.12.3.8	Test Results.....	2.12.3-5
2.12.3.9	Pre-Test and Post-Test Leakage Rate Tests.....	2.12.3-15
2.12.4	Engineering Test Results.....	2.12.4-1
2.12.4.1	Engineering Test Unit Configuration	2.12.4-1
2.12.4.2	Pre-Test Activities	2.12.4-3
2.12.4.3	Summary of Engineering Test Results	2.12.4-4
2.12.5	Fuel Control Structure Evaluation.....	2.12.5-1
2.12.5.1	Summary of Results.....	2.12.5-1
2.12.5.2	Conditions Analyzed.....	2.12.5-2
2.12.5.3	FCS Geometry	2.12.5-2
2.12.5.4	FCS Material Properties.....	2.12.5-3
2.12.5.5	FCS Stress Criteria.....	2.12.5-4
2.12.5.6	FCS Stability Criteria.....	2.12.5-5
2.12.5.7	FCS Vertically Loaded Fuel Load Determination.....	2.12.5-5
2.12.5.8	FCS Horizontal Loaded Fuel Load Determination.....	2.12.5-8
2.12.5.9	Evaluation Assumptions and Methodology	2.12.5-9
2.12.5.10	FCS Finite Element Analysis (FEA)	2.12.5-10
2.12.5.11	Pinned Connection Elastic Analysis.....	2.12.5-11
2.12.5.12	Fastener Analysis.....	2.12.5-13
2.12.5.13	Lock Plate and Hinge Mounting Brackets.....	2.12.5-15
2.12.5.14	Strongback Global Stability.....	2.12.5-21
2.12.5.15	Strongback Local Stability.....	2.12.5-22
2.12.5.16	Strongback Width-Thickness Ratio - Triangular Core.....	2.12.5-23
2.12.5.17	Strongback Width-Thickness Ratio - Plate Extensions	2.12.5-24
2.12.5.18	Strongback Axial Stress.....	2.12.5-24
2.12.5.19	Evaluation of Strongback Response to FCS Loads	2.12.5-25
2.12.5.20	Strongback Stress Calculations – Horizontal Loads.....	2.12.5-27
2.12.6	CASKDROP Computer Program	2.12.6-1

2.12.6.1	Using CASKDROP to Determine Impact Limiter Deformation Behavior	2.12.6-1
2.12.6.2	An Example Problem for the CASKDROP Program	2.12.6-3
2.12.7	Impact Limiter Weld Joint Test Results.....	2.12.7-1
2.12.7.1	Packaging Weld Joint Design	2.12.7-1
2.12.7.2	Certification Test Unit Weld Joint Design	2.12.7-1
2.12.7.3	Bench Test Results.....	2.12.7-1
2.12.7.4	Conclusions.....	2.12.7-2
2.12.8	Effect of Bounding Weight on Package Structural Responses	2.12.8-1
2.12.8.1	Component Weights.....	2.12.8-1
2.12.8.2	Evaluations.....	2.12.8-1
2.12.8.3	Conclusions.....	2.12.8-7
3.0	THERMAL EVALUATION.....	3.1-1
3.1	Description of Thermal Design	3.1-1
3.1.1	Design Features	3.1-1
3.1.1.1	Body.....	3.1-1
3.1.1.2	Impact Limiters.....	3.1-2
3.1.1.3	Strongback	3.1-2
3.1.1.4	Neutron Moderation and Absorption.....	3.1-3
3.1.1.5	Receptacles, Valves, Testing and Sample Ports	3.1-3
3.1.2	Content's Decay Heat.....	3.1-3
3.1.3	Summary of Temperatures	3.1-3
3.1.4	Summary of Maximum Pressures	3.1-4
3.2	Material Properties and Component Specifications	3.2-1
3.2.1	Material Properties	3.2-1
3.2.2	Component Specifications.....	3.2-2
3.3	General Considerations	3.3-1
3.3.1	Evaluation by Analysis.....	3.3-1
3.3.1.1	NCT Analytical Model	3.3-2
3.3.1.2	HAC Analytical Model.....	3.3-4
3.3.2	Evaluation by Test.....	3.3-5
3.3.3	Margins of Safety	3.3-5
3.4	Thermal Evaluation for Normal Conditions of Transport.....	3.4-1
3.4.1	Heat and Cold.....	3.4-1
3.4.1.1	Heat.....	3.4-1
3.4.1.2	Cold.....	3.4-3

3.4.2	Maximum Normal Operating Pressure.....	3.4-3
3.4.3	Maximum Thermal Stresses.....	3.4-5
3.4.4	Evaluation of Package Performance for Normal Conditions of Transport ..	3.4-5
3.5	Thermal Evaluation Under Hypothetical Accident Conditions.....	3.5-1
3.5.1	Initial Conditions.....	3.5-1
3.5.2	Fire Test Conditions.....	3.5-1
3.5.2.1	Analytical Model	3.5-1
3.5.2.2	Performance of Rigid Polyurethane Foam Under HAC Fire Conditions	3.5-3
3.5.3	Maximum Temperatures and Pressures	3.5-6
3.5.3.1	Maximum Temperatures.....	3.5-6
3.5.3.2	Maximum Pressures.....	3.5-7
3.5.4	Accident Conditions for Fissile Material Packages for Air Transport.....	3.5-8
3.5.5	Evaluation of Package Performance for Accident Conditions of Transport	3.5-8
3.6	Appendices	3.6-1
3.6.1	Computer Analysis Results	3.6.1-1
3.6.2	Thermal Model Details.....	3.6.2-1
3.6.2.1	Convection Coefficient Calculation.....	3.6.2-1
3.6.2.2	Effective Thermal Conductivity of MOX Fuel Assemblies	3.6.2-3
4.0	CONTAINMENT	4.1-1
4.1	Description of the Containment System.....	4.1-1
4.1.1	Containment Boundary.....	4.1-1
4.1.1.1	Containment Penetrations	4.1-1
4.1.1.2	Closure	4.1-1
4.1.1.3	Seals	4.1-1
4.1.1.4	Welds	4.1-2
4.1.2	Special Requirements for Plutonium.....	4.1-2
4.2	General Considerations	4.2-1
4.2.1	Type A Fissile Package	4.2-1
4.2.2	Type B Packages	4.2-1
4.3	Containment Requirements for Normal Conditions of Transport.....	4.3-1
4.3.1	Containment of Radioactive Material	4.3-1
4.3.2	Pressurization of the Containment Vessel.....	4.3-1
4.3.3	Containment Criterion.....	4.3-1
4.4	Containment Requirements for Hypothetical Accident Conditions.....	4.4-1

4.4.1	Fission Gas Products	4.4-1
4.4.2	Containment of Radioactive Material	4.4-1
4.4.3	Containment Criteria	4.4-1
4.5	Leakage Rate Tests for Type B Packages	4.5-1
4.5.1	Fabrication Leakage Rate Tests	4.5-1
4.5.2	Maintenance/Periodic Leakage Rate Tests	4.5-1
4.5.3	Preshipment Leakage Rate Tests.....	4.5-1
5.0	SHIELDING EVALUATION.....	5-1
6.0	CRITICALITY EVALUATION	6.1-1
6.1	Description of Criticality Design.....	6.1-1
6.1.1	Design Features Important for Criticality	6.1-1
6.1.2	Summary Table of Criticality Evaluation	6.1-1
6.1.3	Criticality Safety Index	6.1-2
6.2	Fissile Material Contents	6.2-1
6.3	General Considerations	6.3-1
6.3.1	Model Configuration	6.3-1
6.3.1.1	Contents Model.....	6.3-1
6.3.1.2	Packaging Model	6.3-1
6.3.2	Material Properties	6.3-3
6.3.3	Computer Codes and Cross-Section Libraries	6.3-3
6.3.4	Demonstration of Maximum Reactivity.....	6.3-4
6.3.4.1	Single Package.....	6.3-4
6.3.4.2	Arrays of Undamaged Packages	6.3-4
6.3.4.3	Arrays of Damaged Packages	6.3-5
6.4	Single Package Evaluation.....	6.4-1
6.4.1	Single Package Configuration	6.4-1
6.4.1.1	NCT Configuration	6.4-1
6.4.1.2	HAC Configuration.....	6.4-1
6.4.2	Single Package Results.....	6.4-3
6.5	Evaluation of Package Arrays Under Normal Conditions of Transport	6.5-1
6.5.1	NCT Array Configuration	6.5-1
6.5.2	NCT Array Results.....	6.5-1
6.6	Package Arrays Under Hypothetical Accident Conditions	6.6-1
6.6.1	HAC Array Configuration.....	6.6-1
6.6.2	HAC Array Results	6.6-1

6.6.3	Impact of Niobium Content in the Cladding.....	6.6-2
6.7	Fissile Material Packages for Air Transport	6.7-1
6.8	Benchmark Evaluations.....	6.8-1
6.8.1	Applicability of Benchmark Experiments.....	6.8-1
6.8.2	Bias Determination.....	6.8-2
6.9	Appendices	6.9-1
6.9.1	Single Package Model.....	6.9.1-1
6.9.2	Infinite Array Model	6.9.2-1
7.0	OPERATING PROCEDURES.....	7.1-1
7.1	Package Loading.....	7.1-1
7.1.1	Preparation for Loading.....	7.1-1
7.1.1.1	Removal of MFFP from the Transport Conveyance.....	7.1-1
7.1.1.2	Removal of the Closure Lid.....	7.1-1
7.1.1.3	Removal of the Strongback from the MFFP	7.1-1
7.1.2	Loading of Contents	7.1-2
7.1.2.1	Loading of Fuel Assemblies into Strongback.....	7.1-2
7.1.2.2	Loading of the Strongback into the MFFP	7.1-3
7.1.2.3	Closure Lid Installation	7.1-4
7.1.3	Preparation for Transport (Loaded).....	7.1-5
7.2	Package Unloading.....	7.2-1
7.2.1	Receipt of Package from Carrier.....	7.2-1
7.2.2	Removal of Contents	7.2-1
7.2.2.1	Removal of MFFP from the Transport Conveyance.....	7.2-1
7.2.2.2	Removal of the Closure Lid.....	7.2-1
7.2.2.3	Removal of the Strongback from the MFFP.....	7.2-2
7.2.2.4	Unloading of FAs from the Strongback.....	7.2-2
7.2.2.5	Loading of the Strongback into the MFFP	7.2-3
7.2.2.6	Closure Lid Installation	7.2-4
7.2.2.7	Final Package Preparations for Transport (Unloaded)	7.2-4
7.3	Preparation of an Empty Package for Transport	7.3-1
7.4	Preshipment Leakage Rate Test	7.4-1
7.4.1	Gas Pressure Rise Leakage Rate Test Acceptance Criteria	7.4-1
7.4.2	Determining the Test Volume and Test Time	7.4-1
7.4.3	Performing the Gas Pressure Rise Leakage Rate Test	7.4-2
7.4.4	Optional Preshipment Leakage Rate Test	7.4-2

8.0 ACCEPTANCE TESTS AND MAINTENANCE PROGRAM.....	8.1-1
8.1 Acceptance Tests.....	8.1-1
8.1.1 Visual Inspection and Measurements.....	8.1-1
8.1.2 Weld Examinations	8.1-1
8.1.3 Structural and Pressure Tests	8.1-1
8.1.3.1 Lifting Device Load Testing.....	8.1-1
8.1.3.2 Pressure Testing.....	8.1-1
8.1.4 Fabrication Leakage Rate Tests	8.1-2
8.1.4.1 Fabrication Leakage Rate Test Acceptance Criteria.....	8.1-2
8.1.4.2 Helium Leakage Rate Testing the Containment Structure Integrity	8.1-2
8.1.4.3 Helium Leakage Rate Testing the Main O-ring Seal.....	8.1-3
8.1.4.4 Helium Leakage Rate Testing the Vent Port Plug O-ring Seal	8.1-3
8.1.4.5 Helium Leakage Rate Testing the Fill Port Plug O-ring Seal.....	8.1-4
8.1.5 Component and Material Tests.....	8.1-5
8.1.5.1 Polyurethane Foam	8.1-5
8.1.5.2 Neutron Poison Plates.....	8.1-13
8.1.6 Shielding Tests	8.1-13
8.1.7 Thermal Tests	8.1-13
8.2 Maintenance Program	8.2-1
8.2.1 Structural and Pressure Tests	8.2-1
8.2.2 Maintenance/Periodic Leakage Rate Tests	8.2-1
8.2.2.1 Maintenance/Periodic Verification Leakage Rate Test Acceptance Criteria.....	8.2-1
8.2.2.2 Helium Leakage Rate Testing the Main O-ring Seal.....	8.2-1
8.2.2.3 Helium Leakage Rate Testing the Vent Port Plug O-ring Seal	8.2-2
8.2.2.4 Helium Leakage Rate Testing the Fill Port Plug O-ring Seal.....	8.2-3
8.2.3 Component and Material Tests.....	8.2-3
8.2.3.1 Fasteners	8.2-3
8.2.3.2 Seal Areas and Grooves.....	8.2-3
8.2.3.3 Impact Limiters.....	8.2-4
8.2.3.4 Strongback	8.2-4
8.2.3.5 Fuel Control Structures.....	8.2-4
8.2.3.6 Seals	8.2-4
8.2.4 Thermal Tests	8.2-4
8.2.5 Miscellaneous Tests	8.2-4

A

PACTEC

MFFP Safety Analysis Report

Docket No. 71-9295
Revision 2, April 2005

This page intentionally left blank.

1.2.1.10 Lifting and Tie-down Devices

There are no lifting devices integral to the MFFP. The only tie-down devices integral to the MFFP are the doubler plates that attach the impact limiter attachment lugs. The doubler plates serve as an interface between the shipping skid and the MFFP, and provide axial restraint for tie-down. The shipping skid for MFFP is shown in Figure 1.2-11.

1.2.1.11 Pressure Relief Systems

There is no pressure relief system included in the MFFP to relieve pressure from within the containment boundary. Fire-consumable vents in the form of plastic pipe plugs are employed on the exterior surface of the impact limiters. These vents are included to release any gases generated by charring polyurethane foam in the HAC thermal event (fire). During the HAC fire, the plastic pipe plugs melt allowing the release of gases generated by the foam as it flashes to a char. Three vents are used on each impact limiter, located on the inside surface. For optimum performance, the vents are equally spaced around the circumference of the impact limiters.

1.2.1.12 Shielding

The MOX fresh FA payload is not a significant source of radiation. Thus, use of shielding specific components is not required. Further detail of the shielding evaluation is provided in Chapter 5.0, *Shielding Evaluation*.

1.2.2 Containment System

The containment boundary for MFFP is provided by the containment body, closure lid and bolts, and associated sealing components. The containment boundary of the package consists of the cylindrical shell and bottom forging, sealing flange, the inner plate and sealing ring of the closure lid, the vent port plug and elastomeric seal, the fill port plug and elastomeric seal, and the closure lid elastomeric containment O-ring seal. The body has an inner diameter of 28½ inches and an inside length of 165¼ inches. The outer diameter in the closure lid flange area is 32.3 inches, while a majority of the body outer diameter is 29¼ inches. The overall length of the body with the closure lid, excluding impact limiters, is 171¼ inches. The containment boundary is shown in Figure 1.1-2.

1.2.3 Contents of Packaging

The MFFP is designed to carry up to three fresh MOX PWR FAs. The FAs are based on the MK-BW/MOX1 17 × 17 PWR design. For shipping less than three MOX FAs, non-fuel dummy assemblies are utilized in the strongback locations not occupied by the MOX FAs. The physical size and weight of the non-fuel dummy assemblies are nominally the same as the MK-BW/MOX1 17 × 17 design. For criticality analyses, a maximum loading of 6.0^w% plutonium (Pu) is assumed. FA physical parameters are provided in Table 1.2-1.

Burnable poison rod assemblies (BPRAs) may be inserted into a FA as an option. Therefore, a loaded package may contain up to three BPRAs. The 17 × 17 BPRAs (Figure 1.2-12) consists of an arrangement of poison rods and thimble plugs suspended from a flat plate and held in place by a spring-loaded holddown assembly. The holddown assembly fits within the fuel assembly

upper nozzle and rests on the adapter plate. To ensure that the cluster remains seated in the fuel assembly during operation, the holddown springs are compressed by the upper core plate, thereby providing a downward force in excess of the hydraulic lift forces from the reactor coolant. The holddown assembly and the holddown springs are fabricated of Type 304 stainless steel and Inconel[®] 718, respectively.

The burnable poison rod design contains an absorber stack of Al_2O_3 - B_4C pellets. The pellets are encased in cold-worked, stress-relieved annealed Zircaloy-4 cladding with Zircaloy-4 end plugs welded to each end. The upper end plug provides a threaded attachment to the holddown assembly plate, and a bullet nose lower end plug provides lead-in guidance for the rods. A stainless steel spring is located in the plenum above the poison pellet column. Prior to the final seal weld, each rod is pressurized with helium to reduce the pressure differential across the clad wall during operation.

The pellets consist of a uniform sintered dispersion of boron carbide (B_4C) in an alumina (Al_2O_3) matrix. The boron-10 concentrations are adjusted by varying the boron carbide content of the pellets.

In addition to the boron-10 concentration being variable, the number of burnable poison rods on a FA can vary up to a maximum of twenty-four (24) rods. The locations that do not contain a burnable poison rod typically will contain a short thimble plug rod that serves to reduce the coolant flow up the empty guide thimble. The maximum weight of a BPRAs with twenty-four poison rods is 65 pounds.

1.2.3.1 Radionuclide Inventory

The bounding payload nuclear parameters for the MFFP payload are provided in Table 1.2-2. Impurities (e.g., americium) are chemically cleaned from the MOX powder in an aqueous polishing process prior to fuel fabrication.

1.2.3.2 Maximum Payload Weight

The maximum payload weight of the MFFP is 4,740 pounds, based on three MOX PWR fuel assemblies (including BPRAs) with a weight of 1,580 pounds each.

1.2.3.3 Maximum Decay Heat

The maximum heat load for the MFFP is 240 watts for three fuel assemblies.

1.2.3.4 Maximum Pressure Buildup

The maximum normal operating pressure (MNOP) is established at 10 psig. The design pressure of the MFFP is 25 psig. The MFFP is evaluated for the design pressure in Chapter 2.0, *Structural Evaluation*.

1.2.4 Operational Features

The MFFP is not considered to be operationally complex. All operational features are depicted on the drawings provided in Appendix 1.4.2, *Packaging General Arrangement Drawings*. Operating procedures and instructions for loading, unloading, and preparing an empty MFFP for transport are provided in Chapter 7.0, *Package Operations*.

Table 1.2-1 – Fuel Assembly Physical Parameters

Parameter	Value
Fuel Rod Cladding Material	M5
Fuel Rod Array	17 × 17
Fuel Rods per Fuel Assembly	264
Guide Tubes per Fuel Assembly	24
Instrument Tubes per Fuel Assembly	1
Fuel Assembly Length, inches	161.61
Fuel Assembly Maximum Width, inches	8.565
Fuel Rod Pitch, inches	0.496
Fuel Rod Length, inches	152.4
Fuel Rod OD, inches	0.374
Fuel Rod Clad Thickness, inches	0.023
Active Fuel Length, inches	144.0
PuO ₂ + UO ₂ weight, pounds	1,157
Heavy Metal Weight, pounds	1,020
Maximum Fuel Assembly Weight (including BPRA), pounds	1,580
Maximum Initial Pu Loading, weight percent	6.0
Temperature Limits, °F	392 (NCT) 1,337 (HAC)

Table 1.2-2 – Nuclear Design Parameters

Parameter	Value
Pellet Diameter	0.323 inch
Effective Pellet Density	10.31 g/cc
Burnable Poison Rods	Yes – as separate removable assembly
Uranium Concentration Ranges (w/o)	<u>Total Uranium 94.0^{w/o} or greater of which:</u> ²³⁴ U: 0 to 0.05 w/o ²³⁵ U: 0 to 0.30 w/o ²³⁸ U: 99.65 to 100 w/o
Plutonium Concentration Ranges (w/o)	<u>Total Plutonium up to 6.0^{w/o} of which:</u> ²³⁸ Pu: 0 to 0.05 w/o ²³⁹ Pu: 90 to 95 w/o ²⁴⁰ Pu: 5 to 9 w/o ²⁴¹ Pu: 0 to 1 w/o ²⁴² Pu: 0 to 0.1 w/o

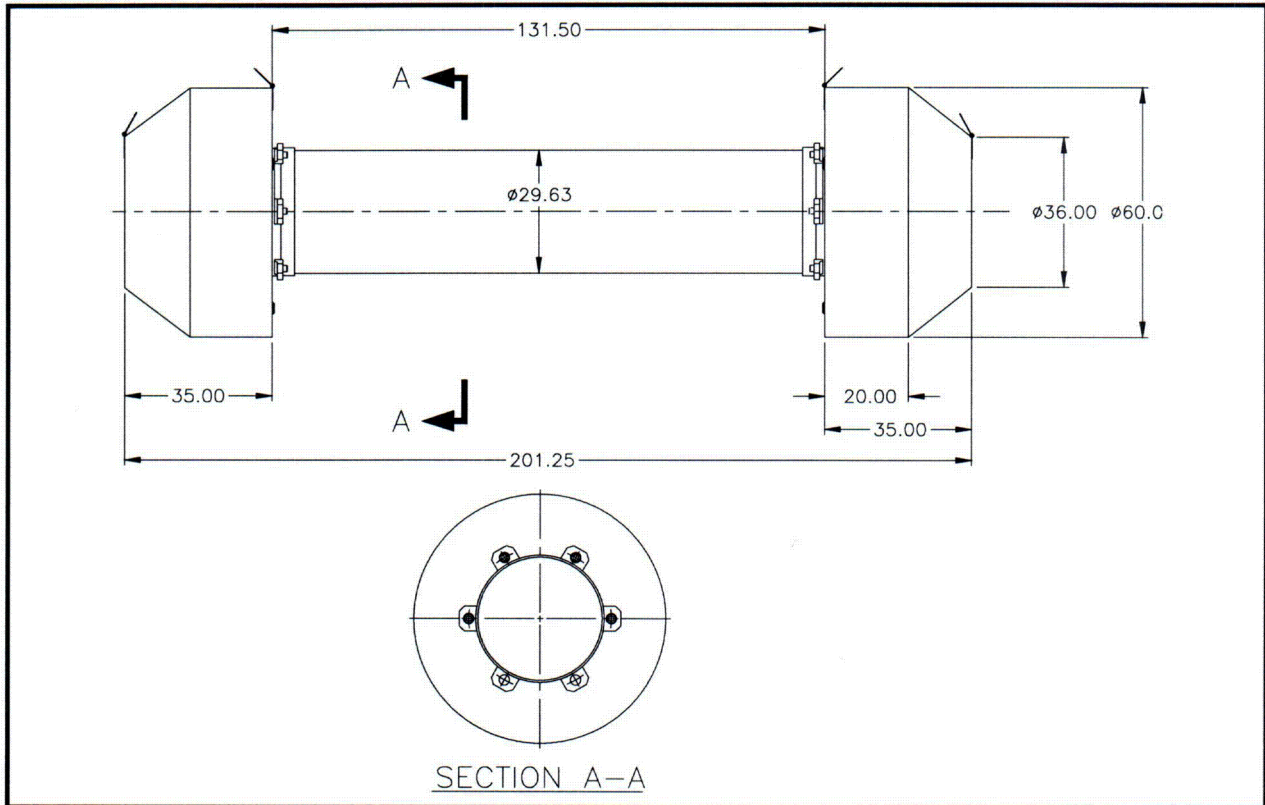


Figure 1.2-1 – MFFP Overall Assembly (inches)

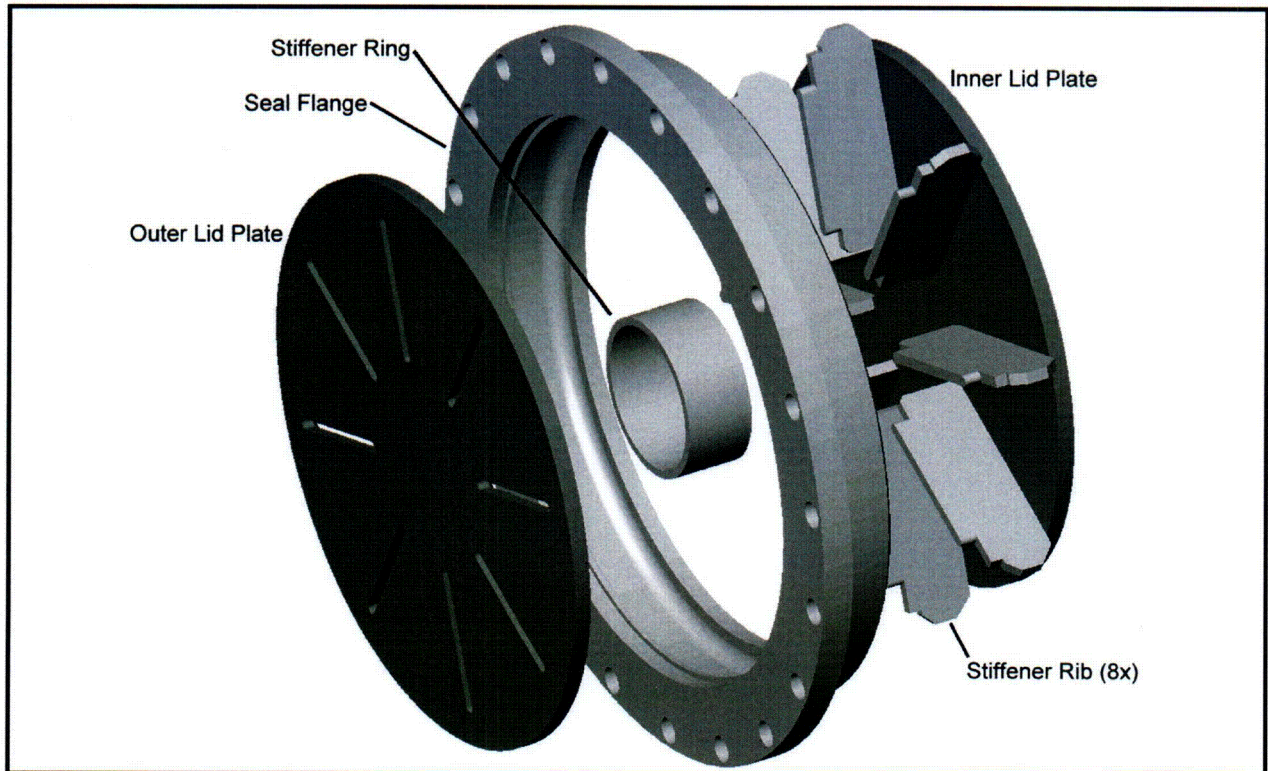


Figure 1.2-2 – Closure Lid (O-Ring Grooves and Ports Removed for Clarity)

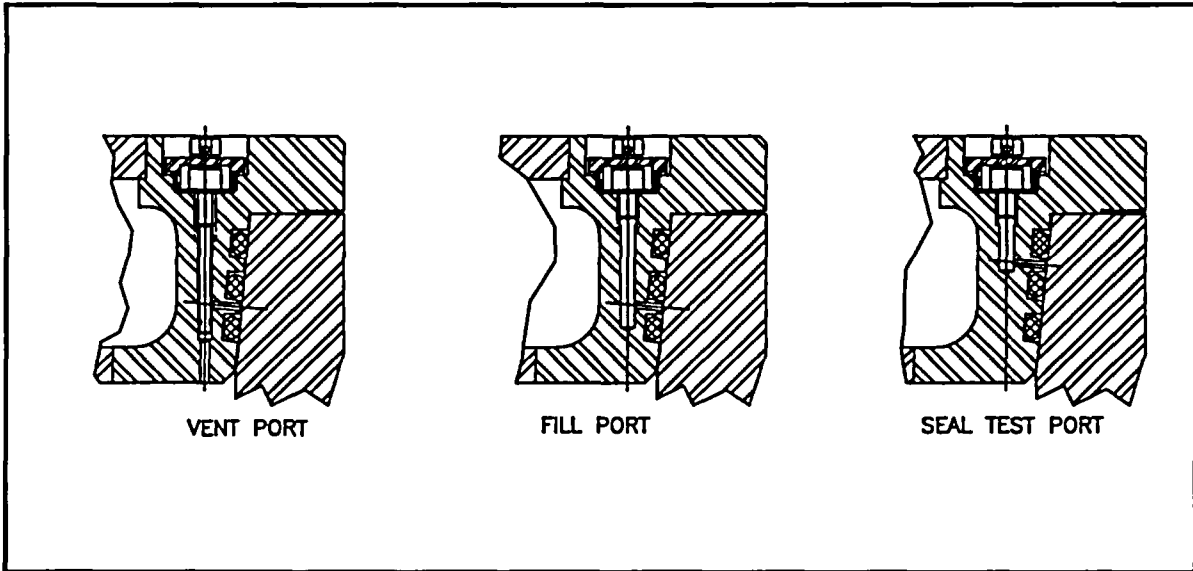


Figure 1.2-3 – MFFP Port Details

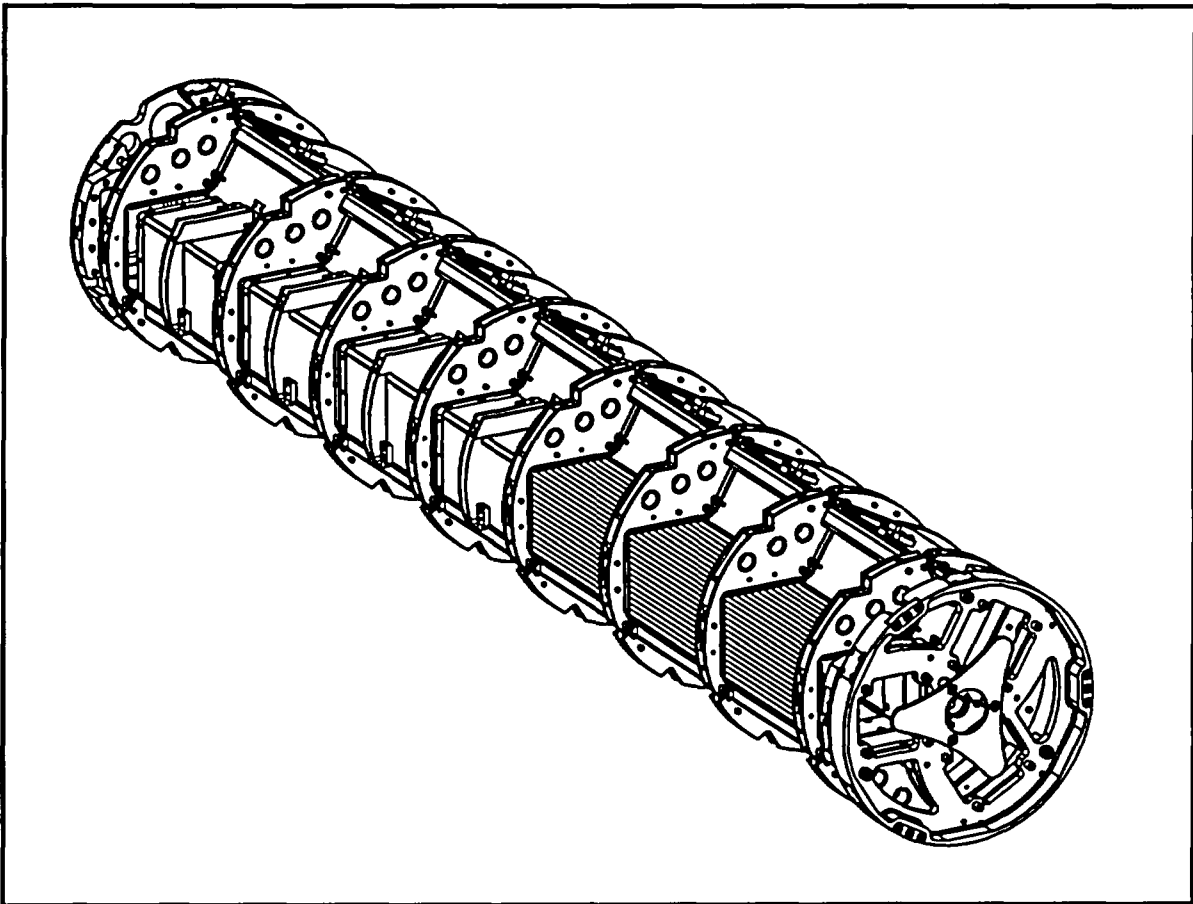


Figure 1.2-4 – Strongback (Shown with FAs installed, Upper (3) FCS Segments Removed)

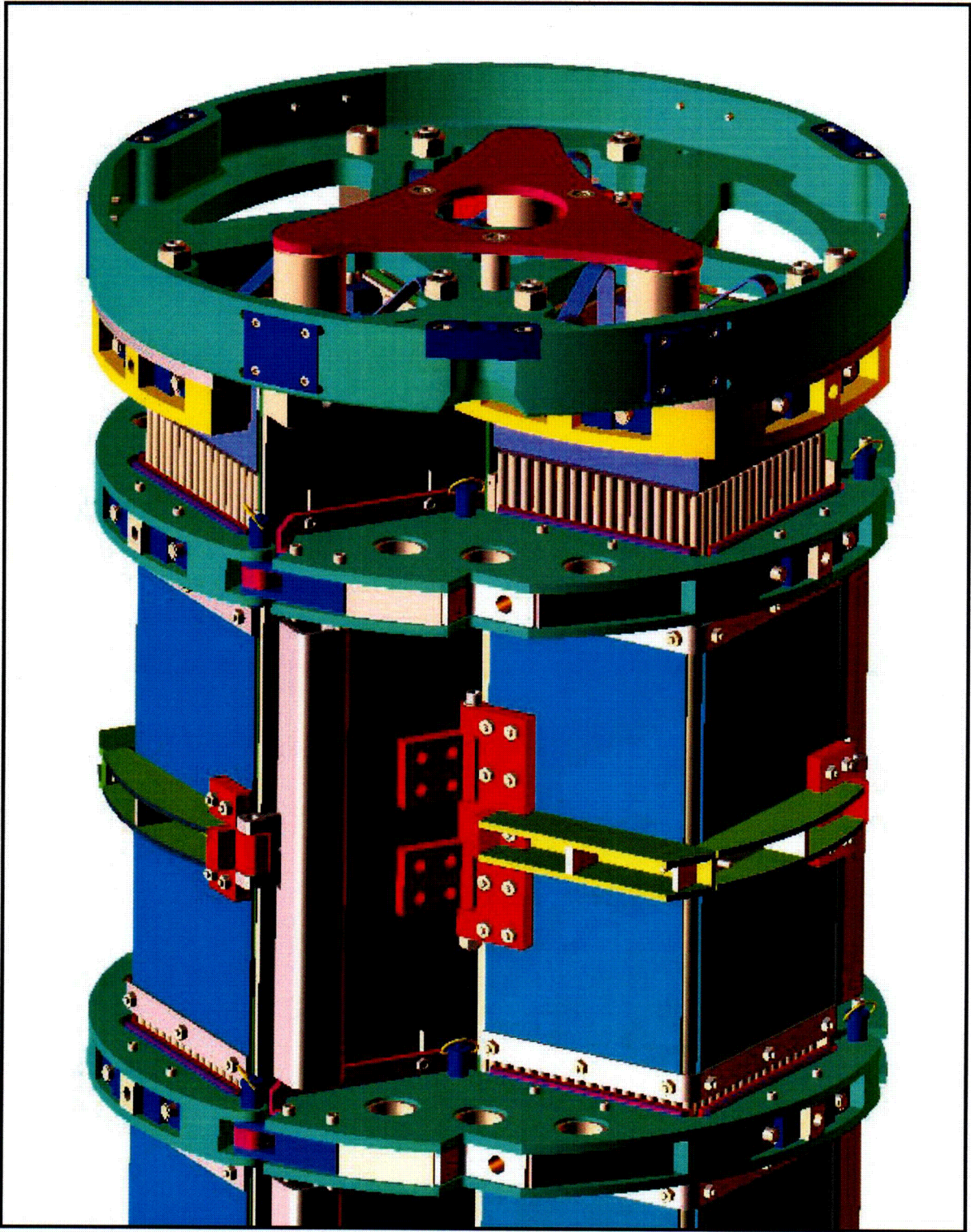


Figure 1.2-5 – Strongback, Top End (Shown with FAs Installed)

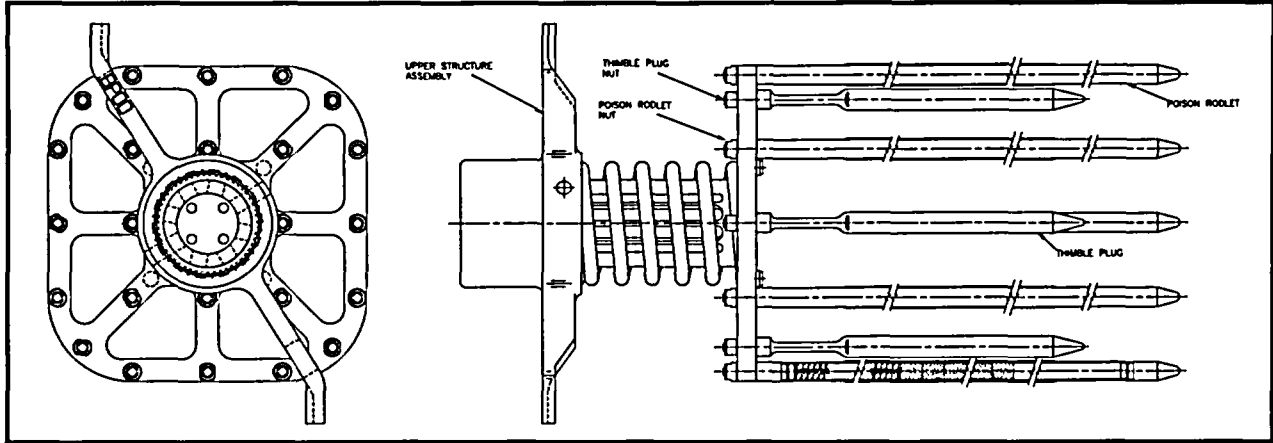


Figure 1.2-12 – BPR Assembly

This page left intentionally blank.

1.4.2 Packaging General Arrangement Drawings

This section presents the MFFP general arrangement drawings¹, consisting of the following drawings:

- 99008-10, Rev. 2, 1 sheet, *MFFP Shipping Package*
- 99008-20, Rev. 2, 5 sheets, *MFFP Body Assembly*
- 99008-30, Rev. 2, 7 sheets, *MFFP Strongback Assembly*
- 99008-31, Rev. 1, 3 sheets, *MFFP Strongback Top Plate Assembly*
- 99008-32, Rev. 0, 2 sheets, *MFFP Strongback Bottom Plate Assembly*
- 99008-33, Rev. 1, 4 sheets, *MFFP Strongback Clamp Arm Assembly*
- 99008-34, Rev. 2, 2 sheets, *MFFP Strongback Fuel Control Structure Assembly*
- 99008-40, Rev. 1, 3 sheets, *MFFP Impact Limiters*

Within the packaging general arrangement drawing, dimensions important to the packaging's safety are dimensioned and toleranced (e.g., shell thicknesses, polyurethane foam thicknesses, and the sealing regions on the seal flanges). All other dimensions are provided as a reference dimension, and are toleranced in accordance with the general tolerance block on the drawings.

¹ The MFFP general arrangement drawings utilize the uniform standard practices of ASME Y14.5M, *Dimensioning and Tolerancing*, American National Standards Institute, Inc. (ANSI).

This page left intentionally blank.

Figure Withheld Under 10 CFR 2.390

A PACTEC	PACKAGING TECHNOLOGY, INC. TACOMA, WA	
	MFFP SHIPPING PACKAGE SAR DRAWING	
	SCHE: 1/B	WT. N/A
	REV: 1	SHEET 1 OF 1
	FIG. NO.	99008-10
	SIZE	D
	CADWAL: 89008_101.DWG	

2

1

A

Figure Withheld Under 10 CFR 2.390

 PACTEC		PACKAGING TECHNOLOGY, INC. TACOMA, WA	
MFP BODY ASSEMBLY SAR DRAWING			
SCALE: N/A	PT. N/A	SHEET 1 OF 5	
REV: 2			
DWG. NO. SIZE	99008-20		
CADD FILE: P9008_3071.DWG			

2 1

Figure Withheld Under 10 CFR 2.390

A		PACKAGING TECHNOLOGY, INC.	
PACTEC		TACOMA, WA	
MFFP BODY ASSEMBLY SAR DRAWING			
SCALE: 1/8		WT	M/A
REV: 2		SHEET 2 OF 5	
DATE BY	DWG NO.		
D	99008-20		
CADD FILE: 99008_2023.DWG			

2 1

Figure Withheld Under 10 CFR 2.390

A PACTEC	PACKAGING TECHNOLOGY, INC. TACOMA, WA	
	MFFP BODY ASSEMBLY SAR DRAWING	
	SCALE: FULL	WT. N/A
	REV: 2	SHEET 4 OF 5
	DWG NO. 99008-20	
	SIZE D	CADLET: 99008_2042.DWG
	2	1

Figure Withheld Under 10 CFR 2.390

A PACTEC	PACKAGING TECHNOLOGY, INC. TACOMA, WA	
	MFP BODY ASSEMBLY SAR DRAWING	
	SCALE: FULL	BY: N/A
	REV: 2	SHEET 5 OF 5
	DWG NO.	
	SIZE	99008-20
	CADFILE: 99008_P2L.DWG	

2 1

2.7 Hypothetical Accident Conditions

The MFFP, when subjected to the sequence of hypothetical accident condition (HAC) tests specified in 10 CFR §71.73¹, subsequent to the sequence of normal conditions of transport (NCT) tests specified in 10 CFR §71.71, is shown to meet the performance requirements specified in Subpart E of 10 CFR 71. As indicated in the introduction to Chapter 2.0, *Structural Evaluation*, with the exception of the thermal and immersion tests that are demonstrated by analysis, the primary proof of performance for the HAC tests is via the use of full-scale testing. In particular, free drop and puncture testing of the MFFP certification test unit (CTU) confirms that the containment boundary will remain leaktight after a worst case HAC sequence. Observations from testing of the CTU also confirm the conservative nature of deformed geometry assumptions used in the thermal and criticality assessments.

Specifically, the certification test program demonstrated the following objectives:

1. **No loss of containment:** The leaktight containment boundary was maintained throughout repeated regulatory test sequences. Additionally, HAC structural loads did not result in deformations (including buckling) that would lead to the degradation of containment under the subsequent HAC fire event.
2. **Maintaining subcriticality:** The strongback structure retained its geometry and retained the neutron poison in their respective positions. Together with the certification testing and the analytical evaluations provided herein, the geometry of the payload is controlled and the MFFP payload remains subcritical.

The basis for the certification testing performed is summarized in the following sections. For a detailed discussion of the basis of the structural certification performed, refer to Appendix 2.12.2, *Certification Test Plan*. The results of the certification testing program are presented in Appendix 2.12.3, *Certification Test Results*. Analyses necessary to supplement or expand the tests results are also presented, as necessary. Development of the MFFP design was facilitated by a half-scale engineering test unit. The engineering tests were focused on development of the puncture resistant impact limiters, but also included a 30-foot free drop (side drop orientation). The results of the engineering test are summarized in Appendix 2.12.4, *Engineering Test Results*.

2.7.1 Free Drop

Subpart F of 10 CFR 71 requires performing a free drop test in accordance with the requirements of 10 CFR §71.73(c)(1). The free drop test involves performing a 30-foot, HAC free drop onto a flat, essentially unyielding, horizontal surface, with the package striking the surface in a position (orientation) for which maximum damage is expected. The ability of the MFFP to adequately withstand this specified free drop condition is demonstrated via testing of a full-scale, certification test unit (CTU) and analytical evaluations. Specifically, the analytical evaluations include:

- Structural analyses of the fuel control structure (FCS), provided in Appendix 2.12.5, *Fuel Control Structure Evaluation*.
- Structural analyses of package weight not accounted for in the certification tests, provided in Appendix 2.12.8, *Effect of Bounding Weight on Package Structural Responses*.

¹ Title 10, Code of Federal Regulations, Part 71 (10 CFR 71), *Packaging and Transportation of Radioactive Material*, Final Rule, 01-26-04.

- Maximum deformation of impact limiters under warm conditions, provided in Appendix 2.12.1, *Impact Limiter Evaluation*.

2.7.1.1 Technical Basis for the Free Drop Tests

Items that could compromise the containment integrity or criticality safety of the package were identified when selecting the worst case package orientations for the 30-foot free drop event. Shielding integrity is not addressed since the MFFP design does not include any components whose primary purpose is shielding. For the MFFP containment body, its ability to remain leaktight is of primary importance. For the strongback, geometric stability, including support of the fuel assemblies and poison plates, is of primary importance.

The types of damage that are the most likely candidates to compromise the leaktight capability of the MFFP are as follows:

- Excessive deformation of the sealing surfaces that would cause reduced seal compression,
- Failure of the closure lid bolts,
- Buckling of the containment shell, and
- Thermal degradation of the seal material resulting from the HAC fire event.

Types of damage that could affect criticality safety are as follows:

- Deformations of the strongback that could change the relative geometric relationships between the fuel assemblies (FAs) and the neutron absorbing material which exceed the bounds established in the criticality analyses, and
- Buckling of the containment shell.

From the above considerations, a total of four 30-foot free drops were selected, including horizontal, vertical, and two near-horizontal slapdown orientations. In the course of testing, an additional free drop test was performed. Multiple tests have been performed to ensure that the most vulnerable package features were subjected to "worst case" loads and deformations, as required by 10 CFR §71.73(c)(1). The certification tests were exceedingly conservative for the containment boundary since a single containment body structure was subject to all the free drops (and punctures). Table 2.7-1 summarizes the free drops performed and the primary aspect of the MFFP performance being tested. Appendix 2.12.2, *Certification Test Plan* discusses, in detail, the justification for the selection of each free drop orientation and the objectives for each test, as well as describing the sequence of free drop and puncture tests, the initial test conditions, the data to be gathered from the test, and the test unit and payload configuration for each test.

As shown in Table 2.7-1, there were three (3) test series. Each series employed a different test payload configuration as subsequently noted. Each series consisted of at least one 30-foot free drop followed by at least one puncture drop, such that each series fulfilled the regulatory requirements for HAC drop testing, i.e., free drop followed by puncture drop. In keeping with the regulatory series philosophy, the containment boundary closure seals were leakage rate tested prior to, and following each series to demonstrate the containment boundary remained leaktight. The entire boundary was leakage rate tested prior to and following the entire set of test series.

For the certification test free drops the CTU impact limiters were chilled to the minimum temperature (-20 °F ambient) condition, in order to maximize crush strength of the foam and

consequent impact magnitude. Since the impact limiters do not “bottom-out” under maximum temperature conditions, see Appendix 2.12.1, *Impact Limiter Evaluation*, maximum impact accelerations are associated with the increased crush stress of chilled foam.

As noted above, three payload configurations were used for certification testing. The mock payload was comprised of a simple bundle of 1/2-inch diameter carbon steel rods. The mock payload was used in lieu of the strongback and FAs in the first test series, which consisted of a HAC side drop and multiple puncture drops. This first test series focused upon demonstrating the behavior of the impact limiters and the integrity of the package containment and structural shells. The details of the mock Payload are presented in Appendix 2.12.2, *Certification Test Plan*. The second and third payload configurations both included the strongback assembly. The second payload configuration consisted of the strongback loaded with two dummy FAs plus one prototypic FA, whereas the third payload configuration consisted of three dummy FAs. The purpose of the second test series was to assess the behavior of an actual MOX FA under hypothetical accident conditions. The purpose of the third test series was to assess the behavior and demonstrate the integrity of the strongback assembly itself.

The dummy FAs were designed to accurately represent the way that an actual MOX FA would apply loads to the strongback, but were not intended to accurately represent the behavior characteristics of the individual fuel rods. The details of the dummy FA are presented in Appendix 2.12.2, *Certification Test Plan*. The prototypic FA was designed to be exactly representative of a MK-BW MOX FA. The only difference between an actual MOX FA and the prototypic FA was that the fuel pellets of the prototypic FA were tungsten carbide. The burnable poison rod assembly (BPRA), optionally shipped assembled with the MOX FA, was not represented. However, the weight of the tungsten carbide pellets was greater than the weight of the actual MOX fuel pellets. Therefore, the prototypic FA included the weight of a BPRA, and thus conservatively represented the actual MOX FA.

2.7.1.2 Summary of Results from the Free Drop Testing

The certification testing successfully demonstrated the robust nature of the containment boundary and stability of the strongback. The containment structure was subjected to five HAC free drops (and six puncture drops, as described in Section 2.7.3) and remained leaktight throughout the testing. Appendix 2.12.3, *Certification Test Results*, contains the details of the free drop results. Significant results of the free drop testing, with respect to the containment boundary, are as follows:

- Containment
 - Following a total of five, 30-foot free drops and six puncture drops, the containment boundary, which was used for all drops, demonstrated its robustness and capability to remain leaktight. The only components of the containment boundary replaced between test series were the butyl O-ring seals.
 - The containment boundary structure did not buckle or permanently deform due to any of the free drops.
 - The side and secondary slapdown impacts (both are effectively 0° impacts) resulted in weld failure in the outside top angle corner of the closure lid end impact limiter (see Figure 2.12.3-7, Appendix 2.12.3, *Certification Test Results*). The impact limiter weld failure was subjected to a subsequent puncture test (see Figure 2.12.3-9, Appendix 2.12.3, *Certification Test Results*). Although the resulting cumulative damage is evaluated in Chapter 3.0, *Thermal Evaluation*, and shown to have no effect on the integrity of the

containment O-ring seals, the fillet weld joint design was revised to a groove butt weld for the packaging design. Demonstration of the weld joint designs is presented in Appendix 2.12.7, *Impact Limiter Weld Joint Test Results*.

- The maximum gross weight of the MFFP, as presented in Section 2.1.3, *Weights and Center of Gravity*, is 14,130 pounds and represents the bounding weight of the package. The CTU Series 1, 2, and 3 configurations weighed 13,815, 13,234, and 13,217 pounds, respectively. These are somewhat lighter than the maximum gross weight, primarily because they are actual fabricated weights (not worst-case maximums) and also do not include the FCS, which was not present in the CTUs. An evaluation of the effect of the additional weight is given in Appendix 2.12.8, *Effect of Bounding Weight on Package Structural Responses*. The effect of the bounding weight on maximum impact limiter deformations under hot conditions is evaluated by analysis in Appendix 2.12.1, *Impact Limiter Evaluation*, where the maximum gross weight is conservatively used to demonstrate that the impact limiters will not 'bottom out'.
- Based on the certification tests and structural analyses, and the conclusions of the thermal analyses in Chapter 3.0, *Thermal Evaluation*, the containment boundary is maintained when the MFFP is subjected to the applicable tests described in Subpart F of 10 CFR 71.

As noted above, the FCS was not present during the certification tests. Presence of the FCS could have an effect on the axial movement of the fuel rods in a top end drop, since the degree of the rod's lateral buckling is strictly limited by the FCS. However, since the degree of buckling of the rods was very small in the absence of the FCS, a further small restriction is unlikely to alter the behavior of the rods significantly. As shown in Figure 2.12.3-23, some rods did pass through the top nozzle plate as a result of the end drop, and some may have struck the closure lid containment plate. Although no significant change to this configuration is expected to occur in the presence of the FCS, a bounding analysis will be performed to evaluate the worst-case loading of the closure lid by the axial movement of fuel rods. This evaluation focuses on the local effect of rods on the closure lid containment plate. The more global effect of the package contents weight on the closure system is discussed in Appendix 2.12.8, *Effect of Bounding Weight on Package Structural Responses*.

Figure 2.12.3-23 shows a view of the top nozzle of the fuel assembly. There are a total of 56 holes through which a fuel rod could pass through. The hole size allows only a single rod to come through each hole. Therefore, the maximum number of fuel rods per FA that could strike the closure lid in an end drop is 56. This analysis will conservatively neglect any friction of the rod with the grids, with other rods that do not move, or with the top nozzle itself. The analysis further assumes that each hole is adequately aligned with a fuel rod to permit passage. Additionally, to ensure that all rods that can move are accounted, the quantity of rods striking the closure lid will be arbitrarily increased by 25%, thus $1.25 \times 56 = 70$ rods will be considered. Per Table 2.12.5-1, the weight of a fuel rod is $W_R = 5.33$ pounds, and from Section 2.12.5.2, *Conditions Analyzed*, the bounding axial impact load is 120g. The maximum load for a FA that could be applied to the lid by the rods is:

$$F = 70W_R (120) = 44,772 \text{ lb}_f$$

The closure lid is a weldment with eight radial ribs. Each 45° segment between the ribs is bounded by the inner diameter of the outer forging of 26.38 inches and the outer diameter of the central support pipe of 7.0 inches. The area of one segment is:

$$A = \left(\frac{1}{8}\right) \frac{\pi}{4} (26.38^2 - 7.0^2) = 63.51 \text{ in}^2$$

The entire load of the displaced rods, F, is conservatively applied to a single segment, so that the pressure loading on the segment is:

$$q = \frac{F}{A} = \frac{44,772}{63.51} = 705 \text{ psi}$$

The maximum stress in the containment plate for a solid circular sector is found using Table 24, Case 27 of Roark², and bounded by the tangential stress, σ_t :

$$\sigma_t = \beta_1 \frac{qr^2}{t^2} = 36,478 \text{ psi}$$

where: $q = 705 \text{ psi (impact load)} + 25 \text{ psi (design pressure)} = 730 \text{ psi}$
 $r = 26.38/2 = 13.19 \text{ inches}$
 $t = 0.63 \text{ inches}$
 $\beta_1 = 0.114 \text{ for } 45^\circ \text{ sector}$

From Table 2.1-1, the allowable primary membrane plus bending stress intensity is equal to the lesser of $3.6S_m$ and S_u , but since this region is near to the closure O-ring seals, a value equal to the yield stress will be conservatively used, equal to 47,100 psi from Table 2.2-1 at a bounding temperature of 200 °F. The margin of safety is:

$$MS = \frac{47,100}{36,478} - 1.0 = +0.29$$

Thus, any additional movement of the fuel rods in an end drop due to the introduction of the FCS is not of concern.

The fuel rods themselves will not be significantly damaged by impact with the lid. As shown in Figures 2.12.3-22 and 2.12.3-23, the damage incurred by the fuel rods in the certification test bounds any damage that could occur in the presence of the FCS.

The burnable poison rod assembly (BPRA) which can optionally be shipped with the fuel was not present during the certification tests. As described in Section 1.2.3, *Contents of Packaging*, the BPRA may be inserted into the top of the FA and weighs up to 65 pounds. During normal transport, it is restrained by the BPRA restraint, shown as Assembly A3 on General Arrangement Drawing Number 99008-30. In a top end drop, the BPRA restraint weldment comes into contact with the inner plate of the closure lid. Therefore, the weight of the BPRA is transferred to the closure lid through the BPRA restraint weldment. Since the surface area of the restraint weldment is relatively large, and since contact between the BPRA, the restraint weldment, and the closure lid is flat without protrusions, the BPRA cannot inflict significant damage to the closure lid inner plate. As stated in Section 2.7.1.1, *Technical Basis for the Free Drop Tests*, the weight of the prototypic and dummy FAs was conservatively slightly greater than the total FA plus BPRA weight. Thus, the presence of a BPRA in any or all of the FAs is not of concern.

² Young, W. C., *Roark's Formulas for Stress and Strain*, Sixth Edition, McGraw-Hill, 1989.

The principal criticality control structure for the MFFP is the strongback. Two strongbacks were used for the certification testing program. Table 2.7-1 summarizes the performance aspect being tested in the respective series.

The first strongback was used in Series 2 and was assembled with two dummy FAs and one prototypic FA. This strongback was subjected to one HAC free drop (and one puncture drop).

The second strongback was used in Series 3 and for the 'Additional Test', and was assembled with three dummy FAs. This strongback was subjected to two HAC free drops (and two puncture drops) as part of Series 3, and then the 'Additional Test' HAC free drop.

Both strongbacks exhibited no significant deformations as a result of the test series. The effectiveness of the neutron poison plates was preserved through maintenance of its integrity and position. Following Series 2, the clamp arms, which restrain the fuel assemblies to the longitudinal strongback plates, were operational following the test and retained both the prototypic and dummy fuel assemblies in position. Although the strongback was not removable from the containment body following Series 3, a borescope inspection of the structure revealed no significant damage or re-configuration of the strongback.

The purpose of Series 2 was to demonstrate the longitudinal stability of the strongback during axial accelerations, and to determine the stability of the prototypic FA as assembled to the strongback. As described above, the strongback performance is acceptable. The fuel rods of the prototypic FA exhibited unacceptable lateral deformations. The lateral fuel rod deformations are best characterized as first mode Euler buckling between the clamp arms nearest the top nozzle (nearest the ground in the near-vertical orientation, see Figure 2.12.3-22, Appendix 2.12.3, *Certification Test Results*). In addition to lateral fuel rod deformations, a number of prototypic fuel rods also slid through the grid straps. An undetermined number of rods contacted the top nozzle, and 8 rods slid through the flow openings in the top nozzle (see Figure 2.12.3-23, Appendix 2.12.3, *Certification Test Results*). To ensure that this lateral fuel rod deformation is positively bounded, a fuel control structure (FCS) has been incorporated into the strongback design. The FCS is analytically evaluated in Appendix 2.12.5, *Fuel Control Structure Evaluation*. As shown in that evaluation, the geometry of the fuel is confined to a maximum cross-section of 8.7 inches square. In addition, since the FCS contains two neutron poison plates, the FAs are surrounded on all four sides by neutron poison materials. Chapter 6.0, *Criticality Evaluation*, concludes that with the neutron poison and geometric control afforded by the strongback/FCS structure, an optimally moderated FA, arranged in the most reactive credible configuration, remains subcritical with significant margin.

Significant results of the free drop testing, with respect to criticality safety, are as follows:

- Criticality safety
 - The strongback structure did not significantly reconfigure. The position of the neutron poison relative to the FAs, and the global position of the FAs relative to each other were maintained.
 - The post-drop configuration of the fuel rods is bounded by the FCS (refer to Section 2.12.5, *Fuel Control Structure Evaluation*), which ensures the assumptions used in the criticality evaluation are valid.
 - Based upon the structural tests and analyses, and upon the conclusions of the criticality analyses, the MFFP, when optimally moderated, remains subcritical when subjected to the applicable tests described in Subpart F of 10 CFR 71.

2.7.2 Crush

Subpart F of 10 CFR 71 requires performing a dynamic crush test in accordance with the requirements of 10 CFR §71.73(c)(2). Since the MFFP weight exceeds 1,100 pounds, the dynamic crush test is not required.

2.7.3 Puncture

Subpart F of 10 CFR 71 requires performing a puncture test in accordance with the requirements of 10 CFR §71.73(c)(3). The puncture test involves a 40-inch free drop of a package onto the upper end of a solid, vertical, cylindrical, mild steel bar mounted on an essentially unyielding, horizontal surface. The bar must be six inches in diameter, with the top surface horizontal and its edge rounded to a radius of not more than 1/4 inch. The package is to be oriented in a position for which maximum damage will occur. The minimum length of the bar is to be eight inches. The ability of the MFFP to adequately withstand this specified puncture drop condition is demonstrated via testing of a full-scale, MFFP certification test unit.

2.7.3.1 Technical Basis for the Puncture Drop Tests

Items that could compromise containment integrity or criticality safety of the package were identified when selecting a worst case package orientation for the puncture drop event. For the MFFP containment body, its ability to remain leaktight is of primary importance. For the strongback, geometric stability, including support of the fuel assemblies and neutron poison plates is of primary importance. Criticality safety could be impacted by excessive deformation of the containment boundary shell which might cause a significant reconfiguration of the fuel and strongback geometry relationship.

The types of damage that are the most likely to compromise the leaktight capability of the MFFP are as follows:

- Excessive deformation of the sealing surfaces that would result in excessive reduction of seal compression caused by a direct puncture impact to the sealing area,
- Puncture of the containment boundary shell, and
- Thermal degradation of the O-ring seal butyl material resulting from the HAC thermal event resulting from the removal of, or excessive damage to, the impact limiter.

Types of damage that could affect criticality safety are as follows:

- Deformations of the strongback that would result in change of the relative geometric relationships between the FAs and the neutron absorbing material, which exceed the limits established in the criticality analyses, and
- Deformation or reconfiguration of the FAs that exceeds the bounds established in the criticality analysis.

From the above considerations, six puncture drops were selected, as shown in Table 2.7-3. Each puncture test was performed following at least one HAC 30-foot free drop. The same MFFP body (body, closure lid, and closure bolts) was conservatively subjected to all six tests. Appendix 2.12.2, *Certification Test Plan*, contains further discussion and provides the detailed logic behind the choice of puncture orientations and test sequence. Section 2.7.3.2, *Summary of Results from the Puncture Drop*

Tests, summarizes the puncture test results and Appendix 2.12.3, *Certification Test Results*, describes the results in detail.

2.7.3.2 Summary of Results from the Puncture Drop Tests

The certification testing successfully demonstrated the robust nature of the containment boundary and stability of the strongback. Appendix 2.12.3, *Certification Test Results*, contains the details of the free drop results.

- Containment
 - The containment boundary shell did not perforate due to any of the puncture drops, including both perpendicular and oblique orientations.
 - The lid end impact limiter shell prevented the puncture bar from directly applying loads to the sealing region. Thus, containment is not affected by direct puncture attack.
 - The lid end impact limiter shell resisted gross perforation, thus preventing excessive removal of polyurethane foam or exposure of the containment seal region to the fire temperatures.
 - The puncture damage, added to the free drop lid end impact limiter weld damage, did not result in loss of containment in the analysis of the HAC thermal event.
- Criticality safety
 - The strongback structure did not significantly reconfigure. The position of the neutron poison relative to the FAs, and the global position of the FAs relative to each other were maintained.
 - The puncture bar was unable to deform the shell body sufficiently to significantly reconfigure the FA rods.

Based upon the puncture tests, the MFFP maintains containment and remains subcritical when subjected to the applicable tests described in Subpart F of 10 CFR 71.

2.7.4 Thermal

Subpart F of 10 CFR 71 requires performing a thermal test in accordance with the requirements of 10 CFR §71.73(c)(4). To demonstrate the performance capabilities of the MFFP when subjected to the HAC thermal test specified in 10 CFR §71.73(c)(4), the worst-case damage from the HAC, 30-foot free drop and puncture tests, as discussed in Section 2.7.1, *Free Drop*, and Section 2.7.3, *Puncture*, was included in the MFFP thermal model, as discussed in Chapter 3.0, *Thermal Evaluation*.

2.7.4.1 Summary of Pressures and Temperatures

Package pressures and temperatures due to the HAC thermal event are presented in Section 3.5.3, *Maximum Temperatures and Pressures*. A brief summary of the thermal analysis results are provided in the following sections.

2.7.4.1.1 Summary of Pressures

From Table 3.5-2, the maximum internal pressure during the HAC thermal event, which includes an assumption of 100% rupture of the fuel rods and the complete combustion of all of the polymer

materials utilized in the strongback, is 123.5 psig, with the package initially at atmospheric pressure. For stress analysis purposes, a pressure of 130 psig is used, which conservatively bounds the maximum internal pressure.

2.7.4.1.2 Summary of Temperatures

From Table 3.5-1, the maximum shell wall temperature is 1,361 °F, and the maximum closure lid temperature is 301 °F, both of which occur at the end of the 30-minute HAC thermal event. The closure lid temperature bounds the bottom end closure temperature. The maximum temperature of the strongback is 599 °F. The maximum temperature in the closure lid sealing region is 339 °F.

2.7.4.2 Differential Thermal Expansion

The maximum temperature of the strongback is $T_{SB} = 599$ °F, but a value of 700 °F is conservatively used and applied to the entire strongback. From Section 2.2.1, *Material Properties and Specifications*, the thermal expansion coefficient of Type 304 stainless steel at this temperature is $\alpha_{SB} = 10.0 \times 10^{-6}$ in/in/°F. Since the length of the strongback is $L_{SB} = 164.90$ inches, the thermal expansion of the strongback is:

$$\delta_{L-SB} = (\alpha_{SB})(T_{SB} - 70)(L_{SB}) = 1.04 \text{ inches}$$

The bounding minimum temperature of the MFFP shell, which is conservatively assumed to apply to the entire shell, is $T_{SH} = 1,200$ °F, a value well below the calculated maximum temperature of 1,361 °F. The linearly extrapolated thermal expansion coefficient of XM-19 is $\alpha_{SH} = 9.8 \times 10^{-6}$ in/in/°F from Section 2.2.1, *Material Properties and Specifications*, using data for 600 °F and 700 °F. Since the length of the shell cavity, L_{SH} , is 165.25 inches, the minimum thermal expansion of the shell is:

$$\delta_{L-SH} = (\alpha_{SH})(T_{SH} - 70)(L_{SH}) = 1.83 \text{ inch}$$

For the HAC thermal event, the strongback grows 0.79 inches less than the cavity, increasing axial clearance. Thus, axial clearance is maintained for the HAC thermal event.

2.7.4.3 Stress Calculations

As discussed in Section 2.7.4.1.1, *Summary of Pressures*, a conservative maximum internal pressure of 130 psig is assumed for the HAC thermal. Shell stresses due to the design pressure of 25 psig are calculated in Section 2.6.1, *Heat*. Therefore, the stress in the shell due to the HAC maximum pressure is found from:

$$\sigma_{HAC} = \frac{130}{25} \sigma_{NCT}$$

The results of this scaling for the shell, bottom end closure, and closure lid are shown in Table 2.7-4. For simplicity, the bottom end and closure lid stresses used in the scaling are peak values, but allowable stresses for membrane-only stress (the lesser of $2.4S_m$ or $0.7S_u$) are conservatively used.

The allowable stress for the bottom end and closure lid is extracted from Section 2.2.1, *Material Properties and Specifications*, for the XM-19 material at a temperature of 301 °F, and is governed by $0.7S_u$, equal to 65,940 psi. Since its temperature exceeds the values given in Section II, Part D of the ASME B&PV Code, the allowable stress for the Type XM-19 shell material is developed by comparing the yield strength behavior versus temperature to Type 304 material, which is included in

the high-temperature ASME B&PV Code. As illustrated in Figure 2.7-1, the yield strengths of Type XM-19 and Type 304 austenitic stainless steels behave similarly up to 1,500 °F. However, the Type XM-19 material is significantly stronger than Type 304 material at all temperatures. Therefore, utilizing the allowable stress extracted from ASME B&PV Code, Section III, Subsection NH³ for Type 304 is conservative for evaluating the shell at elevated temperature. The value of the rupture stress, S_R , for Type 304 is 16.5 ksi for an upper bound shell temperature of 1,400 °F and an exposure of one hour, from Table I-14.6A. The selection of a one-hour temperature duration is conservative since the shell wall temperature falls rapidly after the 30-minute HAC thermal event. The governing allowable stress is equal to $0.67S_r = 11,055$ psi.

The minimum margin of safety for the HAC thermal pressure case, including the significant conservative assumptions described above, is +2.15, as shown in Table 2.7-4. Therefore, stresses in the body shell, bottom end, and closure lid are within acceptable limits.

Per Regulatory Guide 7.6, Paragraph C.7, the extreme range of stress must be considered. Of all the various allowable stresses corresponding to the different conditions evaluated (including fabrication stresses and normal conditions of transport), the largest allowable stress is equal to the material ultimate strength, S_u . It is therefore conservative to assume that S_u bounds all stresses actually developed in the structure. For Type XM-19 stainless steel, $S_u = 100,000$ psi at 70 °F. The maximum possible stress intensity range is twice this value, or 200,000 psi. Applying a factor of four to account for possible stress concentrations at structural discontinuities gives a total stress range of 800,000 psi. The alternating component is one-half of this value, or 400,000 psi. To account for temperature effects, this value of alternating stress is factored by the ratio of modulus of elasticity. This ratio is formed between the modulus of elasticity at room temperature (at which the test data applies directly) and the modulus of elasticity at the design temperature of 160 °F. The adjusted stress is:

$$S_{alt} = 400,000 \frac{E_{70^\circ F}}{E_{160^\circ F}} = 407,194 \text{ psi}$$

where $E_{70^\circ F} = 28.3 \times 10^6$ psi and $E_{160^\circ F} = 27.8 \times 10^6$ psi. Per Figure I-9.2.1 and Table I-9.1 of the ASME B&PV Code, the allowable value for S_{alt} at 10 cycles is 708,000 psi. The margin of safety is:

$$MS = \frac{708,000}{407,194} - 1.0 = +0.74$$

Considering the significant conservatism used in the underlying assumptions (e.g., use of allowable stress rather than smaller actual stresses, assuming worst case stresses are fully reversing, use of the maximum factor of stress concentration), it is apparent that the actual margin of safety is larger than +0.74. Thus, the requirement of paragraph C.7 of Regulatory Guide 7.6 is met.

2.7.5 Immersion – Fissile Material

Subpart F of 10 CFR 71 requires performing an immersion test for fissile material packages in accordance with the requirements of 10 CFR §71.73(c)(5). The criticality evaluation presented in Chapter 6.0, *Criticality Evaluation*, assumes optimum hydrogenous moderation of the contents, thereby conservatively addressing the effects and consequences of water in-leakage.

³ American Society of Mechanical Engineers (ASME) Boiler and Pressure Vessel Code, Section III, *Rules for Construction of Nuclear Power Plant Components*, 2001 Edition, 2002 and 2003 Addenda.

2.7.6 Immersion – All Packages

Subpart F of 10 CFR 71 requires performing an immersion test for all packages in accordance with the requirements of 10 CFR §71.73(c)(6). For the MFFP, this external pressure condition is bounded by the requirements of 10 CFR §71.61, which requires that the undamaged containment system withstand an external water pressure of 290 psi for a period of not less than one hour without collapse, buckling, or in-leakage of water. Section 2.7.7, *Deep Water Immersion Test (for Type B Packages Containing More than 10⁵ A₂)*, demonstrates that the transportation package meets the requirements of 10 CFR §71.61, which bounds the requirements of 10 CFR §71.73(c)(6).

2.7.7 Deep Water Immersion Test (for Type B Packages Containing More than 10⁵ A₂)

Subpart E of 10 CFR 71 specifies performance of a deep immersion test in accordance with the requirements of 10 CFR §71.61. Since the MFFP contains more than 10⁵ A₂ of any isotope, a buckling evaluation for the 200 meter deep immersion test is performed. The evaluation is performed utilizing ASME Code Case N-284-1 and considers an external pressure of 290 psig, which exceeds the pressure of 200 meters of water.

Consistent with Regulatory Guide 7.6 philosophy, a factor of safety corresponding to ASME B&PV Code, Service Level D conditions for the hypothetical accident condition pressure loading is employed. In this case, the applicable factor of safety is 1.34 for accident conditions, as specified in ASME B&PV Code Case N-284-1.

Buckling analysis geometry parameters are provided in Table 2.7-5, and loading parameters are given in Table 2.7-6. The buckling analysis conservatively utilizes shell temperatures consistent with Section 2.6.1, *Heat*, i.e., 160 °F. The stresses are determined using the external pressure of 290 psi. The hoop stress, σ_{θ} , axial stress, σ_{ϕ} , and in-plane shear stress, $\sigma_{\phi\theta}$, are found from:

$$\sigma_{\theta} = \frac{Pr}{t} \quad \sigma_{\phi} = \frac{Pr}{2t} \quad \sigma_{\phi\theta} = \frac{Pr}{4t}$$

where P is the applied pressure, r is the mean radius, and t is the shell thickness. As shown in Table 2.7-7, all the interaction check parameters are less than 1.0, as required. Therefore, buckling of the shell due to a deep immersion is not of concern.

The same analytical methods presented in Section 2.6.1.3.1, *Stresses Due to Pressure Loading*, which are used to determine the stress due to the 25 psig design pressure, are applicable for the 290 psig deep immersion pressure. The stress results are linear and therefore the stress results of Section 2.6.1.3.1, *Stresses Due to Pressure Loading*, are multiplied by the ratio of 290/25 = 11.6. For the HAC MFFP containment design temperature of 160 °F, the allowable primary membrane stress for Type XM-19 stainless steel is the lesser of (2.4)S_m and 0.7S_u, which is equal to 69,748 psi. The allowable primary membrane-plus-bending stress of Type XM-19 stainless steel is the lesser of (3.6)S_m and S_u, which is equal to 99,640 psi. The bottom closure plate, closure lid, and shell stress and resulting margins of safety are shown in Table 2.7-8, which lists the minimum margin of safety as +1.96.

2.7.8 Summary of Damage

As discussed in the previous sections, the cumulative damaging effects of free drop and puncture drop tests are satisfactorily withstood by the MFFP, as demonstrated by certification testing (see Appendix 2.12.3, *Certification Test Results*) and analysis (see Sections 2.7.1, *Free Drop*, through 2.7.7, *Deep Water Immersion (for Type B Packages Containing More than 10⁵ A₂)*, and Appendix 2.12.5, *Fuel Control Structure Evaluation*). Helium leak testing performed prior to and subsequent to each test series confirmed that containment integrity was maintained throughout the test series. The thermal analyses presented in Chapter 3.0, *Thermal Evaluation*, demonstrate that the containment seals, which are the most temperature sensitive material in the MFFP, remain below the limiting temperature of 400 °F. The thermal evaluation includes the effect of accumulated damage from the free and puncture drop tests (conservatively neglecting the improvement to the impact limiter welded corner joint design, described in Appendix 2.12.7, *Impact Limiter Weld Joint Test Results*). The fuel assembly payload remains subcritical, as demonstrated in Chapter 6.0, *Criticality Evaluation*. Therefore, the requirements of 10 CFR §71.73 have been met.

Table 2.7-1 – Free Drop Test Summary

Test No.	Test Description	Addresses
Series 1, Test 1	Horizontal 30-ft free drop	Containment shell buckling
Series 2, Test 1	C.G.-over-corner (80° from horizontal) 30-ft free drop	Closure lid integrity; prototypic fuel integrity
Series 3, Test 1	15° Slapdown 30-ft free drop, lid primary	Strongback deformations
Series 3, Test 2	15° Slapdown 30-ft free drop, lid secondary	Strongback deformations, closure lid integrity
Additional Test (Repeat of Series 2, Test 1)	C.G.-over-corner (80° from horizontal) 30-ft free drop	Using accelerometers to gather more acceleration data for this orientation.

Table 2.7-2 – Summary of Payload Used for Certification Testing

Series No.	Payload
Series 1	Mock Payload, criticality control not tested
Series 2	Strongback, 1 Prototypic FA, 2 Dummy FAs
Series 3	Strongback, 3 Dummy FAs
Additional Test (single free drop)	Strongback, 3 Dummy FAs

Table 2.7-3 – Puncture Drop Test Summary

Test No.	Test Description	Addresses
Series 1, Test 2	Puncture drop axial to limiter	Impact limiter retention, impact limiter shell weld integrity.
Series 1, Test 3	Oblique puncture drop on bottom disk	Perforation of lid end impact limiter skin
Series 1, Test 4	Oblique puncture drop on tapered skin	Perforation of lid end impact limiter skin
Series 2, Test 2	C.G.-over-corner puncture drop on free drop damage	Effect of puncture on prior damage; puncture load on closure region
Series 3, Test 3	Horizontal puncture drop on containment shell	Containment shell leaktight integrity
Series 3, Test 4	Oblique puncture drop on containment shell	Containment shell leaktight integrity

Table 2.7-4 – HAC Thermal Pressure Stresses and Margins of Safety

Component	Stress at 25 psi Internal Pressure (psi)	Stress at 130 psi Internal Pressure (psi)	Allowable Stress (psi)	Margin of Safety
Shell	674	3,505	11,055	+2.15
Closure Lid	1,510	7,852	65,940	+7.40
Bottom End Closure	2,904	15,101	65,940	+3.37

Table 2.7-5 – Buckling Geometry Parameters per Code Case N-284-1

Geometry, Temperature, and Material Input	Shell
Outside Diameter, inch	29.63
Inside Diameter, inch	28.50
Length, inch	168.20
Temperature, °F	160
Geometry Output (nomenclature consistent with ASME Code Case N-284-1)	
R =	14.53
t =	0.56
R/t =	25.72
λ_{ϕ} =	168.20
λ_{θ} =	91.31
M_{ϕ} =	58.70

Table 2.7-6 – Stress Results for 290 psig External Pressure

Direction	Stress (psi)
Axial Stress, σ_{ϕ}	3,762
Hoop Stress, σ_{θ}	7,524
Shear Stress, $\sigma_{\phi\theta}$	1,881

Table 2.7-7 – Buckling Summary for 290 psig External Pressure

Condition	Shell	Remarks
Capacity Reduction Factors (-1511)		
$\alpha_{\phi L} =$	0.5094	
$\alpha_{DL} =$	0.8000	
$\alpha_{\phi\theta L} =$	0.8000	
Plasticity Reduction Factors (-1610)		
$\eta_{\phi} =$	0.1509	
$\eta_{\theta} =$	1.0000	
$\eta_{\phi\theta} =$	0.3567	
Theoretical Buckling Values (-1712.1.1)		
$C_{\phi} =$	0.6050	
$\sigma_{\phi eL} =$	653,895	psi
$C_{\theta r} =$	0.0137	
$\sigma_{\theta eL} = \sigma_{reL} =$	14,809	psi
$C_{\theta h} =$	0.0137	
$\sigma_{\theta eL} = \sigma_{heL} =$	14,809	psi
$C_{\phi\theta} =$	0.0974	
$\sigma_{\phi\theta eL} =$	105,239	psi
Elastic Interaction Equations (-1713.1.1)		
$\sigma_{xa} =$	248,565	psi
$\sigma_{ha} =$	8,841	psi
$\sigma_{ra} =$	8,841	psi
$\sigma_{ia} =$	62,829	psi
Axial + Hoop \Rightarrow Check (a):	...N/A	
Axial + Hoop \Rightarrow Check (b):	...N/A	
Axial + Shear \Rightarrow Check (c):	0.0160	<1 : OK
Hoop + Shear \Rightarrow Check (d):	0.8519	<1 : OK
Axial + Hoop + Shear \Rightarrow Check (e):	...N/A	
Axial + Hoop + Shear \Rightarrow Check (f):	...N/A	
Inelastic Interaction Equations (-1713.2.1)		
$\sigma_{xc} =$	37,507	psi
$\sigma_{rc} =$	8,841	psi
$\sigma_{ic} =$	22,411	psi
Axial + Hoop \Rightarrow Check (a):	0.8510	<1 : OK
Axial + Shear \Rightarrow Check (a):	0.1073	<1 : OK
Hoop + Shear \Rightarrow Check (b):	0.8581	<1 : OK

Table 2.7-8 – Deep Water Immersion Test Stresses (psi) and Margins of Safety

Component	25 psi Internal Pressure Stress	290 psi External Pressure Stress	Allowable Stress	Margin of Safety
Shell	674	7,818	69,748	+7.92
Closure Lid	1,510	17,516	99,640	+4.69
Bottom End Closure	2,904	33,686	99,640	+1.96

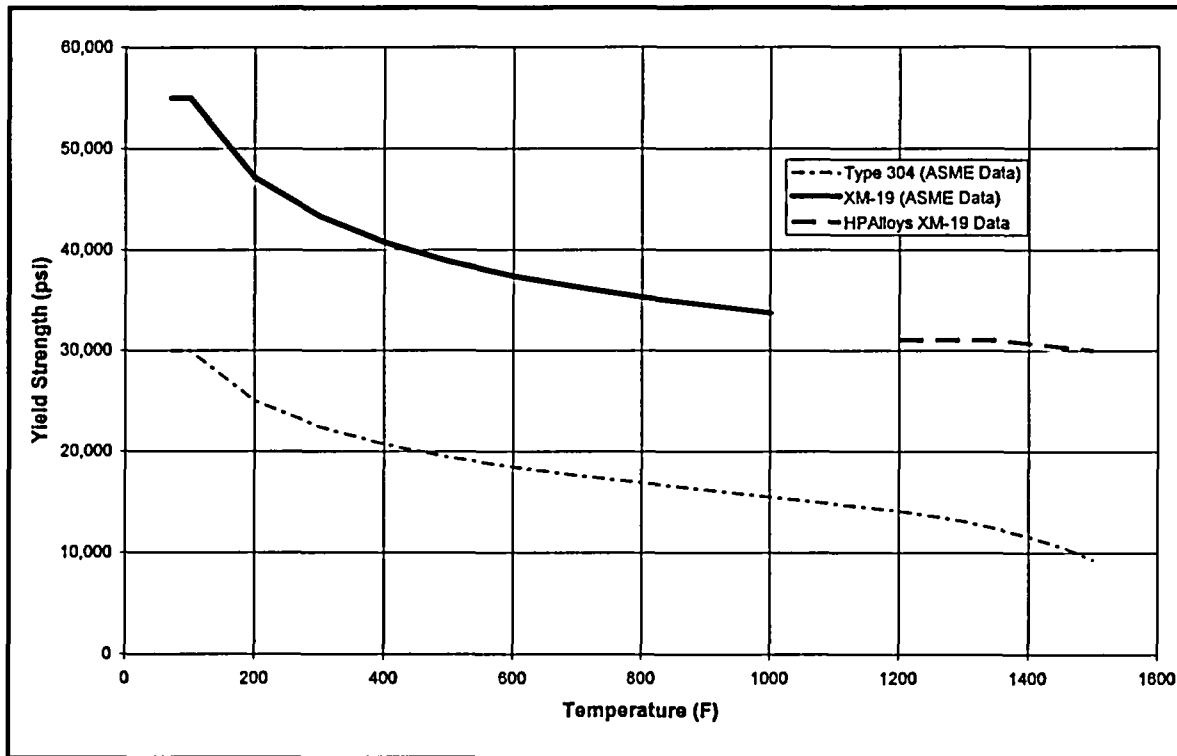


Figure 2.7-1 – Yield Strength vs. Temperature for Type 304 and XM-19 Materials

2.12 Appendices

- 2.12.1 Impact Limiter Evaluation**
- 2.12.2 Certification Test Plan**
- 2.12.3 Certification Test Results**
- 2.12.4 Engineering Test Results**
- 2.12.5 Fuel Control Structure Evaluation**
- 2.12.6 CASKDROP Computer Program**
- 2.12.7 Impact Limiter Weld Joint Test Results**
- 2.12.8 Effect of Bounding Weight on Package Structural Responses**

A

PACTEC

MFFP Safety Analysis Report

**Docket No. 71-9295
Revision 2, April 2005**

This page left intentionally blank.

2.12.8 Effect of Bounding Weight on Package Structural Responses

The free drop and puncture drop testing documented in Appendix 2.12.3, *Certification Test Results*, was performed without the presence of the fuel control structures (FCSs). Since the FCSs are integral with the strongback, they represent an additional contents weight that was not accounted for by the certification testing. This appendix documents the MFFP structural responses that would result from the increased weight of the contents consistent with the addition of the FCS.

2.12.8.1 Component Weights

As shown in Section 2.1.3, *Weights and Center of Gravity*, the maximum gross weight of the MFFP is 14,130 pounds, and the maximum weight of the contents (including the FCS) is equal to the sum of the strongback (2,900 pounds) and three fuel assemblies (4,740 pounds), or 7,640 pounds. The certification test was performed in three series. The maximum gross weight and the weights of the certification test series are compared in Table 2.12.8-1 (Certification test weight data is extracted from Section 2.12.3.6, *Test Unit Description*).

2.12.8.2 Evaluations

The certification test series summary is given in Table 2.12.2-1. Each test is examined in the following paragraphs for the effect of the increased weight on the test results. Each evaluation focuses on the behavior of the package containment structure or impact limiters. The effect of the addition of the FCS on the strongback and fuel assembly behavior is evaluated separately in Appendix 2.12.5, *Fuel Control Structure Evaluation*. A buckling evaluation for the body shell is not needed since the increased weight, which is primarily associated with the contents, does not affect buckling response. The effect of maximum gross weight on the maximum impact limiter deformation in the warm condition is evaluated in Appendix 2.12.1, *Impact Limiter Evaluation*. The maximum deformations reported in Table 2.12.1-8 are based on the maximum licensed package weight of 14,130 pounds (or $36.61 \text{ lb}_m\text{-s}^2/\text{in}$, as shown in Table 2.12.1-6). Impact limiter maximum crush responses are not further evaluated in this appendix.

2.12.8.2.1 Test Series 1

The first test in Series 1 was a 30-ft horizontal free drop. The purpose of this test was to demonstrate that the containment shell would not experience excessive deformation or buckling from the lateral inertia forces. The payload of steel bars weighed 7,500 pounds, or only 140 pounds (i.e., 1.8%) less than the maximum licensed contents weight. In the test, the containment shell did not experience any visible permanent deformation from the side drop impact. For this reason, the small increase of 140 pounds in contents weight will have no effect on the containment shell. Furthermore, as discussed in Section 2.12.2.2.1, *Mock Payload*, the steel bars together have a much smaller bending stiffness than the actual strongback used, and consequently would exert somewhat less self-support than would the strongback, thus diminishing or even eliminating any possible effect due to the extra weight.

The next three tests in Series 1 were puncture bar attacks on various locations of the impact limiters. The weight of the certification test unit, 13,815 pounds, was 315 pounds (i.e., 2.2%) less than the maximum licensed weight of the MFFP. Since the damage due to these impacts was minimal, as described in Section 2.12.3.8.1, *Certification Test Series No. 1*, it is reasonable

to assume that an increase of only 2.2% in available puncture energy would have no effect. Thus, the extra contents weight would have little or no effect on the results from Test Series 1.

2.12.8.2.2 Test Series 2

The first test in Series 2 was a 30-ft, C.G.-over-corner (near vertical) free drop. The purpose of this test was to demonstrate that the closure system could withstand the inertia loading of the contents, and to test fuel assembly integrity. The prototypic strongback, prototypic fuel assembly, and two dummy fuel assemblies together weighed 6,906 pounds, or 734 pounds (i.e., 9.6%) less than the maximum licensed contents weight. Although small, this difference could cause an increase in the loading on the closure system, which is evaluated as follows.

The effect on the closure lid structure is evaluated in two ways:

- Gross bending of the closure lid
- Puncture shear of the closure lid

The effect on the closure bolts is also evaluated.

Gross bending of the closure lid. The MFFP closure lid is a weldment consisting of two plates (3/4-inch thick outer plate and a 5/8-inch thick inner plate), which are connected by an array of radial and ring-shaped stiffeners. The total thickness of the lid weldment is 4.38 inches. During an end impact, the inertia load of the contents is applied to the inner surface of the lid as a pressure. The applied pressure is:

$$q = \frac{(w_{\text{contents}} + w_{\text{lid}})g}{(\pi/4)D_i^2} + p = 1,550 \text{ psi}$$

- where: w_{contents} = 7,640 pounds (maximum weight of contents)
 w_{lid} = 468 pounds (weight of closure lid)
 D_i = 28.5 inches (inner diameter of package/closure lid)
 g = 120g (end impact magnitude, from Section 2.12.5.2)
 p = 25 psi (design pressure from Section 2.6.1.3.1)

For a simply supported circular plate of radius a , the maximum moment per unit width is at the center of the plate. From Roark¹, Table 24, Case 10a, the moment is:

$$M_c = \frac{qa^2(3+\nu)}{16} = 75,326 \text{ lb}\cdot\text{in}/\text{in}$$

where $\nu = 0.3$ and the radius a is conservatively based on the bolt circle diameter of the lid of 30.7 inches. In order to determine the bending stress in the closure lid, its moment of inertia per unit width (I_{total}) is determined by ignoring the stiffeners and taking credit only for the inner and outer lid plates. The vertical centroid, measured from the inner face of the inner plate is:

¹ Young, W. C., *Roark's Formulas for Stress and Strain*, Sixth Edition, McGraw-Hill, 1989.

$$\bar{y} = \frac{\sum Ay}{\sum A} = \frac{(0.75)(4.00) + (0.625)(0.312)}{0.75 + 0.625} = 2.32 \text{ in}$$

The moment of inertia per inch of circumference is:

$$I_{\text{total}} = \sum (I + Ad^2) = \frac{1}{12}(0.75^3 + 0.625^3) + 0.75(4.00 - 2.32)^2 + 0.625(0.312 - 2.32)^2 = 4.69 \text{ in}^4 / \text{in}$$

The bending stress at the center of the plate is then given by:

$$\sigma_c = \frac{M_c \bar{y}}{I_{\text{total}}} = 37,261 \text{ psi}$$

The yield strength of the lid material at a bounding temperature of 200 °F is 47,100 psi from Table 2.2-1. The margin of safety against yield stress is:

$$MS = \frac{47,100}{37,261} - 1.0 = +0.26$$

Therefore, the closure lid remains elastic with the full contents weight when conservatively combining the cold, -20 °F impact to the warm, 200 °F material allowable.

Puncture shear of the closure lid. To evaluate puncture shear, a detailed evaluation of the load paths into and through the lid is made. During an end impact, the inertia load of the contents is sequentially supported as various parts of the strongback structure come into contact with the closure lid. Refer to Figure 2.12.8-1, which is a schematic representation of the structures which participate in the contact between the MFFP contents and the closure lid (the figure is to scale, but represents a composite cross section in order to show all of the elements in a single view). In the progress of the end impact, the first point of contact with the lid inner plate is at the outer rim of the top plate, as shown by the symbol ① in Figure 2.12.8-1. After undergoing approximately 0.3 inches of diaphragm deformation of the top plate, the BPRA Restraint Weldment comes in contact with the center portion of the lid, as shown by the symbol ②. All of the weight of the strongback and FCS is supported by either the top plate outer rim or the BPRA Restraint Weldment. A final contact can occur between the lid and the fuel assembly axial adjustment screws. As shown in Figure 2.12.8-1, these screws are located in the top plate and support the fuel assembly. Once the BPRA Restraint Weldment has come to rest against the closure lid, the fuel assemblies can cause further diaphragm deformation of the top plate by breaking the three, 1/2-13 UNC socket head cap screws which attach the top plate to the strongback (represented by a single bolt labeled 'B' in Figure 2.12.8-1). Note that the contact between the lid and the axial adjustment screws is driven solely by the weight of the fuel. The weight of the strongback and FCS continues to be carried into the closure lid by the top plate outer rim and the BPRA restraint weldment.

The structures of the closure lid which support the impact forces described above are also shown in Figure 2.12.8-1. The outer rim of the top plate is supported by the outer forging of the lid. The BPRA restraint weldment consists of three, 1-inch diameter hollow bars through which the bolts ('A' in the figure) pass. The three bars are placed on a 6.38-inch bolt circle, which are supported by the stiffening ring (7-inch diameter OD, 6-inch diameter ID) of the closure lid. The fuel assembly axial adjustment screws are supported by the inner plate of the closure lid.

The increase in contents weight arises from the following:

- Addition of 148 pounds to account for the maximum possible manufactured weight of the strongback.
- Addition of the FCS weight of 650 pounds.
- Reduction of 64 pounds since the simulated fuel weighed slightly more than the maximum FA weight (including BPRA) of 4,740 pounds total.

As seen from this breakdown, all of the increase in weight is either part of the strongback structure, or, in the case of the FCS, is fully carried by the strongback. Consequently, in an end drop, the added weight will be carried into the closure lid by the same paths as was the weight of the strongback in the Series 2 free drop, namely, through the top plate outer rim and through the BPRA Restraint Weldment. Since these two pathways are well supported by internal closure lid structure, the added weight does not create a risk of puncture shear in the closure lid inner plate. The only source of load path into the closure lid that is not fully supported by internal structure is the fuel assembly axial adjustment screws. However, the maximum weight of the MOX FA is slightly less than the weight of the simulated fuel assembly actually tested. For this reason, no risk of puncture shear of the closure lid is presented by the increased contents weight.

Closure bolts. As for the normal conditions of transport bolt analysis given in Section 2.6.1.3.4, *Closure Bolt Evaluation*, NUREG/CR-6007² will be used to evaluate the closure bolts. The analysis makes the following assumptions:

- From Section 2.6.1.3.4, *Closure Bolt Evaluation*, the maximum force due to pre-load ($F_{a_{max}}$) is equal to 22,420 pounds. Differential thermal expansion ($F_{a_{therm}}$) is not applicable for HAC. Therefore, $F_{a_{pt}}$ as discussed in Table 4.9 of NUREG/CR-6007 is equal to 22,420 pounds.
- The sum of the tensile forces for the remaining loads ($F_{a_{al}}$) is equal to the sum of the forces resulting from the internal pressure load ($F_{a_{pressure}} = 687$ pounds) as calculated in Section 2.6.1.3.4, *Closure Bolt Evaluation*, and the vertical component of the impact load ($F_{a_{impact}}$) calculated below.
- In Appendix V of NUREG/CR-6007, $F_{a_{impact}}$ is calculated based on the very conservative assumption that the package is supported only at the impact corner of the package, and ignores any support provided by the impact limiter. The following analysis assumes some support is provided by the impact limiter. A modified derivation of $F_{a_{impact}}$ follows below.
- The closure lid has a step located at the bolt circle diameter that precludes prying forces.
- There are no applied shear stresses from the horizontal component of the impact force since the shear load is carried by the closure lid.
- Per Table 6.3 of NUREG/CR-6007, the "tension plus shear plus bending plus residual torsion" stress limit is not evaluated for HAC. Therefore, the residual torsion stress is not considered in the calculation.

The maximum bolt impact force is now determined. Because of the cold conditions, the impact limiter crush zone has a minimum possible volume, resulting in the smallest possible crush foot print. Moreover, the regulatory test articles weighed slightly less than the maximum MFFP weight, which

² G.C. Mok, L.E. Fischer, S.T. Hsu, *Stress Analysis of Closure Bolts for Shipping Casks*, NUREG/CR-6007, UCRL-ED-110637, U.S. Nuclear Regulatory Commission, April 1992.

also results in a smaller crush volume. Consequently, the crush zone resulting from the regulatory drop predicts a conservative minimum backing of the closure bolts by the impact limiter.

The shape of the impact limiter crush zone is a wedge shape due to the impact angle as illustrated in Figure 2.12.8-2. The maximum depth of the deformation is measured as 6.1 inches as stated in Section 2.12.3.8.2.2, *Series 2, Test 1: HAC 80-Degree Oblique C.G.-Over-Corner 30-foot Drop*. Given this crush depth, the impact footprint extends nearly to the edge of the impact limiter's 36 inch diameter face, as shown in Figure 2.12.8-2. The impact limiter has a 20-inch diameter hole on its end having a depth of 8 inches. Conservatively, no support is assumed for the area of the 20-inch diameter hole.

At a minimum, the impact limiter will provide support to the closure lid over the vertical projection of the footprint area onto the lid. Rather than assuming that the zone extends to the edge of the impact limiter's 36 inch diameter face, it is conservatively assumed that the zone will extend only to the edge of the 20 inch hole. The force distribution will be a maximum at the impact corner of the closure lid, and will linearly decrease to zero at the opposite edge of the supported zone. Figure 2.12.8-2 illustrates the force distribution.

Using the nomenclature from NUREG/CR-6007 for the impact gs (ai) and the drop angle (πi), the total reaction force provided by the impact limiter equals the vertical component of the weight supported by the impact limiter multiplied by the impact gs and is given by:

$$R_{IL,y} = (W_{TOTAL-IL} \sin(\pi i)) \times ai$$

Because of the shape and distribution of the reaction force, the center of pressure of the distributed reaction force acts at location 8.28 inches from the impact corner of the closure lid as determined by 3D computer-aided design (CAD) software, and shown in Figure 2.12.8-2. This arm length is referred to as (yf).

As shown on the free body diagram V.1 in Appendix V of NUREG/CR-6007, the vertical component of the load applied by the lid (Wl) and payload (Wc) during impact is equal to L , or:

$$L = ((Wl + Wc) \sin(\pi i)) \times ai$$

Taking into consideration the support force $R_{IL,y}$, the summation of moments about the impact point (Appendix V, equation V.1) becomes:

$$\sum fb yb = L (yL) - R_{IL,y} (yf)$$

where (yL) is the distance from the impact point to the center of the applied load (L), which equals the outside radius of the lid (Rlo). Following the derivation in Appendix V, the maximum bolt force, $(fb)_{max}$, for a bolt pattern having a total number of bolts (Nb) becomes:

$$(fb)_{max} = \frac{4 L(yL) - R_{IL,y} (yf)}{3 (Rlo)(Nb)}$$

In summary, the moment in the direction of opening the lid is $L(yL)$, the moment of the impact limiter in resisting that moment is $R_{IL,y}(yf)$, and the balance is resisted by the closure bolt forces.

Substituting the above equation into the equation for the axial force in Table 4.5 of NUREG/CR-6007 for an unprotected closure lid gives the following equation:

$$F_{a_impact} = \frac{1.34(ai)\sin(\pi i)[(Wl + Wc)Rlo - W_{TOTAL-IL}(yf)]}{Nb(Rlo)} = 10,739 \text{ lb}_m$$

where: Wl = 468 pounds (weight of closure lid)
Wc = 7,640 pounds (maximum weight of contents)
W_{TOTAL-IL} = 12,640 pounds (MFFP weight (14,130 lb_m) - lower limiter weight (1,490 lb_m)
Rlo = 16.15 inches (outer radius of closure lid)
yf = 8.28 inches (location of reaction force centroid from lid edge)
πi = 80° (package orientation)
ai = 120g (impact magnitude)
Nb = 24 (number of bolts)

The combined maximum tensile bolt forces are equal to:

$$F_{a_al} = F_{a_pressure} + F_{a_impact} = 687 + 10,739 = 11,426 \text{ lb}$$

A comparison of F_{a_pt} with F_{a_al} per Table 4.9, Step 1.4 of NUREG/CR-6007, shows that F_{a_pt}, equal to 22,420 pounds, is greater than F_{a_al}. Therefore, calculation of the average bolt stress (S_{ba}) is based on the pre-load, not the impact loads:

$$S_{ba} = (1.2732) \frac{F_{a_pt}}{D_{ba}^2} = 66,943 \text{ psi}$$

where D_{ba} = 0.653 inches from Section 2.6.1.3.4. From Table 2.1-1, the HAC allowable average tensile stress is the lesser of S_y (equal to 106,300 psi) or 0.7S_u (equal to 0.7 × 140,000 = 98,000 psi), with material properties taken from Table 2.2-5 at 200 °F. The corresponding margin of safety on average tensile stress, S_{ba}, is:

$$MS = \frac{98,000}{66,943} - 1.0 = +0.46$$

Since the calculated stress is less than the material yield strength of 106,300 psi, there is no plastic deformation in the closure lid or seal region. Because there is no resulting shear stress, the "Average Shear Stress" and the "Average Tensile + Average Shear" criteria are met.

The second test in Series 2 was a puncture drop test on the impact damage from the prior free drop. The weight of the certification test unit, 13,234 pounds, was 896 pounds (i.e., 6.3%) less than the maximum licensed weight of the MFFP. However, based on the very minimal damage done to the impact limiter as a result of this test (see Figure 2.12.3-18), an increase in available puncture energy of 6.3% will have a negligible effect. Thus, the extra contents weight would have little or no effect on the results from Test Series 2.

2.12.8.2.3 Test Series 3

The first two tests in Test Series 3 were 30-ft free drops in a slapdown orientation, one with the closure lid end striking first, and one with the closure lid end striking second. Each test also featured a different azimuth orientation of the strongback. As stated in Table 2.12.2-1, these two drops were planned to test the strongback and the closure system in the lateral direction. The

effect of the added FCS weight on the strongback structure is evaluated in Appendix 2.12.5, *Fuel Control Structure Evaluation*. The added contents weight will have no effect on the behavior of the closure system in a slapdown orientation, since the secondary impact orientation was essentially horizontal.

The second two tests were puncture attacks on the containment boundary shell. The weight of the certification test unit, 13,217 pounds, was 913 pounds (i.e., 6.5%) less than the maximum licensed weight of the MFFP. The governing case was Test 3, which was oriented perpendicular to the surface and directed through the package C.G. As stated in Section 2.12.3.8.3.4, *Series 3, Test 3: HAC Horizontal Puncture Drop*, the damage consisted of an indentation of approximately 2.13 inches deep. As shown in Figure 2.12.3-35, the deformation was not severe, and no cracking or loss of leaktight condition was noted from the test. An additional available puncture energy of 6.5% could produce an additional deformation of approximately $0.065 \times 2.13 = 0.14$ inches. This modest increase in deformation would not cause containment boundary failure or loss of a leaktight condition. Thus, the extra contents weight would have little or no effect on the results from Test Series 3.

2.12.8.3 Conclusions

As shown in the foregoing calculations, the additional weight of the MFFP, up to the maximum licensed weight, will have little or no effect on the results obtained from full-scale certification testing.

Table 2.12.8-1 – Summary of Certification Test Unit Weights (pounds)

Component	Maximum Licensed	Test Series 1	Test Series 2	Test Series 3
Strongback	2,900	N/A	2,102	2,100
Fuel Assemblies	4,740	7,500*	4,804	4,788
<i>Contents Sum</i>	7,640	7,500	6,906	6,888
Empty Package**	6,490	6,315	6,328	6,329
<i>Gross Package</i>	14,130	13,815	13,234	13,217

*Mock payload composed of small steel rods.

**Empty package, without strongback.

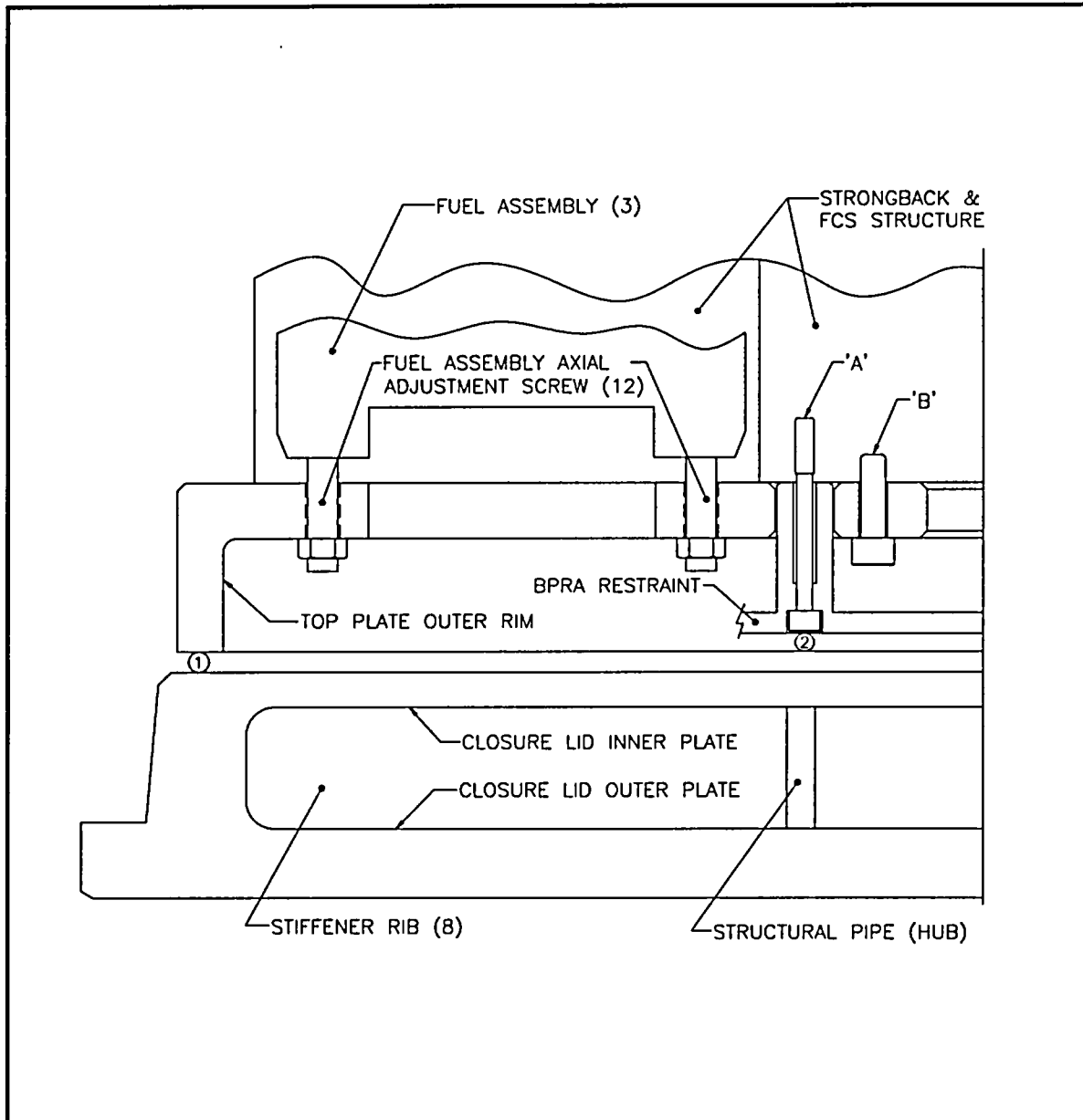


FIGURE 2.12.8-1 – Impact Conditions at the Top Plate – Closure Lid Interface

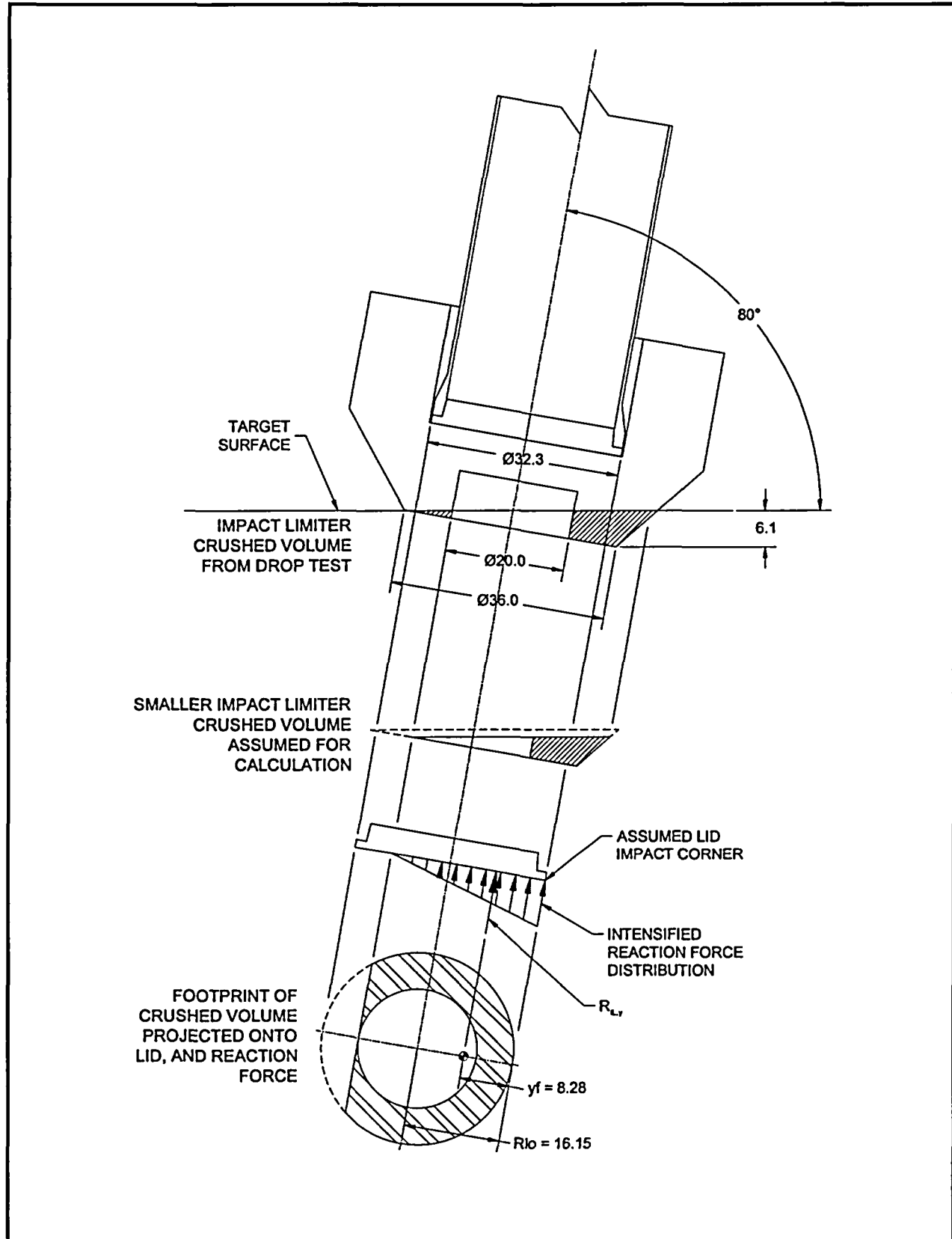


FIGURE 2.12.8-2 – Support Provided by the Impact Limiter

This page left intentionally blank.

6.0 CRITICALITY EVALUATION

The following analyses demonstrate that the MFFP complies with the requirements of 10 CFR §71.55¹ and §71.59. The analyses presented herein show that the criticality requirements are satisfied when limiting the MFFP package to a maximum of three pressurized water reactor (PWR) mixed-oxide (MOX) fresh fuel assemblies (FAs) as described in Section 1.2.3, *Contents of Packaging*.

6.1 Description of Criticality Design

6.1.1 Design Features Important for Criticality

A comprehensive description of the MFFP package is provided in Section 1.2, *Packaging Description*, and in the drawings in Appendix 1.4.2, *Packaging General Arrangement Drawings*. This section summarizes those design features important for criticality.

The primary design feature used to ensure criticality safety is the use of neutron poison plates (boral) with a minimum B-10 areal density of 0.035 g/cm². The neutron poison plates surround each fuel assembly on all four sides. Neutron poison plates that span the active fuel length are fastened to the radial and tangential strongback angles. The remaining two sides of each assembly are constrained by fuel control structures (FCSs), which are hinged angles placed between the clamp arms. Neutron poison plates (boral) are bolted to the exterior surface of each FCS.

Criticality safety is also ensured by the structural design of the MFFP. The stainless steel strongback angles and clamp arms firmly secure the FAs to the package. The FCS provides additional support in the event of an accident and prevents unrestrained pitch expansion of the fuel. Finally, the stainless steel shell of the package itself provides separation from adjacent packages and provides a leaktight containment boundary that excludes water from the package.

6.1.2 Summary Table of Criticality Evaluation

The upper subcritical limit (USL) for ensuring that the MFFP (package or package array) is acceptably subcritical, as determined in Section 6.8, *Benchmark Evaluations*, is:

$$USL = 0.9288$$

The package is considered to be acceptably subcritical if the computed k_{safe} (k_s), which is defined as $k_{effective}$ (k_{eff}) plus twice the statistical uncertainty (σ), is less than the USL, or:

$$k_s = k_{eff} + 2\sigma < USL$$

The USL is determined on the basis of a benchmark analysis and incorporates the combined effects of code computational bias, the uncertainty in the bias based on both benchmark-model and computational uncertainties, and an administrative margin. The results of the benchmark analyses indicate that the USL is adequate to ensure subcriticality of the MFFP.

¹ Title 10, Code of Federal Regulations, Part 71 (10 CFR 71), *Packaging and Transportation of Radioactive Material*, Final Rule, 01-26-04.

The results of the criticality calculations are summarized in Table 6.1-1. The maximum calculated k_s is 0.9037 which occurs for the HAC infinite array case with fully moderated internal region and void external region. Under NCT, the maximum calculated k_s is 0.6039 for the array case.

The NCT cases assume no moderation. This assumption is credible because of the leaktight performance of the MFFP under both NCT and HAC. Consequently, NCT reactivities are negligibly low.

For HAC, water is assumed to be present in the containment system. Reactivity increases monotonically as water density is increased to a maximum of 100% water density. For the HAC cases, the pitch is also allowed to expand to the maximum possible extent allowed by the FCS to simulate possible fuel assembly damage. Reactivity is a maximum when the pitch is the maximum allowed by the FCS, indicating that the system is undermoderated.

6.1.3 Criticality Safety Index

For both NCT and HAC, an infinite number of MFFPs are evaluated in a close-packed hexagonal array. Therefore, "N" is infinite, and in accordance with 10 CFR §71.59 the criticality safety index (CSI) is $50/N = 0$.

Table 6.1-1 – Summary of Criticality Analysis Results

Normal Conditions of Transport (NCT)			
Case	k_{eff}	σ	k_s
Single Unit Maximum k_s	0.2858	0.0008	0.2874
Infinite Array Maximum k_s	0.6027	0.0006	0.6039
Hypothetical Accident Conditions (HAC)			
Case	k_{eff}	σ	k_s
Single Unit Maximum k_s	0.8981	0.0010	0.9001
Infinite Array Maximum k_s	0.9017	0.0010	0.9037
USL	0.9288		

6.3 General Considerations

Criticality calculations for the MFFP package are performed using the three-dimensional Monte Carlo computer code MCNP5¹. Descriptions of the fuel assembly geometric models are given in Section 6.3.1, *Model Configuration*. The material properties for all materials used in the models are provided in Section 6.3.2, *Material Properties*. The computer code and cross section libraries used are provided in Section 6.3.3, *Computer Codes and Cross-Section Libraries*. Finally, the most reactive configuration for each case is provided in Section 6.3.4, *Demonstration of Maximum Reactivity*.

6.3.1 Model Configuration

6.3.1.1 Contents Model

The MFFP contents are represented by a conservative model of the MOX fresh fuel assembly. The model contains fuel loading that exceeds the designs currently being considered. In addition, the fuel assembly model conservatively:

- Neglects fuel rod zoning
- Assumes the maximum fuel loading, including fissile isotope distribution, possible
- Ignores any effect of burnable poison fuel assemblies, even if present.

Table 6.2-1, Table 6.2-2, and Table 6.2-3 contain the significant parameters used in the contents model. The contents model uses nominal dimensions with the exception of the pitch, which is optimized to maximize reactivity.

Each fuel pin is modeled explicitly, including the top and bottom end plugs, plenum, and pellet/cladding gap. The 24 empty guide thimbles are modeled explicitly, and the center instrument tube is assumed to be the same as a guide thimble. The grid straps are conservatively ignored, as well as the top and bottom nozzles, which are modeled as variable density water. The fuel pin pellet-cladding gap is also filled with variable density water to match the moderation assumed in the package cavity. The HAC models also consider the reactivity effects of the fuel pins shifting axially.

6.3.1.2 Packaging Model

A comprehensive description of the MFFP packaging is provided in Section 1.2, *Packaging Description*, and in the packaging drawings in Appendix 1.4.2, *Packaging General Arrangement Drawings*. The packaging includes a containment vessel, an internal strongback assembly, and impact limiters. The impact limiters cover each end of the body and are steel shells filled with polyurethane form.

The packaging is lightweight due to the weight constraints built into the design. For modeling simplicity, the impact limiters are neglected for both NCT and HAC models. Ignoring the impact limiters conservatively:

¹ MCNP5, "MCNP – A General Monte Carlo N-Particle Transport Code, Version 5; Volume II: User's Guide," LA-CP-03-0245, Los Alamos National Laboratory, April, 2003.

- Allows for greater reflection in the single package cases (because the reflector is closer to the contents).
- Accounts for any HAC damage to the limiters (due to crush during impact).
- Conservatively places packages closer together for the array calculations (because the impact limiters would provide additional spacing and reduce moderation or reflection).

Because the containment shell sustains only localized puncture damage during HAC (refer to Figure 2.12.3-35 for puncture damage) and because minor variations in the package dimensions have little effect on the criticality calculations, nominal packaging dimensions are used for both the basic NCT and HAC models.

Details of the packaging model are provided in the following figures. Figures are presented to scale and are generated from the MCNP input files. The packaging model represents geometrically significant structural and poison materials. Key dimensions used in the MCNP models are provided in Table 6.3-1. Notations are made in the table when the model dimensions differ from the final design. The model is more conservative than the final design because the FCS poison plates as modeled are smaller than actual size.

Figure 6.3-1 shows the model geometry through a planar slice of the package for the NCT case. The strongback is modeled as a simplified triangular shaped structure. Because the design allows for easy water migration through the strongback, any water moderation is modeled to completely fill all void spaces. Water reflector (12 inches) surrounds the package on all sides. Figure 6.3-2 shows an axial view of the NCT geometry.

Figure 6.3-3 and Figure 6.3-4 present a close-up view of the lower fuel assembly at different axial elevations with labels on all major components. Each fuel assembly is completely surrounded on all four sides to restrict movement. As shown in Figure 6.3-3, the top and right boundary of the assembly is bounded by the strongback. Borated aluminum (boral) neutron poison plates are bolted to the strongback between the strongback and neutron poison cover plates.

The strongback and strongback boral are continuous pieces, while the neutron poison cover plates are segmented and are located only opposite each clamp arm. Steel bolts are explicitly modeled in the strongback boral to reduce the boron loading. As shown in Figure 6.3-3, the left and bottom boundary of each assembly is supported by eight clamp arms and seven fuel control structures (FCSs). Each FCS segment has neutron poison plates attached on the outer surface of the FCS. For simplicity, the clamp arms and strongback support triangles are not explicitly modeled, although the seven steel segments that form the FCS are modeled as one continuous piece because the steel clamp arms will be present between the segments. The impact of including the clamp arms and strongback triangles is assessed in additional calculations in which these components are homogenized into the water region.

The FCS neutron poison plates are modeled as discrete segments. The FCS neutron poison plates are not modeled with bolt holes as with the strongback boral, although the FCS neutron poison plates are modeled conservatively short to minimize the amount of boral.

Figure 6.3-5 shows a close-up view of the model corner. Note that the neutron poison plate is explicitly modeled as a B_4C -Al matrix clad on each side by aluminum.

Figure 6.3-6 and Figure 6.3-7 show the top and bottom of the package. Note that the top and bottom nozzles are modeled as variable density water. Also, these figures explicitly show the

fuel pin end caps and plenum regions. Figure 6.3-8 and Figure 6.3-9 show the strongback and FCS poison plates and the extent to which they overlap the active fuel region.

6.3.2 Material Properties

All material compositions used in the models are representative of the actual materials used in the MFFP. The compositions and densities of all packaging materials as input to MCNP are provided in Table 6.3-2 through Table 6.3-6. Note that most materials (Type 304, XM-19, fuel) are input with weight fractions on the material card and gram density on the cell card. The boral is input with number densities on the material card and total number density on the cell card.

As fuel isotopics are provided as ranges in Table 6.2-3, the fuel isotopics selected for the criticality model are chosen to maximize reactivity. As Pu-241 is more reactive than Pu-239 for moderated systems (which are the most reactive cases for the MFFP), the Pu-241 content is maximized. As Pu-240 acts as a poison, the Pu-240 content is minimized. The balance of Pu is assumed to be Pu-239. The U-235 content is conservatively assumed to be at the maximum value. The fuel isotopics utilized are provided in Table 6.3-2.

The effective density of the fuel is computed to be 10.31 g/cm³ based on the mass of fuel in a pin (95% theoretical density), pellet diameter, and active fuel length, as shown in Table 6.3-2. The fuel density assuming 100% theoretical density is 10.85 g/cm³.

Type 304 stainless steel is used for the strongback angles and poison cover plates; its composition and density are provided in Table 6.3-3.

Most of the models used in the analysis assume M5 fuel cladding, end caps, and thimble tubes; M5 composition and density are provided in Table 6.3-4. Final runs were made with a more generic zirconium-based material with niobium in the range 0 to 3%.

Type XM-19 stainless steel is used for the MFFP structural shell; its composition and density are provided in Table 6.3-5.

The neutron poison plates have a minimum B-10 areal density of 0.035 g/cm². Only 75% credit is taken for the B-10 number density. The number densities of the B₄C-Al boral matrix are provided in Table 6.3-6. The boral is clad with aluminum assumed to be pure and with a density of 2.713 g/cm³.

Water used in the models is assumed to be pure; density is case dependent.

6.3.3 Computer Codes and Cross-Section Libraries

The Monte Carlo computer program MCNP5 is used for this criticality analysis and has been verified for proper operation on the machine(s) on which it is installed. MCNP5 and its predecessor codes (MCNP4C, MCNP4B, etc.) have been an industry standard for neutron transport and criticality analysis for several decades.

MCNP5 primarily uses continuous energy ENDF/B-VI cross sections at room temperature, although ENDF/B-V cross sections are used when ENDF/B-VI cross sections are not available (i.e., iron, chromium, and nickel). A summary of the neutron cross sections utilized are provided in Table 6.3-7. Note that these cross sections are the default cross sections utilized by the program when no particular cross section set is specified. The S(α,β) card [LWTR.01t] is used to simulate hydrogen in room temperature water.

The NCT cases are run with 500 generations and 1,000 particles per generation. These files converge quickly because of the absence of moderating material. The HAC cases are run with 500 generations and 2,000 particles per generation. All cases use the SDEF card to distribute the starting neutrons over the length of every fuel pin. This ensures a uniform starting distribution and stable convergence. A $1-\sigma$ standard deviation of approximately 0.001 is considered acceptable for the results.

6.3.4 Demonstration of Maximum Reactivity

6.3.4.1 Single Package

The most reactive single package model is for the HAC case `max_hac_single_su1`. To ensure this is the most reactive case, the following parameters have been investigated:

- The internal moderation is varied from 0 to 1.0 g/cm^3 . The water in the pellet-cladding gap is also assumed to vary with the internal moderation. The most reactive condition is for full-density water.
- The pitch is varied from the “nominal-minus-tolerance” value to the maximum pitch such that the fuel assembly completely fills the space constrained by the FCS. The pitch is expanded uniformly over all three assemblies. Note that in the fully expanded position, the steel neutron poison cover plates that hold the borated aluminum to the strongback are artificially removed from the package model to allow room for this expansion. The case with a maximum pitch is the most reactive.
- The package is reflected with steel, which is shown to be slightly more reactive than either water or lead reflectors.
- Miscellaneous minor steel components in the package are homogenized into the water region for the most reactive case. This addition of steel further raises the reactivity slightly.
- The zirconium based alloy cladding has no niobium content, which is shown to be slightly more reactive than with niobium present.
- The fuel pellets are assumed to be 100% dense.
- The most reactive number of fuel pins are allowed to shift either up or down to the maximum possible extent.
- The most reactive single package therefore has full density moderator inside the package and the pellet-cladding gap, maximum pitch, steel reflector, homogenized minor steel components, pure-zirconium cladding, 100% dense fuel pellets, and axially shifted fuel pins.

6.3.4.2 Arrays of Undamaged Packages

The most reactive NCT array case is `max_nct_array`. An infinite hexagonal array is assumed. Because the MFFP is leaktight under NCT conditions, the package cavity is assumed to be dry. In the absence of moderation, the reactivity is very low and only one pitch is investigated. The only parameter investigated is the external water density, which is allowed to vary over the range 0 to 1.0 g/cm^3 . The fuel pellets are assumed to be 100% dense and the zirconium based alloy cladding has no niobium content. Maximum reactivity is obtained with no water between the packages.

6.3.4.3 Arrays of Damaged Packages

The most reactive HAC array case is max_hac_array_sd2. An infinite hexagonal array is assumed. To ensure this is the most reactive case, the following parameters have been investigated:

- The internal moderation is varied from 0 to 1.0 g/cm³. The water in the pellet-cladding gap is also assumed to vary with the internal moderation. The most reactive condition is for full-density water.
- The external moderation is varied from 0 to 1.0 g/cm³. The most reactive condition is for no external moderation.
- The pitch is varied from the “nominal minus tolerance” value to the maximum pitch such that the fuel assembly completely fills the space constrained by the FCS. The pitch is expanded uniformly over all three assemblies. Note that in the fully expanded position, the steel neutron poison cover plates that hold the borated aluminum to the strongback are artificially removed from the package model to allow room for this expansion. The case with a maximum pitch is the most reactive.
- Miscellaneous minor steel components in the package are homogenized into the water region for the most reactive case. This addition of steel further raises the reactivity slightly.
- The zirconium based alloy cladding has no niobium content, which is shown to be slightly more reactive than with niobium present.
- The fuel pellets are assumed to be 100% dense.
- The most reactive number of fuel pins are allowed to shift either up or down to the maximum possible extent.
- The most reactive package array therefore has full density moderator inside the package and the pellet-cladding gap, no external moderation, maximum pitch, homogenized minor steel components, pure-zirconium cladding, 100% dense fuel pellets, and axially shifted fuel pins.

Table 6.3-1 – Key Packaging Model Dimensions

Description	English Value (in)	Metric Value (cm)
Total package length	171.3	435.2
Body shell OD	29.625	75.248
Body shell ID	28.50	72.39
Bottom end thickness	1.50	3.81
Closure lid thickness (total)	4.38	11.13
Closure lid upper plate thickness	0.75	1.91
Closure lid lower plate thickness	0.63	1.60
Length of “tangential” strongback angle	8.30	21.08
Length of “radial” strongback angle	9.07	23.04
Strongback thickness	0.25	0.64
Strongback length (excluding top/bottom plate assemblies)	160.11	406.68
Radial poison plate hole diameter (same as tangential)	0.375	0.953
Radial poison plate hole axial location (same as tangential)	Refer to drawings in §1.4.2	Refer to drawings in §1.4.2
Radial poison plate width (same as tangential)	8.43	21.41
Radial poison plate, radial distance between bolt holes (used for all pairs)	4.352	11.054
Radial poison plate, axial distance between bolt holes (used for all pairs, same as tangential)	2.848	7.234
Radial poison plate, distance from inner hole to edge of plate	2.12	5.39
Tangential poison plate, radial distance between bolt holes (used for all pairs)	5.50	13.97
Tangential poison plate, distance from inner hole to edge of plate	0.97	2.46
Poison cover plate thickness	0.1874 (7-gauge)	0.4760
Poison cover plate width	8.43	21.41
Poison cover plate height (Note: used for both radial and tangential for simplicity, although radial dimension is 3.75 inches)	4.25	10.80
End poison cover plate height (Note: modeled as 1.25 inches at the top for simplicity)	1.0	2.54
Middle triangle base length (also used for upper triangle)	7.36	18.69

6.4 Single Package Evaluation

Compliance with the requirements of 10 CFR §71.55 is demonstrated by analyzing optimally moderated damaged and undamaged, single-unit MFFP packages. The figures and descriptions provided in Section 6.3.1, *Model Configuration*, describe the basic geometry of the single-unit models.

6.4.1 Single Package Configuration

Because the engineering drop tests show no measurable change in the package external dimensions but expansion of the assembly pitch, the NCT and HAC models are the same, except (1) optimized internal water (within voids inside containment) is included in the HAC calculations, (2) the HAC cases allow for pitch expansion up to the maximum allowed extent, and (3) the HAC cases consider axial shifting of the fuel pins.

Each of the three FAs are radially symmetric about the origin. The model is constructed by building the lower assembly in the correct geometrical location using the MCNP LATTICE feature and then simply rotating copies of this assembly counterclockwise to build the other two assemblies. To simplify model preparation, the strongback assembly and outer FCS are modeled in separate MCNP “universes” and then inserted into the primary universe by use of the MCNP FILL command. This allows for simple rotation of these components to generate the complete model.

6.4.1.1 NCT Configuration

The largest allowable pin pitch in the undamaged condition is assumed (0.502 inches, 1.2751 cm). The package is reflected on all sides with 12 inches of three common reflectors: water, steel, and lead (cases `nct_single_b35pnomplustol`, `nct_single_b35pnomplustol_Rsteel`, `nct_single_b35pnomplustol_Rlead`). The lead reflector case is the most reactive of the three reflectors analyzed. Other reflectors might yield slightly higher results, although in the absence of internal moderation, the reactivity is extremely low (<0.3) and no further analysis is warranted. Because no water is present within the package for the NCT cases and the reactivity is low, parametric studies on the pitch are not warranted.

All cases except the final maximum case (`max_nct_single`) are run with a pellet density of 10.31 g/cm^3 and M5 cladding. To bound possible future fluctuations in the pellet density and cladding composition, the lead reflector case is run with a pellet density of 10.85 g/cm^3 and pure-zirconium cladding. It is shown in Section 6.6.3, *Impact of Niobium Content in the Cladding*, that pure zirconium cladding is slightly more reactive than cladding containing niobium.

6.4.1.2 HAC Configuration

The FCS limits the expansion of the fuel assemblies to a maximum of 8.8 inches. This dimension of 8.8 inches is defined from the surface of the strongback boral to the inner surface of the FCS, see Figure 6.4-1. In the HAC single package models, the pitch is allowed to range from a minimum value of nominal minus tolerance (0.490 inches) to a maximum value such that the OD of the outer fuel pins fill a region 8.8 inches square (0.5266 inches). In the MCNP models, the steel poison cover plates are “sliced off” to allow for this pin expansion. The various pitches used in the analysis, along with the nomenclature utilized, are provided in Table 6.4-1.

For the HAC single package model, it is assumed that water has completely flooded the package internals, including the pellet-cladding gap. The package is reflected with 12 inches of water on all sides. Note that reactivity increases with increasing pitch, indicating that the system is under moderated. The maximum reactivity is calculated for the maximum pitch expansion.

Using this model with maximum pitch and 12 inches water reflector, a further series of cases are run to investigate the effects of reduced internal moderation by reducing the internal water density. Because water is free to flow throughout the internals of the package, it is assumed that all internal water densities are uniformly reduced. As expected for an under moderated system, the reactivity decreases with decreasing water density.

The worst-case pitch geometry is also run with full-water moderation and both steel and lead reflectors. The increase in k_s with these reflectors is small (only a few mk), and the system is most reactive with a steel reflector. Because the difference in k_s between the three reflectors studied is small (~3 mk), analysis of other reflectors is not warranted.

Because the high-density steel and lead reflector cases (cases hac_single_b35pmax2_Rsteel, hac_single_b35pmax2_Rlead) are slightly more reactive than the water reflectors, additional cases (denoted with _hsteel in case name) are run to investigate the effect of including minor steel components that have been ignored in the model, namely, the clamp arms and the strongback triangles. The clamp arms are steel structures that weigh approximately 36 pounds each and secure the fuel assembly to the strongback. The strongback triangles fit into the triangular region between the strongbacks and provide support. The top and bottom triangles are primarily solid steel, while the triangle pieces in the central regions are fabricated from 1/2-inch thick steel plate and are mostly void.

For simplicity, this additional steel is not modeled explicitly but is homogenized into the water surrounding the assemblies. Water between the fuel pins remains unchanged and does not contain the homogenized steel. The triangle steel represents approximately 5.8% (by volume) of the region between the strongbacks, while the clamp arm steel represents approximately 3.2% (by volume) of the region between the fuel and the body shell wall. To maximize the amount of steel within the model, 5.8% steel is assumed for both regions. The reactivity for this case is slightly higher than the case without the homogenized steel, although the increase is within the statistical uncertainty of the calculations.

All cases except the final maximum cases (beginning max_hac_single) are run with a pellet density of 10.31 g/cm^3 and M5 cladding. To bound possible future fluctuations in the pellet density and cladding composition, the case with a steel reflector and homogenized minor steel components is run with a pellet density of 10.85 g/cm^3 and pure-zirconium cladding. It is shown in Section 6.6.3, *Impact of Niobium Content in the Cladding*, that pure zirconium cladding is slightly more reactive than cladding containing niobium.

The last set of calculations allows axial shifting of the fuel pins. These models use a pellet density of 10.85 g/cm^3 and pure-zirconium cladding. Approximately 8 fuel pins shifted upward through the holes in the top nozzle during the drop tests. In order to bound any potential axial displacement of the fuel pins, models are developed in which pins are allowed to shift up to the top lid or down to the bottom of the package. Models are developed with 8, 24, 60, and 116 pins shifted either up or down in a regular pattern, see Figure 6.4-2. Pins are shifted every other row to increase moderation between pins at the ends. To approximate the actual test results, models are also developed with only 10 or 20 randomly selected rods shifting either up or down. Cases are also developed in which all of the rods displace either up or down.

Pins are assumed to shift either up or down within a model, as the direction of shift will be dependent upon the package orientation upon impact. It is not possible for the some pins to shift up and other pins to shift down as a result of the same accident.

The relation of fuel to the top and bottom of the strongback for the nominal (unshifted) geometry is shown in Figure 6.3-6 and Figure 6.3-7, respectively. Fuel pins shifted up and down are shown in Figure 6.4-3 and Figure 6.4-4, respectively. Note that the top and bottom nozzles, as well as elements of the strongback, are necessarily ignored to allow the pins to shift in this fashion. Such extreme shifting would likely be incredible and was not observed in the drop tests.

6.4.2 Single Package Results

Criticality results for the NCT single package analysis is provided in Table 6.4-2. For the NCT case, the maximum $k_s = 0.2874$ is below the USL and is obtained for the case with a lead reflector, a pellet density of 10.85 g/cm^3 , and pure zirconium cladding.

Criticality results for the HAC single package analysis without and with axially shifted fuel pins are provided in Table 6.4-3 and Table 6.4-4, respectively. For the HAC case, the maximum $k_s = 0.9001$ is below the USL and is obtained for the case with full-density water (with homogenized minor steel components) in the package cavity, maximum pin pitch, a steel reflector, a pellet density of 10.85 g/cm^3 , pure zirconium cladding, and shifted fuel pins. The maximum $k_s = 0.9001$ occurs for two different cases, 20 fuel pins randomly shifted down, and 8 fuel pins shifted up. Allowing various combinations of fuel pins to shift axially has a small, positive effect on the reactivity, although the effect is in typically within the uncertainty of the Monte Carlo method.

NCT cases are run with 1,000 particles per generation, 530 generations, with 30 generations skipped. HAC cases are run with 2,000 particles per generation, 530 generations, with 30 generations skipped. MCNP5 performs statistical checks on k-collision, k-absorption, and k-track length. These cycle values should be normally distributed at the 99% confidence level or below. All of the reported results meet this convergence criteria. Convergence plots for the limiting NCT and HAC cases are provided in Figure 6.4-5 and Figure 6.4-6, respectively.

This page left intentionally blank.

Table 6.4-1 – Summary of Fuel Pin Pitch Nomenclature and Dimensions

Fuel Pin Pitch	Case label abbreviation	Pin Pitch (cm)	Pin Pitch (inches)
Nominal minus the tolerance	pnomminustol	1.2446	0.4900
Nominal	pnom	1.2598	0.4960
Nominal plus the tolerance	pnomplustol	1.2751	0.5020
Mid-point value	pmid	1.2952	0.5099
Maximum	pmax	1.3150	0.5177
Maximum with removal of poison cover plates	pmax2	1.3376	0.5266

Table 6.4-2 – Criticality Results for NCT Single Package

Case Identifier	Internal Water Density (g/cm ³)	EALF (MeV)	H/ (²³⁹ Pu+ ²³⁵ U)	V ^m /V ^t	²³⁹ Pu/ (U+Pu)	k _{eff}	σ	k _s (k _{eff} +2σ)
max_nct_single	0	3.62E-01	0	1.740	0.056	0.2858	0.0008	0.2874
nct_single_b35pnomplustol_Rsteel	0	2.66E-01	0	1.740	0.056	0.2627	0.0008	0.2642
nct_single_b35pnomplustol_Rlead	0	3.52E-01	0	1.740	0.056	0.2766	0.0008	0.2781
nct_single_b35pnomplustol	0	1.03E-01	0	1.740	0.056	0.2076	0.0005	0.2086



Table 6.4-3 – Criticality Results for HAC Single Package (no shifted pins)

Case Identifier	Internal Water Density (g/cm ³)	EALF (MeV)	H/ (²³⁹ Pu+ ²³⁵ U)	V ^m /V ^f	²³⁹ Pu/ (U+Pu)	k _{eff}	σ	k _s (k _{eff} +2σ)
max_hac_single_0Nb	1	7.32E-7	96.044	2.050	0.056	0.8958	0.0009	0.8976
hac_single_b35pmax2_Rsteel_hsteel	1	6.59E-07	101.074	2.050	0.056	0.8910	0.0010	0.8930
hac_single_b35pmax2_Rlead_hsteel	1	6.66E-07	101.074	2.050	0.056	0.8902	0.0010	0.8921
hac_single_b35pmax2_Rsteel	1	6.53E-07	101.074	2.050	0.056	0.8880	0.0010	0.8900
hac_single_b35pmax2_Rlead	1	6.68E-07	101.074	2.050	0.056	0.8860	0.0009	0.8879
hac_single_b35pmax2	1	6.60E-07	101.074	2.050	0.056	0.8854	0.0009	0.8872
hac_single_b35pmax	1	7.23E-07	95.466	1.936	0.056	0.8752	0.0010	0.8771
hac_single_b35pamid	1	7.82E-07	90.631	1.838	0.056	0.8626	0.0010	0.8646
hac_single_b35pnomplustol	1	8.45E-07	85.793	1.740	0.056	0.8511	0.0010	0.8532
hac_single_b35pnom	1	9.11E-07	82.179	1.667	0.056	0.8448	0.0010	0.8468
hac_single_b35pnominustol	1	9.76E-07	78.609	1.594	0.056	0.8335	0.0010	0.8354
hac_single_b35pmax2_i95	0.95	7.49E-07	96.021	2.050	0.056	0.8621	0.0009	0.8640
hac_single_b35pmax2_i90	0.9	8.61E-07	90.967	2.050	0.056	0.8347	0.0010	0.8367
hac_single_b35pmax2_i75	0.75	1.41E-06	75.806	2.050	0.056	0.7527	0.0009	0.7546
hac_single_b35pmax2_i50	0.5	5.51E-06	50.537	2.050	0.056	0.5873	0.0008	0.5890
hac_single_b35pmax2_i25	0.25	9.77E-05	25.269	2.050	0.056	0.3993	0.0007	0.4007
hac_single_b35pmax2_i10	0.1	3.04E-03	10.107	2.050	0.056	0.2838	0.0005	0.2847
hac_single_b35pmax2_i0	0	9.90E-02	0.000	2.050	0.056	0.2064	0.0004	0.2071

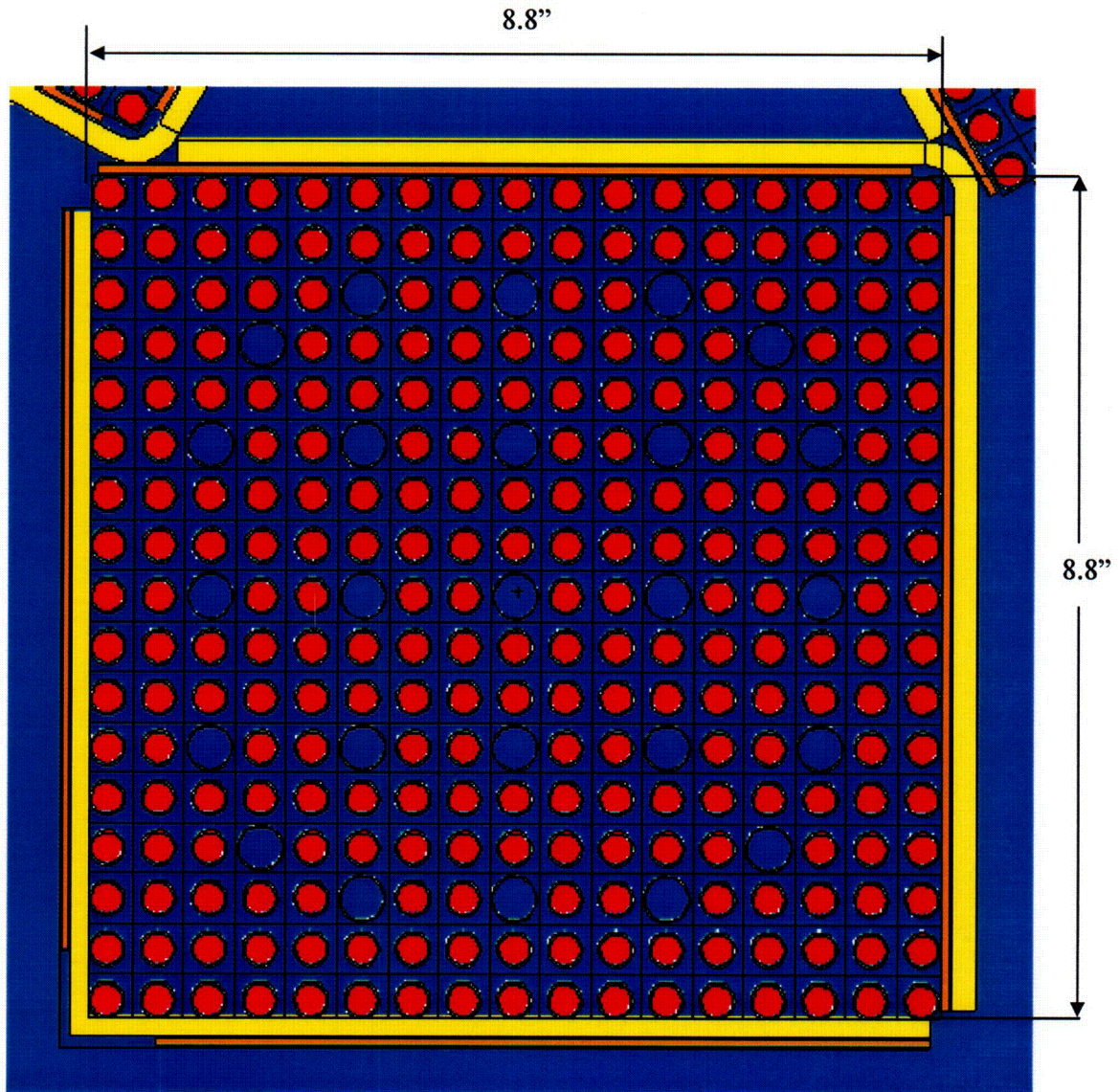


Table 6.4-4 – Criticality Results for HAC Single Package (with shifted pins)

Case Identifier	Internal Water Density (g/cm ³)	Shifted Pins	EALF (MeV)	H/ (²³⁹ Pu+ ²³⁵ U)	V ^m /V ^f	²³⁹ Pu/ (U+Pu)	k _{eff}	σ	k _s (k _{eff} +2σ)
max_hac_single_srddn10	1	10 down random	7.28E-07	96.044	2.050	0.056	0.8970	0.0009	0.8988
max_hac_single_srddn20	1	20 down random	7.15E-07	96.044	2.050	0.056	0.8983	0.0009	0.9001
max_hac_single_sd1	1	8 down	7.22E-07	96.044	2.050	0.056	0.8957	0.0010	0.8976
max_hac_single_sd2	1	24 down	7.19E-07	96.044	2.050	0.056	0.8958	0.0010	0.8977
max_hac_single_sd3	1	60 down	7.17E-07	96.044	2.050	0.056	0.8960	0.0009	0.8978
max_hac_single_sd4	1	116 down	7.22E-07	96.044	2.050	0.056	0.8956	0.0010	0.8976
max_hac_single_salldn	1	All down	7.30E-07	96.044	2.050	0.056	0.8963	0.0010	0.8983
max_hac_single_srndup10	1	10 up random	7.14E-07	96.044	2.050	0.056	0.8968	0.0010	0.8987
max_hac_single_srndup20	1	20 up random	7.26E-07	96.044	2.050	0.056	0.8964	0.0010	0.8983
max_hac_single_su1	1	8 up	7.24E-07	96.044	2.050	0.056	0.8981	0.0010	0.9001
max_hac_single_su2	1	24 up	7.25E-07	96.044	2.050	0.056	0.8958	0.0010	0.8979
max_hac_single_su3	1	60 up	7.08E-07	96.044	2.050	0.056	0.8962	0.0009	0.8981
max_hac_single_su4	1	116 up	7.13E-07	96.044	2.050	0.056	0.8964	0.0010	0.8985
max_hac_single_sallup	1	All up	7.26E-07	96.044	2.050	0.056	0.8953	0.0009	0.8972



This page left intentionally blank. |



Note that the pitch has expanded to the maximum possible extent (8.8-inch square) and that the poison holders have been "sliced off" to allow for this expansion.

Figure 6.4-1 – HAC Model Geometry, Worst-Case Pitch

10 randomly shifted pins

1	1	1	1	1	1	1	1	1	1	1	1	1	1	1	1
1	1	1	1	1	1	1	1	1	1	1	1	1	1	1	1
1	1	1	1	1	4	1	1	4	1	1	4	1	1	1	1
1	1	1	4	1	3	1	1	1	1	1	1	1	4	1	1
1	1	1	1	1	1	1	1	1	1	1	3	1	1	1	1
1	1	4	1	1	4	1	1	4	1	1	4	1	1	4	1
1	1	1	3	1	1	3	1	1	1	1	1	1	1	1	1
1	1	1	1	1	1	1	1	1	1	1	1	1	3	1	1
1	1	4	1	1	4	1	1	4	1	3	4	1	1	4	1
1	1	1	1	1	1	3	1	1	1	1	1	1	1	1	1
1	1	1	1	1	1	1	1	1	1	1	1	1	3	1	1
1	1	4	1	1	4	1	1	4	1	1	4	1	1	4	1
1	1	1	1	1	1	1	1	1	1	3	1	1	1	1	1
1	1	1	4	1	1	3	1	1	1	1	1	1	4	1	1
1	1	1	1	1	4	1	1	4	1	1	4	1	1	1	1
1	1	1	1	1	1	1	1	1	1	1	1	1	1	1	1
1	1	1	1	1	1	1	1	1	1	1	1	1	1	1	1

20 randomly shifted pins

1	1	1	1	1	1	1	1	1	1	1	1	1	1	1	1
1	1	1	1	1	1	1	1	1	1	1	1	1	1	1	1
1	1	1	1	1	4	1	1	4	1	1	4	1	1	1	1
1	1	1	4	1	3	1	1	1	1	1	1	1	4	1	1
1	1	1	1	1	1	1	3	1	1	1	3	1	1	1	1
1	1	4	1	1	4	1	1	4	1	1	4	1	1	4	1
1	1	1	3	1	1	3	1	1	1	3	1	1	1	1	1
1	1	1	1	1	1	1	3	1	1	1	1	1	3	1	1
1	1	4	1	1	4	1	1	4	1	3	4	1	1	4	1
1	1	1	3	1	1	3	1	1	3	1	1	1	1	1	1
1	1	1	1	1	1	1	1	1	1	3	1	1	3	1	1
1	1	4	3	1	4	1	3	4	1	1	4	1	1	4	1
1	1	1	1	1	1	1	1	1	1	3	1	1	1	1	1
1	1	1	4	1	1	3	1	1	3	1	1	3	4	1	1
1	1	1	1	1	4	1	1	4	1	1	4	1	1	1	1
1	1	1	1	1	1	1	1	1	1	1	1	1	1	1	1
1	1	1	1	1	1	1	1	1	1	1	1	1	1	1	1

1 is a fuel pin in the standard axial position
3 is a shifted fuel pin (either up or down)
4 is a guide thimble

Figure 6.4-2 – Fuel Pin Loading Patterns for Axially Shifted Fuel

8 shifted pins

1	1	1	1	1	1	1	1	1	1	1	1	1	1	1	1
1	1	1	1	1	1	1	1	1	1	1	1	1	1	1	1
1	1	1	1	1	4	1	1	4	1	1	4	1	1	1	1
1	1	1	4	1	1	1	1	1	1	1	1	1	4	1	1
1	1	1	1	1	1	1	1	1	1	1	1	1	1	1	1
1	1	4	1	1	4	1	1	4	1	1	4	1	1	4	1
1	1	1	1	1	1	1	1	1	1	1	1	1	1	1	1
1	1	1	1	1	1	1	3	3	3	1	1	1	1	1	1
1	1	4	1	1	4	1	3	4	3	1	4	1	1	4	1
1	1	1	1	1	1	1	3	3	3	1	1	1	1	1	1
1	1	1	1	1	1	1	1	1	1	1	1	1	1	1	1
1	1	4	1	1	4	1	1	4	1	1	4	1	1	4	1
1	1	1	1	1	1	1	1	1	1	1	1	1	1	1	1
1	1	1	4	1	1	1	1	1	1	1	1	1	4	1	1
1	1	1	1	1	4	1	1	4	1	1	4	1	1	1	1
1	1	1	1	1	1	1	1	1	1	1	1	1	1	1	1
1	1	1	1	1	1	1	1	1	1	1	1	1	1	1	1

24 shifted pins

1	1	1	1	1	1	1	1	1	1	1	1	1	1	1	1
1	1	1	1	1	1	1	1	1	1	1	1	1	1	1	1
1	1	1	1	1	4	1	1	4	1	1	4	1	1	1	1
1	1	1	4	1	1	1	1	1	1	1	1	1	4	1	1
1	1	1	1	1	1	1	1	1	1	1	1	1	1	1	1
1	1	4	1	1	4	3	3	4	3	3	4	1	1	4	1
1	1	1	1	1	3	1	1	1	1	1	3	1	1	1	1
1	1	1	1	1	3	1	3	3	3	1	3	1	1	1	1
1	1	4	1	1	4	1	3	4	3	1	4	1	1	4	1
1	1	1	1	1	3	1	3	3	3	1	3	1	1	1	1
1	1	1	1	1	3	1	1	1	1	1	3	1	1	1	1
1	1	4	1	1	4	3	3	4	3	3	4	1	1	4	1
1	1	1	1	1	1	1	1	1	1	1	1	1	1	1	1
1	1	1	4	1	1	1	1	1	1	1	1	1	4	1	1
1	1	1	1	1	4	1	1	4	1	1	4	1	1	1	1
1	1	1	1	1	1	1	1	1	1	1	1	1	1	1	1
1	1	1	1	1	1	1	1	1	1	1	1	1	1	1	1

1 is a fuel pin in the standard axial position
3 is a shifted fuel pin (either up or down)
4 is a guide thimble

Figure 6.4-2 – Fuel Pin Loading Patterns for Axially Shifted Fuel (2/3)

60 shifted pins

1	1	1	1	1	1	1	1	1	1	1	1	1	1	1	1
1	1	1	1	1	1	1	1	1	1	1	1	1	1	1	1
1	1	1	1	1	4	1	1	4	1	1	4	1	1	1	1
1	1	1	4	3	3	3	3	3	3	3	3	3	4	1	1
1	1	1	3	1	1	1	1	1	1	1	1	1	3	1	1
1	1	4	3	1	4	3	3	4	3	3	4	1	3	4	1
1	1	1	3	1	3	1	1	1	1	1	3	1	3	1	1
1	1	1	3	1	3	1	3	3	3	1	3	1	3	1	1
1	1	4	3	1	4	1	3	4	3	1	4	1	3	4	1
1	1	1	3	1	3	1	3	3	3	1	3	1	3	1	1
1	1	1	3	1	3	1	1	1	1	1	3	1	3	1	1
1	1	4	3	1	4	3	3	4	3	3	4	1	3	4	1
1	1	1	3	1	1	1	1	1	1	1	1	1	3	1	1
1	1	1	4	3	3	3	3	3	3	3	3	3	4	1	1
1	1	1	1	1	4	1	1	4	1	1	4	1	1	1	1
1	1	1	1	1	1	1	1	1	1	1	1	1	1	1	1
1	1	1	1	1	1	1	1	1	1	1	1	1	1	1	1

116 shifted pins

1	1	1	1	1	1	1	1	1	1	1	1	1	1	1	1
1	3	3	3	3	3	3	3	3	3	3	3	3	3	3	1
1	3	1	1	1	4	1	1	4	1	1	4	1	1	1	3
1	3	1	4	3	3	3	3	3	3	3	3	3	4	1	3
1	3	1	3	1	1	1	1	1	1	1	1	1	3	1	3
1	3	4	3	1	4	3	3	4	3	3	4	1	3	4	3
1	3	1	3	1	3	1	1	1	1	1	3	1	3	1	3
1	3	1	3	1	3	1	3	3	3	1	3	1	3	1	3
1	3	4	3	1	4	1	3	4	3	1	4	1	3	4	3
1	3	1	3	1	3	1	3	3	3	1	3	1	3	1	3
1	3	1	3	1	3	1	1	1	1	1	3	1	3	1	3
1	3	4	3	1	4	3	3	4	3	3	4	1	3	4	3
1	3	1	3	1	1	1	1	1	1	1	1	1	3	1	3
1	3	1	4	3	3	3	3	3	3	3	3	3	4	1	3
1	3	1	1	1	4	1	1	4	1	1	4	1	1	1	3
1	3	3	3	3	3	3	3	3	3	3	3	3	3	3	3
1	1	1	1	1	1	1	1	1	1	1	1	1	1	1	1

1 is a fuel pin in the standard axial position
3 is a shifted fuel pin (either up or down)
4 is a guide thimble

Figure 6.4-2 – Fuel Pin Loading Patterns for Axially Shifted Fuel (3/3)

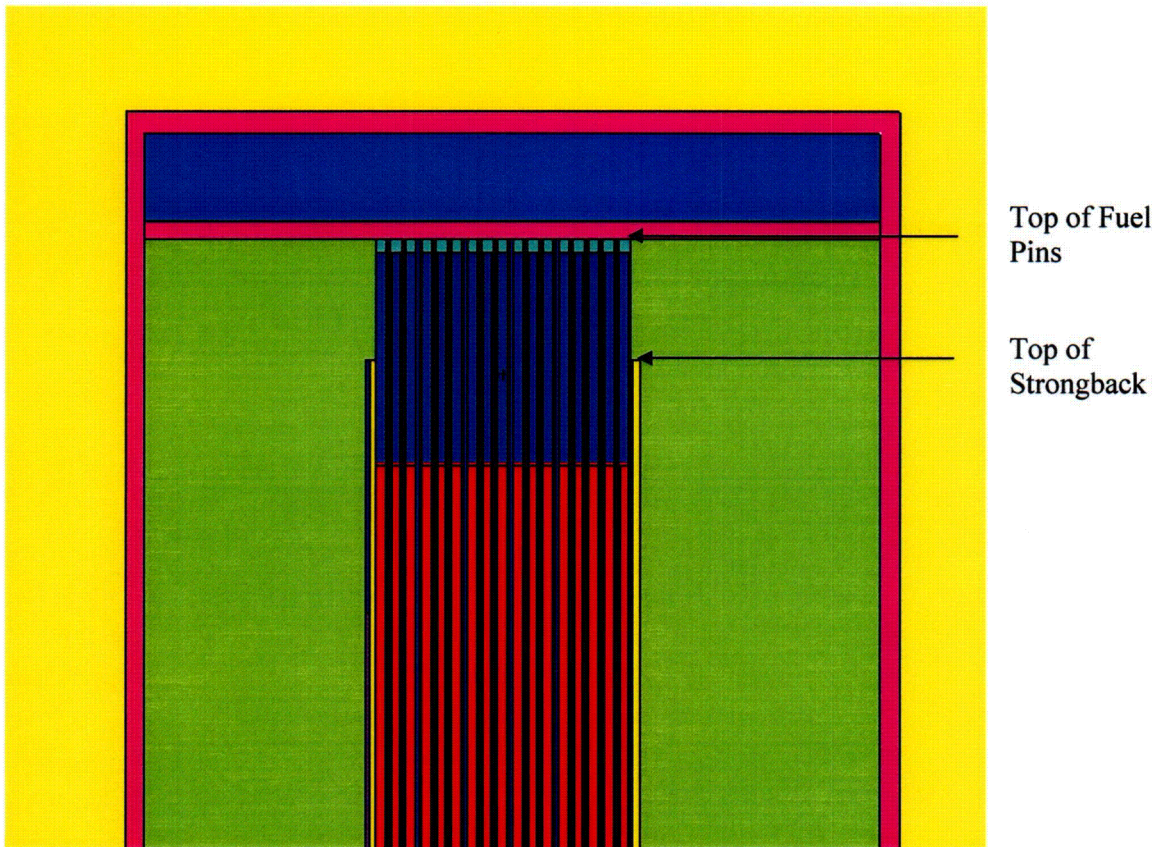


Figure 6.4-3 – HAC Model Geometry, Pins Shifted Up

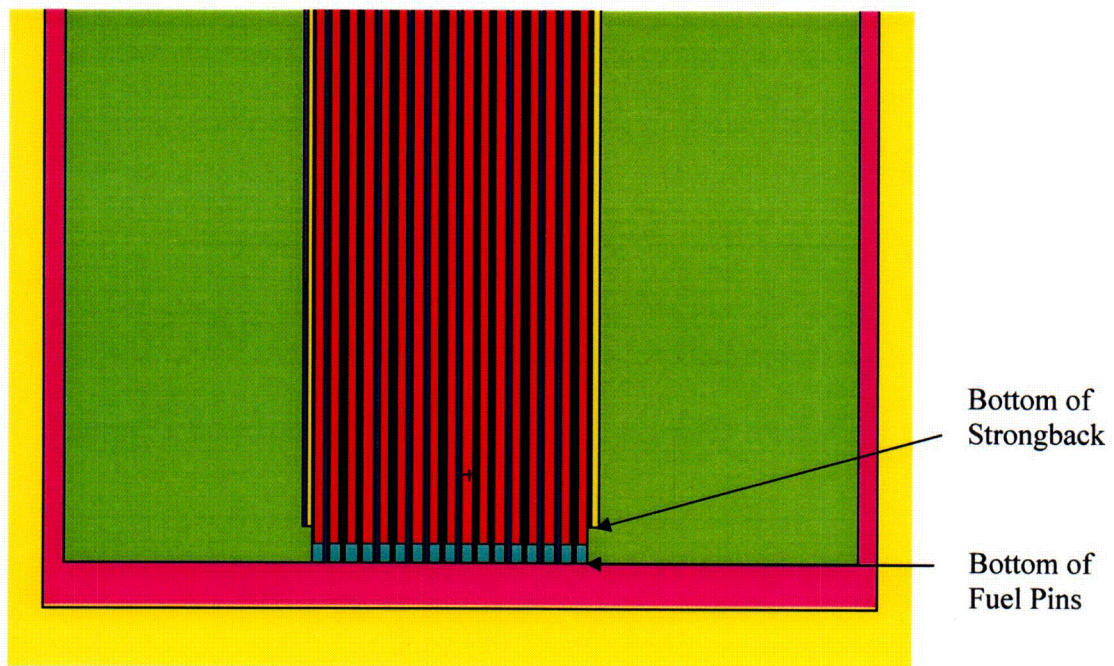


Figure 6.4-4 – HAC Model Geometry, Pins Shifted Down

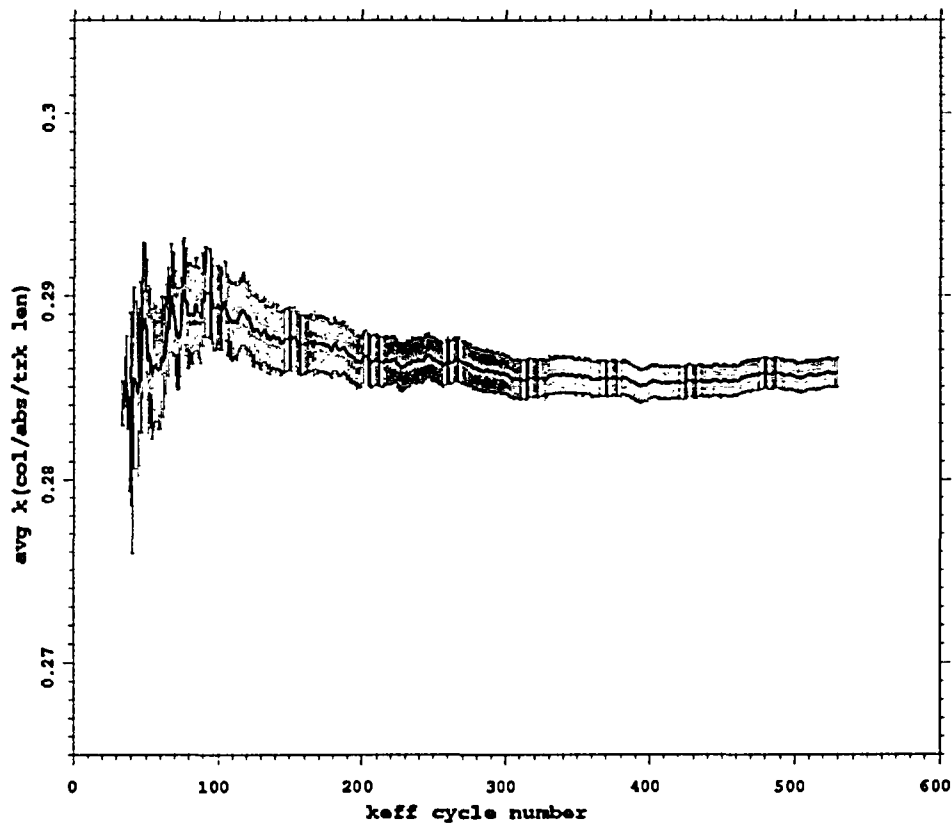


Figure 6.4-5 – Convergence of Maximum NCT Single Case (max_nct_single)

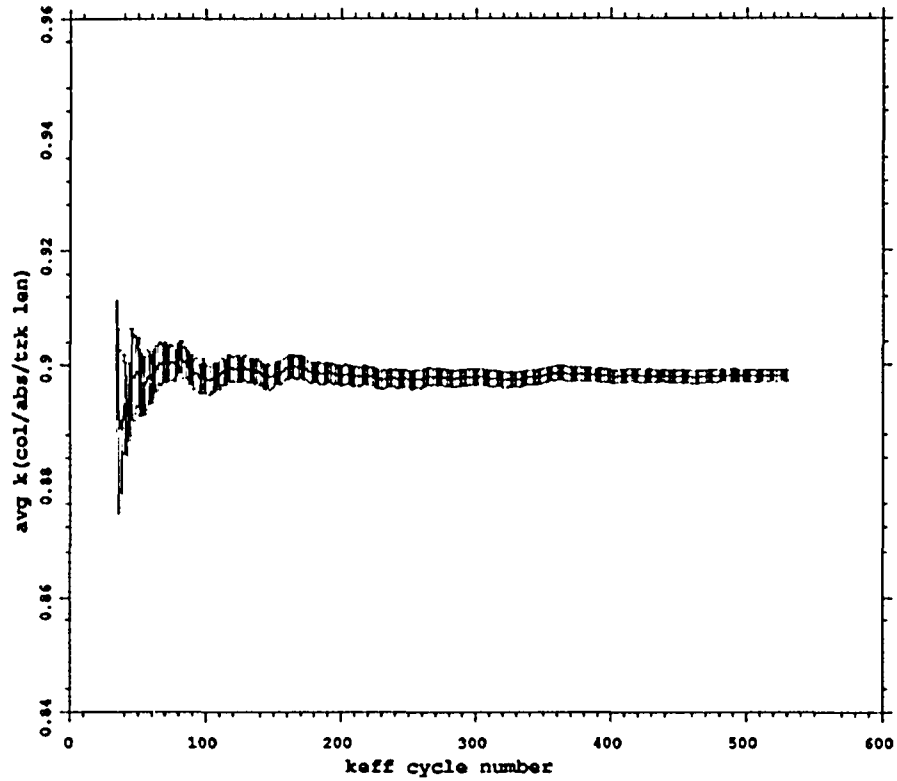


Figure 6.4-6 – Convergence of Maximum HAC Single Case (max_hac_single_su1)

6.6 Package Arrays Under Hypothetical Accident Conditions

6.6.1 HAC Array Configuration

The HAC array models are developed in the same manner as the NCT array models. The worst-case pitch from the single package HAC case (0.5266 inches) is assumed for all models. Internal and external water densities are varied independently to obtain the most reactive configuration. Because water is free to flow throughout the internals of the package, it is assumed that all internal water densities are uniformly reduced. Initially, the clamp arms and strongback angles are ignored. The maximum reactivity for the cases without clamp arms or strongback angles is obtained for the case with full internal moderation and no moderation between packages.

Although full-density internal water results in the worst-case reactivity, water also serves to isolate the fuel assemblies from one another. Therefore, ignoring the minor steel components, such as the clamp arms and strongback triangles, is a small non-conservative assumption because neutrons pass easily through steel and thus steel within the package will increase reactivity. As with the HAC single package models, the effect of ignoring small amounts of steel (i.e., the clamp arms and strongback angles) is quantified by assuming 5.8% (by volume) steel is homogenized within the body (case hac_array_b35pmax2_i100o0_hsteel). The reactivity increase when including the homogenized steel is insignificant and is within the uncertainty of this calculation.

All cases except the final maximum cases (beginning max_hac_array) are run with a pellet density of 10.31 g/cm³ and M5 cladding. To bound possible future fluctuations in the pellet density and cladding composition, the case with no external moderator, 100% internal moderator, and homogenized minor steel components is run with a pellet density of 10.85 g/cm³ and pure-zirconium cladding. It is shown in Section 6.6.3, *Impact of Niobium Content in the Cladding*, that pure zirconium cladding is slightly more reactive than cladding containing niobium.

A final set of cases is run that allow the fuel pins to shift axially, as described in Section 6.4.1.2. These cases have a pellet density of 10.85 g/cm³ and pure-zirconium cladding.

Because the MFFP may transport either one or two assemblies instead of the maximum of three, dummy assemblies are used to balance the package weight. These dummy assemblies are fabricated out of steel. To examine the impact on reactivity of the dummy assemblies, reference HAC array models are run with both one and two fuel assemblies and dummy "assemblies" of void, water, and steel. The reactivity drops in all cases, indicating that any dummy fuel assembly design is acceptable.

6.6.2 HAC Array Results

The maximum $k_s = 0.9037$ is below the USL and is obtained for full internal moderation, no moderation between packages, a homogenized steel/water mixture surrounding the assemblies, a pellet density of 10.85 g/cm³, pure-zirconium cladding, and 24 fuel pins shifted down. This value is only ~4 mk higher than the single package HAC result, indicating that communication between the packages is minimal. Note that allowing various combinations of fuel pins to shift axially has a small, positive effect on the reactivity, although the effect is in typically within the uncertainty of the Monte Carlo method. The detailed results for a full (3 assembly) package

without and with shifted fuel pins are provided in Table 6.6-1 and Table 6.6-2, respectively. The detailed results for a partially filled package are provided in Table 6.6-3.

Cases are run with 2,000 particles per generation, 530 generations, with 30 generations skipped. Convergence is well-behaved and the convergence plot as a function of generation for the limiting case is provided in Figure 6.6-1.

6.6.3 Impact of Niobium Content in the Cladding

The importance of the niobium content in the fuel assembly cladding is evaluated for 0 and 3% niobium by weight. Niobium perturbation calculations (using the MCNP perturbation feature) for single and array HAC cases are evaluated to identify the most reactive niobium content in the cladding under flooded conditions. Both cases indicate that 0 wt% niobium is more reactive than the 3 wt% niobium in the cladding. The difference in the reactivity is on the order of 0.001, which is also the approximate magnitude of the convergence of the remaining calculations. Thus, ignoring the niobium in the cladding for the maximum criticality calculations will be a small conservatism.

For the HAC array case (`max_hac_array_pertNb`) the removal of the niobium (3% by weight) results in a 0.00110 ± 0.00025 increase in the reactivity. The second order contribution of the perturbation is calculated as 0.00010 ± 0.00004 . The HAC single package case (`max_hac_single_pertNb`) gives an increase in the reactivity of 0.00065 ± 0.00024 (with a second order term of 0.00004 ± 0.00003) for the removal of 3% by weight niobium from the cladding. The perturbation reactivity values are not directly used for comparison to the USL and are used simply to identify the most reactive case to be evaluated. Due to the small change in k , statistical fluctuations can randomly exceed the effect seen from the niobium content variation.

Table 6.6-1 – Criticality Results for an Infinite Array of HAC Packages (no shifted pins)

Case Identifier	Water Density (g/cm ³)		EALF (MeV)	H/ (²³⁹ Pu+ ²³⁵ U)	V ^m /V ^f	²³⁹ Pu/ (U+Pu)	k _{eff}	σ	k _s (k _{eff} +2σ)
	Internal	External							
max_hac_array_rho_0Nb	1	0	7.26E-7	96.044	2.050	0.056	0.8996	0.0010	0.9016
hac_array_b35pmax2_i100o0_hsteel	1	0	6.61E-07	101.074	2.050	0.056	0.8951	0.0010	0.8971
hac_array_b35pmax2_i100o100	1	1.0	6.67E-07	101.074	2.050	0.056	0.8883	0.0010	0.8903
hac_array_b35pmax2_i100o50	1	0.5	6.60E-07	101.074	2.050	0.056	0.8893	0.0010	0.8913
hac_array_b35pmax2_i100o10	1	0.10	6.48E-07	101.074	2.050	0.056	0.8930	0.0009	0.8948
hac_array_b35pmax2_i100o05	1	0.05	6.57E-07	101.074	2.050	0.056	0.8909	0.0010	0.8929
hac_array_b35pmax2_i100o01	1	0.01	6.51E-07	101.074	2.050	0.056	0.8932	0.0010	0.8952
hac_array_b35pmax2_i100o001	1	0.001	6.55E-07	101.074	2.050	0.056	0.8919	0.0010	0.8938
hac_array_b35pmax2_i100o0	1	0	6.60E-07	101.074	2.050	0.056	0.8912	0.0010	0.8931
hac_array_b35pmax2_i95o0	0.95	0	7.43E-07	96.021	2.050	0.056	0.8683	0.0010	0.8702
hac_array_b35pmax2_i90o0	0.9	0	8.55E-07	90.967	2.050	0.056	0.8470	0.0010	0.8489
hac_array_b35pmax2_i75o0	0.75	0	1.39E-06	75.806	2.050	0.056	0.7662	0.0010	0.7682
hac_array_b35pmax2_i50o0	0.5	0	4.90E-06	50.537	2.050	0.056	0.6221	0.0009	0.6238
hac_array_b35pmax2_i25o0	0.25	0	5.19E-05	25.269	2.050	0.056	0.4926	0.0007	0.4940
hac_array_b35pmax2_i10o0	0.1	0	6.08E-04	10.107	2.050	0.056	0.4849	0.0006	0.4862
hac_array_b35pmax2_i0o100	0	1.0	2.47E-02	0	2.050	0.056	0.3270	0.0004	0.3278
hac_array_b35pmax2_i0o90	0	0.9	2.27E-02	0	2.050	0.056	0.3342	0.0005	0.3351
hac_array_b35pmax2_i0o50	0	0.5	1.82E-02	0	2.050	0.056	0.3847	0.0005	0.3856
hac_array_b35pmax2_i0o10	0	0.10	2.51E-02	0	2.050	0.056	0.5343	0.0005	0.5352
hac_array_b35pmax2_i0o01	0	0.01	7.55E-02	0	2.050	0.056	0.5880	0.0005	0.5889
hac_array_b35pmax2_i0o001	0	0.001	9.35E-02	0	2.050	0.056	0.5905	0.0004	0.5913
hac_array_b35pmax2_i0o0	0	0	9.76E-02	0	2.050	0.056	0.5917	0.0004	0.5926

Table 6.6-2 – Criticality Results for an Infinite Array of HAC Packages (with shifted pins)

Case Identifier	Water Density (g/cm ³)		Shifted Pins	EALF (MeV)	H/ (²³⁹ Pu+ ²³⁵ U)	V ^m /V ^f	²³⁹ Pu/ (U+Pu)	k _{eff}	σ	k _s (k _{eff} +2σ)
	Internal	External								
max_hac_array_smddn10	1	0	10 down random	7.18E-07	96.044	2.050	0.056	0.9004	0.0010	0.9025
max_hac_array_smddn20	1	0	20 down random	7.23E-07	96.044	2.050	0.056	0.9002	0.0011	0.9023
max_hac_array_sd1	1	0	8 down	7.20E-07	96.044	2.050	0.056	0.9001	0.0010	0.9020
max_hac_array_sd2	1	0	24 down	7.36E-07	96.044	2.050	0.056	0.9017	0.0010	0.9037
max_hac_array_sd3	1	0	60 down	7.27E-07	96.044	2.050	0.056	0.8992	0.0010	0.9012
max_hac_array_sd4	1	0	116 down	7.02E-07	96.044	2.050	0.056	0.9008	0.0009	0.9026
max_hac_array_salldn	1	0	All down	7.21E-07	96.044	2.050	0.056	0.9001	0.0010	0.9020
max_hac_array_smdup10	1	0	10 up random	7.33E-07	96.044	2.050	0.056	0.8991	0.0009	0.9010
max_hac_array_smdup20	1	0	20 up random	7.14E-07	96.044	2.050	0.056	0.8998	0.0009	0.9016
max_hac_array_su1	1	0	8 up	7.30E-07	96.044	2.050	0.056	0.9004	0.0009	0.9023
max_hac_array_su2	1	0	24 up	7.10E-07	96.044	2.050	0.056	0.8999	0.0010	0.9020
max_hac_array_su3	1	0	60 up	7.13E-07	96.044	2.050	0.056	0.9003	0.0010	0.9022
max_hac_array_su4	1	0	116 up	7.01E-07	96.044	2.050	0.056	0.8979	0.0010	0.8998
max_hac_array_sallup	1	0	All up	7.30E-07	96.044	2.050	0.056	0.8997	0.0010	0.9016



PACTEC

MFFP Safety Analysis Report

Docket No. 71-9295

Revision 2, April 2005

Table 6.6-3 – Criticality Results for an Infinite Array of HAC Partially Filled Packages (no shifted pins)

Case Identifier	Number of Assemblies	Dummy Assembly Material	EALF (MeV)	H/ (²³⁹ Pu+ ²³⁵ U)	V ^m /V ^f	²³⁹ Pu/ (U+Pu)	k _{eff}	σ	k _s (k _{eff} +2σ)
hac_array_b35pmax2_i100o0_hsteel	3	null	6.61E-07	101.074	2.050	0.056	0.8951	0.0010	0.8971
hac_array_b35pmax2_i100o0_hsteel_1asss	1	Steel	6.61E-07	101.074	2.050	0.056	0.8577	0.0010	0.8596
hac_array_b35pmax2_i100o0_hsteel_1assv	1	Void	6.70E-07	101.074	2.050	0.056	0.8548	0.0010	0.8568
hac_array_b35pmax2_i100o0_hsteel_1assw	1	Water	6.68E-07	101.074	2.050	0.056	0.8568	0.0010	0.8588
hac_array_b35pmax2_i100o0_hsteel_2asss	2	Steel	6.56E-07	101.074	2.050	0.056	0.8772	0.0009	0.8791
hac_array_b35pmax2_i100o0_hsteel_2assv	2	Void	6.73E-07	101.074	2.050	0.056	0.8753	0.0009	0.8771
hac_array_b35pmax2_i100o0_hsteel_2assw	2	Water	6.65E-07	101.074	2.050	0.056	0.8741	0.0010	0.8761



PACTEC

This page left intentionally blank.

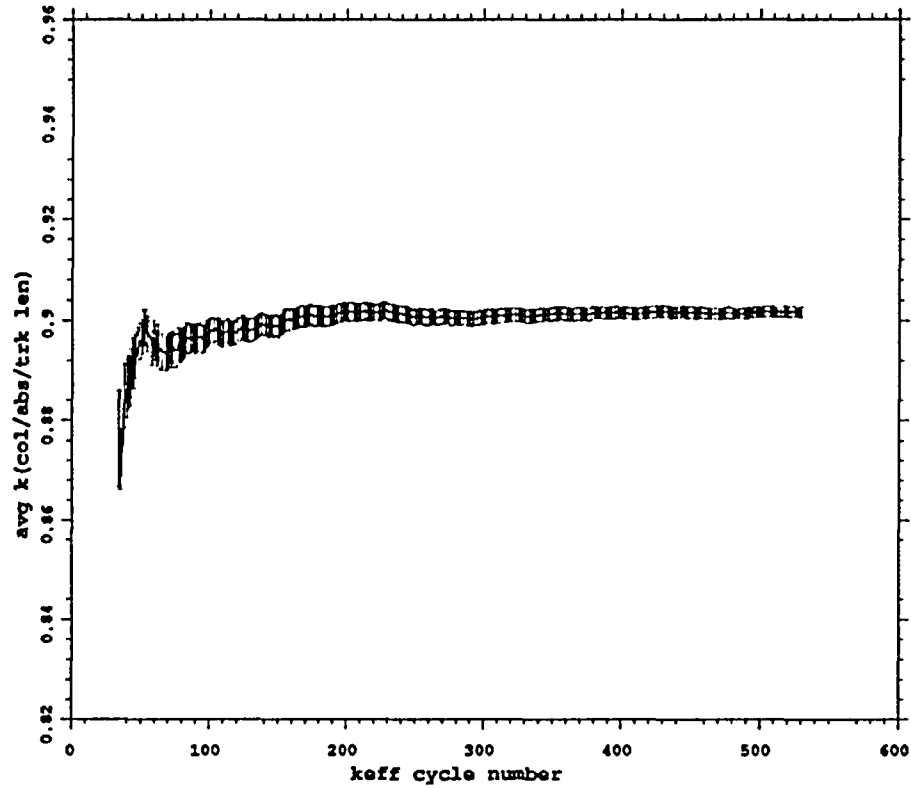


Figure 6.6-1 – Convergence of Maximum HAC Array Case (max_hac_array_sd2)

This page left intentionally blank.

6.8 Benchmark Evaluations

The MCNP, Version 5, Monte Carlo computer code¹ with point-wise ENDF/B-V and -VI cross sections has been used extensively in criticality evaluations. This section justifies the validity of this computation tool and data library combination for application to the MFFP package criticality analysis and a bias factor is obtained from these calculations of the critical experiments.

The MCNP code uses room temperature continuous-energy (point-wise) cross sections that are thoroughly documented in Appendix G of the manual. These cross sections are defined with a high-energy resolution that describes each resolved cross section resonance for the isotope. All of the cross-sections used for these analyses were generated from the U.S. Evaluated Nuclear Data Files (ENDF/B).

The validation of the point-wise cross sections is conducted using 84 experimental criticality benchmarks applicable to the MFFP. The statistical analysis of the benchmark experiments results in a USL of 0.9288.

6.8.1 Applicability of Benchmark Experiments

The experimental benchmarks are taken from the OECD Nuclear Energy Agency's *International Handbook of Evaluated Criticality Safety Benchmark Experiments*². This Handbook discusses each experiment in detail. It includes estimates of the uncertainty in the measurements, detailed information regarding dimensions and material compositions, comparisons between the multiplication factor calculated by various computer codes, and a list of input files that were used in their calculations. The only changes made to the input files involve changing to a consistent set of cross section libraries, as needed.

The critical experiment benchmarks are selected for use in this USL determination based upon their similarity to the MOX fresh fuel assembly. The important constituents of the MOX assembly are: mixed oxide fuel (plutonium with depleted uranium), borated absorber plates and a steel container and components. The nominal pin cell moderator volume to fuel volume ratio is 1.60 for MFFP fuel. Cases are selected based on plutonium being the dominant fissile material in a solid form (i.e., solutions were excluded). This first selection criteria identified critical experiments with composite mixed oxide fuel rods with uranium enrichments of less than 2%, greater than 1% Pu/(U+Pu) and moderator to fuel ratios of less than 20. This set of 145 experiments is filtered to remove those cases that contained cadmium and hafnium absorber materials which are not present in this analysis (leaving only boron as the accepted absorber material). The remaining 77 experiments have mixed plutonium/uranium fuel in a lattice with a thermal spectrum, similar to MOX fuel.

To provide benchmarks with harder neutron spectra, a second selection is performed over the metal fuel experiments with the same criteria. From this second search, 7 more critical benchmark experiments are identified. These later experiments use metal fuel in a graphite moderator/reflector.

¹ MCNP5, "MCNP – A General Monte Carlo N-Particle Transport Code, Version 5; Volume II: User's Guide," LA-CP-03-0245, Los Alamos National Laboratory, April, 2003.

² OECD Nuclear Energy Agency, *International Handbook of Evaluated Criticality Safety Benchmark Experiments*, NEA/NSC/DOC(95)03, September, 2003.

The overall selection of cases is weighted to the thermal spectra where calculated MOX assembly reactivity is highest. The critical experiments selected are listed in Table 6.8-1.

6.8.2 Bias Determination

The ORNL USLSTATS code³, described in Appendix C of NUREG/CR-6361⁴, is used to establish an upper subcritical limit (USL) for the analysis. Computed multiplication factors, k_{eff} , for the MOX package are deemed to be adequately subcritical if the computed value of k_{eff} plus two standard deviations is below the USL as follows:

$$k_s = k_{eff} + 2\sigma < USL$$

The USL includes the combined effects of code bias, uncertainty in the benchmark experiments, uncertainty in the computational evaluation of the benchmark experiments, and an administrative margin of subcriticality. The USL is determined using the confidence band with administrative margin technique (USLSTATS Method 1).

USLSTATS takes as input the k_{eff} as calculated by MCNP5, the total 1- σ uncertainty (combined benchmark and computational uncertainties), and a trending parameter. For the current analysis, four trending parameters have been selected (1) moderator to fuel volume ratio (v^m/v^f), (2) H/(Pu239+U235) ratio, (3) Pu239/(Pu+U), and (4) Energy of the Average Lethargy causing Fission (EALF). Parameters (1) and (2) are applied to only to the first 77 benchmarks because these parameters are not directly applicable to dry, non-lattice benchmarks. Parameters (3) and (4) are applied to all 84 benchmarks. The USL is computed by trending upon these variables and selecting the lowest USL.

The uncertainty value, σ_{tot} , assigned to each case is a combination of the benchmark-model uncertainty for each experiment, σ_{bench} , and the Monte Carlo uncertainty associated with the particular computational evaluation of the case, σ_{comp} , or:

$$\sigma_{tot} = (\sigma_{bench}^2 + \sigma_{comp}^2)^{1/2}$$

These values are input into the USLSTATS program in addition to the following parameters, which are the values suggested by the USLSTATS user's manual:

- P, proportion of population falling above lower tolerance level = 0.995
- 1- γ , confidence on fit = 0.95
- α , confidence on proportion P = 0.95
- Δk_m , administrative margin used to ensure subcriticality = 0.05.

³ USLSTATS, "USLSTATS: A Utility To Calculate Upper Subcritical Limits For Criticality Safety Applications," Version 1.3.6, Oak Ridge National Laboratory, December 15, 1998.

⁴ J. J. Lichtenwalter, S. M. Bowman, M. D. DeHart, C. M. Hopper, *Criticality Benchmark Guide for Light-Water-Reactor Fuel in Transportation and Storage Packages*, NUREG/CR-6361, ORNL/TM-13211, March 1997.

This data is followed by triplets of trending parameter value, computed k_{eff} , and uncertainty for each case. The USL Method 1 performs a confidence band analysis on the data for the trending parameter. All benchmark data used as input to USLSTATS are reported in Table 6.8-2.

Note that USLSTATS assumes that all benchmark experiments have a $k_{eff} = 1.000$. However, some of the benchmark k_{eff} are greater or less than 1.000. The most accurate value for the model reactivity is used and the k_{eff} input into USLSTATS is normalized by dividing by the benchmark k_{eff} . The benchmark-model reactivity may be different than 1.000 due to experiments that were not exactly critical or due to model simplifications. For example, for experiments with fixed rod patterns, the addition of one more rod may bring the experiment from sub-critical to super-critical without the possibility of being exactly critical. Other known model assumptions may be evaluated with the experiment and may be included in the benchmark reactivity. Corrections may be based on analytical evaluation or measurements and the uncertainties in these adjustments are included in the benchmark's overall uncertainty. Typically the combined corrections are small and benchmark-model k_{eff} are close to 1.000.

The USL generated for each of the three trending parameters utilized is provided below.

Trending parameter	USL equation	Range of Applicability
v^m/v^f	USL1 = 0.9289 + (4.0398E-04)*X	1.1112 ≤ X ≤ 17.5
H/ (Pu239+U235)	USL1 = 0.9309 + (1.4706E-06)*X	51.000 ≤ X ≤ 1145.
Pu239/(U+Pu)	USL1 = 0.9297 + (1.0963E-02)*X (X < 0.709) = 0.9374 (X ≥ 0.709)	0.014 ≤ X ≤ 0.95
EALF	USL1 = 0.9288 + (3.6369E-02)*X (X < 0.20144) = 0.9362 (X ≥ 0.201)	8.07E-8 ≤ X ≤ 0.40 MeV

All of the trending parameters show little correlation, thus the use of a constant USL is appropriate. The MCNP results show an average negative bias (under prediction) in the reactivity for the selected benchmarks of about 0.007 ± 0.006 . The minimum USL value of 0.9288 is used which includes the bias, trend corrections, administrative margin (0.05) and the 95% confidence band width of the data.

Results for v^m/v^f

The volume ratio is equivalent to trending by pin pitch and was used as a selection criteria for the 77 lattice benchmark cases. The volume fractions are used to better represent the mixture of hexagonal and square lattice geometries used in the benchmarks. The USL1 value is a minimum at the minimum moderator to fuel volume ratio. As shown in Figure 6.8-1 there is little correlation with this variable and the calculated benchmark reactivity. The calculations for the MOX package have v^m/v^f ratios from about 1.6 to 2 with full density water. Not adjusting for the water density provides a trending that will be similar to trending on fuel pin pitch. The possible influence with water density is covered with the H/Pu+U ratio below.

Results for H/(Pu239+U235)

This parameter is utilized with the 77 lattice benchmark cases. Reactivity trend with respect to the ratio of the primary moderator (H) to the primary fissile isotopes (Pu239 and U235) within the pin cell was not significant. The smeared atom densities in the pin cells are used. For the

MOX package analyses, the H/(Pu239+U235) ratio ranges from 0 to 101. As shown on Figure 6.8-2, the benchmark data for low H/(Pu239+U235) ratios is sparse and variable. However, for this analysis the higher reactivity and more important cases occur with the larger H/(Pu239+U235) values (around 100) and in this range there is adequate benchmark data. The more important MFFP cases occur with more moderation which is also apparent in the EALF trending as discussed below.

Results for Pu239/(U+Pu)

This parameter is utilized with all 84 benchmark cases. The Pu239/(U+Pu) trending parameter was selected to identify any bias resulting from the selection of benchmark cases with different plutonium and uranium concentrations. The MOX package has a Pu239/(U+Pu) ratio of 0.056, which is within the range of applicability for the benchmark data as shown in Figure 6.8-3.

Results for EALF

This parameter is utilized with all 84 benchmark cases. The EALF comparison provides a means to observe neutron spectral dependencies or trends. The USL1 for the EALF parameter has a negligible increase with increasing EALF as shown in Figure 6.8-4 for the benchmark cases. The MOX analyses have EALF values from 6.5E-7 to 0.35 MeV. As shown in Figure 6.8-5 cases with a high EALF have a lower calculated reactivity. The MOX case with the peak reactivity has an EALF of 7.36E-7 MeV which is well represented by the benchmarks. Additional refinement of the benchmarks for high EALF values is not warranted due to the low calculated reactivity in this range, and thus large margin for safety.

Table 6.8-1 – Experimental Benchmarks

Used Y/N	Identification	Solid poison	EALF (eV)	Pu/(U+Pu) ratio	Pitch type	Pitch size (cm)
Y	MIX-COMP-THERM-001-001	null	1.07	0.2237	Square	0.9525
Y	MIX-COMP-THERM-001-002	null	0.292	0.2237	Square	1.258
Y	MIX-COMP-THERM-001-003	null	0.174	0.2237	Square	1.5342
Y	MIX-COMP-THERM-001-004	null	0.12	0.2237	Square	1.905
Y	MIX-COMP-THERM-002-001	null	0.581	0.0204	Square	1.778
Y	MIX-COMP-THERM-002-002	null	0.769	0.0204	Square	1.778
Y	MIX-COMP-THERM-002-003	null	0.197	0.0204	Square	2.20914
Y	MIX-COMP-THERM-002-004	null	0.288	0.0204	Square	2.20914
Y	MIX-COMP-THERM-002-005	null	0.142	0.0204	Square	2.51447
Y	MIX-COMP-THERM-002-006	null	0.188	0.0204	Square	2.51447
Y	MIX-COMP-THERM-003-001	null	0.922	0.0659	Square	1.3208
Y	MIX-COMP-THERM-003-002	null	0.559	0.0659	Square	1.4224
Y	MIX-COMP-THERM-003-003	null	0.663	0.0659	Square	1.4224
Y	MIX-COMP-THERM-003-004	null	0.192	0.0659	Square	1.8679
Y	MIX-COMP-THERM-003-005	null	0.159	0.0659	Square	2.01158
Y	MIX-COMP-THERM-003-006	null	0.103	0.0659	Square	2.6416
Y	MIX-COMP-THERM-004-001	null	0.149	0.03	Square	1.825
Y	MIX-COMP-THERM-004-002	null	0.148	0.0299	Square	1.825
Y	MIX-COMP-THERM-004-003	null	0.147	0.028	Square	1.825
Y	MIX-COMP-THERM-004-004	null	0.123	0.03	Square	1.956
Y	MIX-COMP-THERM-004-005	null	0.122	0.0299	Square	1.956
Y	MIX-COMP-THERM-004-006	null	0.121	0.0298	Square	1.956

Used Y/N	Identification	Solid poison	EALF (eV)	Pu/(U+Pu) ratio	Pitch type	Pitch size (cm)
Y	MIX-COMP-THERM-004-007	null	0.0951	0.03	Square	2.225
Y	MIX-COMP-THERM-004-008	null	0.0948	0.0299	Square	2.225
Y	MIX-COMP-THERM-004-009	null	0.0944	0.0298	Square	2.225
Y	MIX-COMP-THERM-004-010	null	0.082	0.03	Square	2.474
Y	MIX-COMP-THERM-004-011	null	0.0916	0.0299	Square	2.474
Y	MIX-COMP-THERM-005-001	null	0.399	0.0399	Hexagonal	2.159
Y	MIX-COMP-THERM-005-002	null	0.263	0.0399	Hexagonal	2.3622
Y	MIX-COMP-THERM-005-003	null	0.18	0.0399	Hexagonal	2.667
Y	MIX-COMP-THERM-005-004	null	0.15	0.0399	Hexagonal	2.90322
Y	MIX-COMP-THERM-005-005	null	0.111	0.0399	Hexagonal	3.52044
Y	MIX-COMP-THERM-005-006	null	0.0956	0.0399	Hexagonal	4.064
Y	MIX-COMP-THERM-005-007	null	0.0912	0.0399	Hexagonal	4.318
Y	MIX-COMP-THERM-006-001	null	0.383	0.0204	Hexagonal	2.032
Y	MIX-COMP-THERM-006-002	null	0.2	0.0204	Hexagonal	2.3622
Y	MIX-COMP-THERM-006-003	null	0.145	0.0204	Hexagonal	2.667
Y	MIX-COMP-THERM-006-004	null	0.123	0.0204	Hexagonal	2.90322
Y	MIX-COMP-THERM-006-005	null	0.101	0.0204	Hexagonal	3.3528
Y	MIX-COMP-THERM-006-006	null	0.0954	0.0204	Hexagonal	3.52044
Y	MIX-COMP-THERM-006-007	null	0.144	0.0204	Hexagonal	2.667
N	MIX-COMP-THERM-006-008	Hf	0.145	0.0204	Hexagonal	2.667
N	MIX-COMP-THERM-006-009	Hf	0.145	0.0204	Hexagonal	2.667
N	MIX-COMP-THERM-006-010	Hf	0.145	0.0204	Hexagonal	2.667
N	MIX-COMP-THERM-006-011	Hf	0.145	0.0204	Hexagonal	2.667
N	MIX-COMP-THERM-006-012	Hf	0.146	0.0204	Hexagonal	2.667
Y	MIX-COMP-THERM-006-013	Boron	0.145	0.0204	Hexagonal	2.667
Y	MIX-COMP-THERM-006-014	Boron	0.145	0.0204	Hexagonal	2.667
Y	MIX-COMP-THERM-006-015	Boron	0.145	0.0204	Hexagonal	2.667
Y	MIX-COMP-THERM-006-016	Boron	0.146	0.0204	Hexagonal	2.667
N	MIX-COMP-THERM-006-017	Cd	0.147	0.0204	Hexagonal	2.667
N	MIX-COMP-THERM-006-018	Cd + Hf	0.147	0.0204	Hexagonal	2.667
N	MIX-COMP-THERM-006-019	Cd + Hf	0.146	0.0204	Hexagonal	2.667
N	MIX-COMP-THERM-006-020	Cd + Hf	0.147	0.0204	Hexagonal	2.667
N	MIX-COMP-THERM-006-021	Cd + Hf	0.146	0.0204	Hexagonal	2.667
N	MIX-COMP-THERM-006-022	Cd + Hf	0.146	0.0204	Hexagonal	2.667
N	MIX-COMP-THERM-006-023	B + Cd	0.146	0.0204	Hexagonal	2.667
N	MIX-COMP-THERM-006-024	B + Cd	0.146	0.0204	Hexagonal	2.667
N	MIX-COMP-THERM-006-025	B + Cd	0.146	0.0204	Hexagonal	2.667
N	MIX-COMP-THERM-006-026	B + Cd	0.147	0.0204	Hexagonal	2.667
N	MIX-COMP-THERM-006-027	Cd	0.146	0.0204	Hexagonal	2.667
N	MIX-COMP-THERM-006-028	Cd	0.147	0.0204	Hexagonal	2.667
Y	MIX-COMP-THERM-006-029	null	0.101	0.0204	Hexagonal	3.3528
N	MIX-COMP-THERM-006-030	Hf	0.101	0.0204	Hexagonal	3.3528
N	MIX-COMP-THERM-006-031	Hf	0.101	0.0204	Hexagonal	3.3528
N	MIX-COMP-THERM-006-032	Hf	0.101	0.0204	Hexagonal	3.3528
N	MIX-COMP-THERM-006-033	Hf	0.101	0.0204	Hexagonal	3.3528
N	MIX-COMP-THERM-006-034	Hf	0.101	0.0204	Hexagonal	3.3528
Y	MIX-COMP-THERM-006-035	Boron	0.1	0.0204	Hexagonal	3.3528
Y	MIX-COMP-THERM-006-036	Boron	0.101	0.0204	Hexagonal	3.3528
Y	MIX-COMP-THERM-006-037	Boron	0.101	0.0204	Hexagonal	3.3528
Y	MIX-COMP-THERM-006-038	Boron	0.101	0.0204	Hexagonal	3.3528
N	MIX-COMP-THERM-006-039	Cd	0.101	0.0204	Hexagonal	3.3528

Used Y/N	Identification	Solid polson	EALF (eV)	Pu/(U+Pu) ratio	Pitch type	Pitch size (cm)
N	MIX-COMP-THERM-006-040	Cd + Hf	0.101	0.0204	Hexagonal	3.3528
N	MIX-COMP-THERM-006-041	Cd + Hf	0.101	0.0204	Hexagonal	3.3528
N	MIX-COMP-THERM-006-042	Cd + Hf	0.101	0.0204	Hexagonal	3.3528
N	MIX-COMP-THERM-006-043	Cd + Hf	0.101	0.0204	Hexagonal	3.3528
N	MIX-COMP-THERM-006-044	Cd + Hf	0.101	0.0204	Hexagonal	3.3528
N	MIX-COMP-THERM-006-045	B + Cd	0.101	0.0204	Hexagonal	3.3528
N	MIX-COMP-THERM-006-046	B + Cd	0.101	0.0204	Hexagonal	3.3528
N	MIX-COMP-THERM-006-047	B + Cd	0.101	0.0204	Hexagonal	3.3528
N	MIX-COMP-THERM-006-048	B + Cd	0.101	0.0204	Hexagonal	3.3528
N	MIX-COMP-THERM-006-049	Cd	0.101	0.0204	Hexagonal	3.3528
N	MIX-COMP-THERM-006-050	Cd	0.101	0.0204	Hexagonal	3.3528
Y	MIX-COMP-THERM-007-001	null	0.203	0.0199	Hexagonal	2.3622
Y	MIX-COMP-THERM-007-002	null	0.146	0.0199	Hexagonal	2.667
Y	MIX-COMP-THERM-007-003	null	0.123	0.0199	Hexagonal	2.9032
Y	MIX-COMP-THERM-007-004	null	0.1	0.0199	Hexagonal	3.3528
Y	MIX-COMP-THERM-007-005	null	0.0954	0.0199	Hexagonal	3.5204
Y	MIX-COMP-THERM-007-006	null	0.145	0.0199	Hexagonal	2.667
Y	MIX-COMP-THERM-007-007	Boron	0.146	0.0199	Hexagonal	2.667
Y	MIX-COMP-THERM-007-008	Boron	0.146	0.0199	Hexagonal	2.667
Y	MIX-COMP-THERM-007-009	Boron	0.146	0.0199	Hexagonal	2.667
Y	MIX-COMP-THERM-007-010	Boron	0.145	0.0199	Hexagonal	2.667
N	MIX-COMP-THERM-007-011	Hf	0.146	0.0199	Hexagonal	2.667
N	MIX-COMP-THERM-007-012	Hf	0.146	0.0199	Hexagonal	2.667
N	MIX-COMP-THERM-007-013	Hf	0.146	0.0199	Hexagonal	2.667
N	MIX-COMP-THERM-007-014	Hf	0.146	0.0199	Hexagonal	2.667
N	MIX-COMP-THERM-007-015	Hf	0.145	0.0199	Hexagonal	2.667
N	MIX-COMP-THERM-007-016	Cd	0.147	0.0199	Hexagonal	2.667
N	MIX-COMP-THERM-007-017	B + Cd	0.147	0.0199	Hexagonal	2.667
N	MIX-COMP-THERM-007-018	B + Cd	0.147	0.0199	Hexagonal	2.667
N	MIX-COMP-THERM-007-019	B + Cd	0.147	0.0199	Hexagonal	2.667
N	MIX-COMP-THERM-007-020	B + Cd	0.147	0.0199	Hexagonal	2.667
N	MIX-COMP-THERM-007-021	Cd + Hf	0.147	0.0199	Hexagonal	2.667
N	MIX-COMP-THERM-007-022	Cd + Hf	0.147	0.0199	Hexagonal	2.667
N	MIX-COMP-THERM-007-023	Cd + Hf	0.147	0.0199	Hexagonal	2.667
N	MIX-COMP-THERM-007-024	Cd + Hf	0.147	0.0199	Hexagonal	2.667
N	MIX-COMP-THERM-007-025	Cd + Hf	0.147	0.0199	Hexagonal	2.667
N	MIX-COMP-THERM-007-026	Cd	0.146	0.0199	Hexagonal	2.667
N	MIX-COMP-THERM-007-027	Cd	0.147	0.0199	Hexagonal	2.667
Y	MIX-COMP-THERM-008-001	null	0.408	0.02	Hexagonal	2.032
Y	MIX-COMP-THERM-008-002	null	0.205	0.02	Hexagonal	2.3622
Y	MIX-COMP-THERM-008-003	null	0.147	0.02	Hexagonal	2.667
Y	MIX-COMP-THERM-008-004	null	0.124	0.02	Hexagonal	2.9032
Y	MIX-COMP-THERM-008-005	null	0.101	0.02	Hexagonal	3.3528
Y	MIX-COMP-THERM-008-006	null	0.0952	0.02	Hexagonal	3.5204
Y	MIX-COMP-THERM-008-007	null	0.146	0.02	Hexagonal	2.667
N	MIX-COMP-THERM-008-008	Hf	0.146	0.02	Hexagonal	2.667
N	MIX-COMP-THERM-008-009	Hf	0.147	0.02	Hexagonal	2.667
N	MIX-COMP-THERM-008-010	Hf	0.147	0.02	Hexagonal	2.667
N	MIX-COMP-THERM-008-011	Hf	0.147	0.02	Hexagonal	2.667
N	MIX-COMP-THERM-008-012	Hf	0.147	0.02	Hexagonal	2.667
Y	MIX-COMP-THERM-008-013	Boron	0.146	0.02	Hexagonal	2.667

A

PACTEC

MFFP Safety Analysis Report

Docket No. 71-9295
Revision 2, April 2005

Used Y/N	Identification	Solid poison	EALF (eV)	Pu/(U+Pu) ratio	Pitch type	Pitch size (cm)
Y	MIX-COMP-THERM-008-014	Boron	0.147	0.02	Hexagonal	2.667
Y	MIX-COMP-THERM-008-015	Boron	0.147	0.02	Hexagonal	2.667
Y	MIX-COMP-THERM-008-016	Boron	0.147	0.02	Hexagonal	2.667
N	MIX-COMP-THERM-008-017	Cd	0.148	0.02	Hexagonal	2.667
N	MIX-COMP-THERM-008-018	Cd + Hf	0.147	0.02	Hexagonal	2.667
N	MIX-COMP-THERM-008-019	Cd + Hf	0.148	0.02	Hexagonal	2.667
N	MIX-COMP-THERM-008-020	Cd + Hf	0.148	0.02	Hexagonal	2.667
N	MIX-COMP-THERM-008-021	Cd + Hf	0.148	0.02	Hexagonal	2.667
N	MIX-COMP-THERM-008-022	Cd + Hf	0.148	0.02	Hexagonal	2.667
N	MIX-COMP-THERM-008-023	B + Cd	0.147	0.02	Hexagonal	2.667
N	MIX-COMP-THERM-008-024	B + Cd	0.148	0.02	Hexagonal	2.667
N	MIX-COMP-THERM-008-025	B + Cd	0.148	0.02	Hexagonal	2.667
N	MIX-COMP-THERM-008-026	B + Cd	0.148	0.02	Hexagonal	2.667
N	MIX-COMP-THERM-008-027	Cd	0.148	0.02	Hexagonal	2.667
N	MIX-COMP-THERM-008-028	Cd	0.148	0.02	Hexagonal	2.667
Y	MIX-COMP-THERM-009-001	null	0.537	0.015	Hexagonal	1.397
Y	MIX-COMP-THERM-009-002	null	0.304	0.015	Hexagonal	1.524
Y	MIX-COMP-THERM-009-003	null	0.158	0.015	Hexagonal	1.8034
Y	MIX-COMP-THERM-009-004	null	0.119	0.015	Hexagonal	2.032
Y	MIX-COMP-THERM-009-005	null	0.0972	0.015	Hexagonal	2.286
Y	MIX-COMP-THERM-009-006	null	0.093	0.015	Hexagonal	2.3622
Y	MIX-MET-INTER-001-001	null	36800	0.4525	null	null
Y	MIX-MET-FAST-008-002	null	347000	0.4525	null	null
Y	MIX-MET-FAST-008-003	null	83400	0.4525	null	null
Y	MIX-MET-FAST-008-004	null	186000	0.4525	null	null
Y	MIX-MET-FAST-008-005	null	285000	0.4525	null	null
Y	MIX-MET-INTER-001-006	null	26600	0.191	null	null
Y	PU-MET-FAST-033-001	null	422000	0.5255	null	null

This page left intentionally blank.

6.9.1 Single Package Model

This file is for the worst-case HAC model (max_hac_single_sul). Other files may be generated by adjusting the water density in the desired cells and modifying the pin pitch to the desired value.

```

MOX package max single conditions with 10.85 g/cc Fuel no Nb
c
c *****Fuel Assembly*****
c cells 1 to 3 transform the 3 assemblies to their locations
c 1 4 -1.0 -21 22 -23 24 -25 6 imp:n=1 $ top nozzle, void
c 2 4 -1.0 -21 22 -23 24 -7 26 imp:n=1 $ bottom nozzle, void
c 7 0 -21 22 -23 24 126 -25 fill=20 imp:n=1 $ pins
c
c 201 like 1 but trcl=53 $ assembly 2
c 202 like 2 but trcl=53
c 207 like 7 but trcl=53
c 220 like 1 but trcl=54 $ assembly 3
c 221 like 2 but trcl=54
c 222 like 7 but trcl=54
c
c -- "box" around fuel
c
c 301 0 (302 -303 300 -304 -906 26):
      (303 -305 300 -301 -906 26) fill=30 imp:n=1 $ "box" cutout
c 302 like 301 but trcl=53
c 303 like 301 but trcl=54
c
c perimeter containing strongback #1 in -y
c 50 0 (26 -906 902 -909 904 -910):
      (26 -906 909 -912 904 -901):
      (26 -906 912 904 -908):
      (26 -906 911 905 -904 -908):
      (26 -906 905 -900 903 -911) fill=7 imp:n=1
c perimeter containing strongback #2
c 51 like 50 but trcl=53
c perimeter containing strongback #3
c 52 like 50 but trcl=54
c
c *****water beyond three units*****
c 131 9 -1.4 -61 -69 64 #7 #50 #51 #52 #301 #302 #303
      #207 #222 imp:n=1
c
c *****containment*****
c 141 5 -7.94 -62 -66 63 (61:65:-64) imp:n=1 $ outer steel
c 143 5 -7.94 -61 -70 69 imp:n=1 $ upper inner steel
c 145 4 -1.0 -61 -65 70 imp:n=1 $ upper void
c *****beyond containment*****
c 195 6 -7.94 -72 -76 73 (62:66:-63) imp:n=0.25 $ one foot refl
c 199 0 (72:76:-73) imp:n=0 $ outside world
c
c Universe 20: Fuel Lattice
c
c 200 4 -1.0 -12 11 -14 13 u=20 lat=1 trcl=30 fill=0:16 0:16 0:0
      1 1 1 1 1 1 1 1 1 1 1 1 1 1 1 1 1 1 $ row 17
      1 1 1 1 1 1 1 1 1 1 1 1 1 1 1 1 1 1 $ row 16
      1 1 1 1 1 4 1 1 4 1 1 4 1 1 1 1 1 1 $ row 15
      1 1 1 4 1 1 1 1 1 1 1 1 1 4 1 1 1 1 $ row 14
      1 1 1 1 1 1 1 1 1 1 1 1 1 1 1 1 1 1 $ row 13
      1 1 4 1 1 4 1 1 4 1 1 4 1 1 4 1 1 1 $ row 12
      1 1 1 1 1 1 1 1 1 1 1 1 1 1 1 1 1 1 $ row 11
      1 1 1 1 1 1 1 2 2 2 1 1 1 1 1 1 1 1 $ row 10
      1 1 4 1 1 4 1 2 4 2 1 4 1 1 4 1 1 1 $ row 9
      1 1 1 1 1 1 1 2 2 2 1 1 1 1 1 1 1 1 $ row 8
      1 1 1 1 1 1 1 1 1 1 1 1 1 1 1 1 1 1 $ row 7
      1 1 4 1 1 4 1 1 4 1 1 4 1 1 4 1 1 1 $ row 6
      1 1 1 1 1 1 1 1 1 1 1 1 1 1 1 1 1 1 $ row 5
      1 1 1 4 1 1 1 1 1 1 1 1 1 4 1 1 1 1 $ row 4
      1 1 1 1 1 4 1 1 4 1 1 4 1 1 1 1 1 1 $ row 3
      1 1 1 1 1 1 1 1 1 1 1 1 1 1 1 1 1 1 $ row 2
      1 1 1 1 1 1 1 1 1 1 1 1 1 1 1 1 1 1 imp:n=1 $ row 1 (top)
c
c Universe 1: Fuel pin in normal position

```

```

c
10 1 -10.85 -1 -4 5 u=1 imp:n=1 $ fuel
11 4 -1.0 -2 1 -4 5 u=1 imp:n=1 $ radial gap
12 7 -6.5 -3 2 -8 5 u=1 imp:n=1 $ clad
13 4 -1.0 3 7 -6 u=1 imp:n=1 $ radially beyond pin
14 4 -1.0 -2 -8 4 u=1 imp:n=1 $ above fuel void
15 7 -6.5 -3 -6 8 u=1 imp:n=1 $ top of fuel cap
16 7 -6.5 -3 -5 7 u=1 imp:n=1 $ bottom of fuel cap
17 4 -1.0 6 u=1 imp:n=1 $ top water to infinity
18 4 -1.0 -7 u=1 imp:n=1 $ bottom water to infinity
c
c Universe 2: Fuel pin shifted up
c
410 1 -10.85 -1 -4 5 trcl=(0 0 23.7109) u=2 imp:n=1 $ fuel
411 4 -1.0 -2 1 -4 5 trcl=(0 0 23.7109) u=2 imp:n=1 $ radial gap
412 7 -6.5 -3 2 -8 5 trcl=(0 0 23.7109) u=2 imp:n=1 $ clad
413 4 -1.0 3 7 -6 trcl=(0 0 23.7109) u=2 imp:n=1 $ radially beyond pin
414 4 -1.0 -2 -8 4 trcl=(0 0 23.7109) u=2 imp:n=1 $ above fuel void
415 7 -6.5 -3 -6 8 trcl=(0 0 23.7109) u=2 imp:n=1 $ top of fuel cap
416 7 -6.5 -3 -5 7 trcl=(0 0 23.7109) u=2 imp:n=1 $ bottom of fuel cap
417 4 -1.0 6 trcl=(0 0 23.7109) u=2 imp:n=1 $ top water to infinity
418 4 -1.0 -7 trcl=(0 0 23.7109) u=2 imp:n=1 $ bottom water to
infinity
c
c Universe 3: Fuel pin shifted down
c
420 1 -10.85 -1 -4 5 trcl=(0 0 -9.4361) u=3 imp:n=1 $ fuel
421 4 -1.0 -2 1 -4 5 trcl=(0 0 -9.4361) u=3 imp:n=1 $ radial gap
422 7 -6.5 -3 2 -8 5 trcl=(0 0 -9.4361) u=3 imp:n=1 $ clad
423 4 -1.0 3 7 -6 trcl=(0 0 -9.4361) u=3 imp:n=1 $ radially beyond pin
424 4 -1.0 -2 -8 4 trcl=(0 0 -9.4361) u=3 imp:n=1 $ above fuel void
425 7 -6.5 -3 -6 8 trcl=(0 0 -9.4361) u=3 imp:n=1 $ top of fuel cap
426 7 -6.5 -3 -5 7 trcl=(0 0 -9.4361) u=3 imp:n=1 $ bottom of fuel cap
427 4 -1.0 6 trcl=(0 0 -9.4361) u=3 imp:n=1 $ top water to infinity
428 4 -1.0 -7 trcl=(0 0 -9.4361) u=3 imp:n=1 $ bottom water to infinity
c
c Universe 4: Instrument/guide tube
c
41 4 -1.0 -18 5 -8 u=4 imp:n=1 $ inside
42 7 -6.5 -19 18 5 -8 u=4 imp:n=1 $ tube
43 4 -1.0 19 5 -8 u=4 imp:n=1 $ beyond tube
44 4 -1.0 8 u=4 imp:n=1
45 4 -1.0 -5 u=4 imp:n=1
c
c Universe 14: Water only
c
46 4 -1.0 -998 u=14 imp:n=1
47 4 -1.0 998 u=14 imp:n=1
c
c Universe 7: Strongback
c
700 6 -7.94 715 -710 u=7 imp:n=1 $ tangential strongback
701 6 -7.94 (710 711 718):(-711 713) u=7 imp:n=1 $ radial strongback+bend
702 2 -2.713 714 -719 -716 u=7 imp:n=1 $ tan Al clad
703 21 9.2244E-02 719 -720 -716
730 731 732 733 734 735 736 737 738
739 740 741 742 743 744 745 746 747
750 751 752 753 754 755 756 757 758
759 760 761 762 763 764 765 766 767 u=7 imp:n=1 $ tangential boral
704 2 -2.713 720 -715 -716 u=7 imp:n=1 $ tan Al clad
706 2 -2.713 712 -722 -717 u=7 imp:n=1 $ rad Al clad
707 21 9.2244E-02 722 -723 -717
770 771 772 773 774 775 776 777 778
779 780 781 782 783 784 785 786 787
790 791 792 793 794 795 796 797 798
799 800 801 802 803 804 805 806 807 u=7 imp:n=1 $ radial boral
708 2 -2.713 723 -713 -717 u=7 imp:n=1 $ rad Al
710 4 -1.0 (710 711 -718):(716 -710 717 -715):
(710 -713 717 -711) u=7 imp:n=1
719 6 -7.94 ((-717 -712):(-716 -714 717)) -809 u=7 imp:n=1 $ poison holder
720 4 -1.0 ((-717 -712):(-716 -714 717)) 809 -810 u=7 imp:n=1
721 6 -7.94 ((-717 -712):(-716 -714 717)) 810 -811 u=7 imp:n=1
722 4 -1.0 ((-717 -712):(-716 -714 717)) 811 -812 u=7 imp:n=1
723 6 -7.94 ((-717 -712):(-716 -714 717)) 812 -813 u=7 imp:n=1
724 4 -1.0 ((-717 -712):(-716 -714 717)) 813 -814 u=7 imp:n=1

```

725	6	-7.94	((-717 -712):(-716 -714 717))	814 -815	u=7	imp:n=1	
726	4	-1.0	((-717 -712):(-716 -714 717))	815 -816	u=7	imp:n=1	
727	6	-7.94	((-717 -712):(-716 -714 717))	816 -817	u=7	imp:n=1	
728	4	-1.0	((-717 -712):(-716 -714 717))	817 -818	u=7	imp:n=1	
729	6	-7.94	((-717 -712):(-716 -714 717))	818 -819	u=7	imp:n=1	
730	4	-1.0	((-717 -712):(-716 -714 717))	819 -820	u=7	imp:n=1	
731	6	-7.94	((-717 -712):(-716 -714 717))	820 -821	u=7	imp:n=1	
732	4	-1.0	((-717 -712):(-716 -714 717))	821 -822	u=7	imp:n=1	
733	6	-7.94	((-717 -712):(-716 -714 717))	822 -823	u=7	imp:n=1	
734	4	-1.0	((-717 -712):(-716 -714 717))	823 -824	u=7	imp:n=1	
735	6	-7.94	((-717 -712):(-716 -714 717))	824 -825	u=7	imp:n=1	
736	4	-1.0	((-717 -712):(-716 -714 717))	825 -826	u=7	imp:n=1	
737	6	-7.94	((-717 -712):(-716 -714 717))	826	u=7	imp:n=1	
c							
750	6	-7.94	719 -720 -750		u=7	imp:n=1	\$ screws in boral
751	6	-7.94	719 -720 -751		u=7	imp:n=1	
752	6	-7.94	719 -720 -752		u=7	imp:n=1	
753	6	-7.94	719 -720 -753		u=7	imp:n=1	
754	6	-7.94	719 -720 -754		u=7	imp:n=1	
755	6	-7.94	719 -720 -755		u=7	imp:n=1	
756	6	-7.94	719 -720 -756		u=7	imp:n=1	
757	6	-7.94	719 -720 -757		u=7	imp:n=1	
758	6	-7.94	719 -720 -758		u=7	imp:n=1	
759	6	-7.94	719 -720 -759		u=7	imp:n=1	
760	6	-7.94	719 -720 -760		u=7	imp:n=1	
761	6	-7.94	719 -720 -761		u=7	imp:n=1	
762	6	-7.94	719 -720 -762		u=7	imp:n=1	
763	6	-7.94	719 -720 -763		u=7	imp:n=1	
764	6	-7.94	719 -720 -764		u=7	imp:n=1	
765	6	-7.94	719 -720 -765		u=7	imp:n=1	
766	6	-7.94	719 -720 -766		u=7	imp:n=1	
767	6	-7.94	719 -720 -767		u=7	imp:n=1	
c							
770	6	-7.94	722 -723 -770		u=7	imp:n=1	
771	6	-7.94	722 -723 -771		u=7	imp:n=1	
772	6	-7.94	722 -723 -772		u=7	imp:n=1	
773	6	-7.94	722 -723 -773		u=7	imp:n=1	
774	6	-7.94	722 -723 -774		u=7	imp:n=1	
775	6	-7.94	722 -723 -775		u=7	imp:n=1	
776	6	-7.94	722 -723 -776		u=7	imp:n=1	
777	6	-7.94	722 -723 -777		u=7	imp:n=1	
778	6	-7.94	722 -723 -778		u=7	imp:n=1	
779	6	-7.94	722 -723 -779		u=7	imp:n=1	
780	6	-7.94	722 -723 -780		u=7	imp:n=1	
781	6	-7.94	722 -723 -781		u=7	imp:n=1	
782	6	-7.94	722 -723 -782		u=7	imp:n=1	
783	6	-7.94	722 -723 -783		u=7	imp:n=1	
784	6	-7.94	722 -723 -784		u=7	imp:n=1	
785	6	-7.94	722 -723 -785		u=7	imp:n=1	
786	6	-7.94	722 -723 -786		u=7	imp:n=1	
787	6	-7.94	722 -723 -787		u=7	imp:n=1	
c							
790	6	-7.94	722 -723 -790		u=7	imp:n=1	
791	6	-7.94	722 -723 -791		u=7	imp:n=1	
792	6	-7.94	722 -723 -792		u=7	imp:n=1	
793	6	-7.94	722 -723 -793		u=7	imp:n=1	
794	6	-7.94	722 -723 -794		u=7	imp:n=1	
795	6	-7.94	722 -723 -795		u=7	imp:n=1	
796	6	-7.94	722 -723 -796		u=7	imp:n=1	
797	6	-7.94	722 -723 -797		u=7	imp:n=1	
798	6	-7.94	722 -723 -798		u=7	imp:n=1	
799	6	-7.94	722 -723 -799		u=7	imp:n=1	
800	6	-7.94	722 -723 -800		u=7	imp:n=1	
801	6	-7.94	722 -723 -801		u=7	imp:n=1	
802	6	-7.94	722 -723 -802		u=7	imp:n=1	
803	6	-7.94	722 -723 -803		u=7	imp:n=1	
804	6	-7.94	722 -723 -804		u=7	imp:n=1	
805	6	-7.94	722 -723 -805		u=7	imp:n=1	
806	6	-7.94	722 -723 -806		u=7	imp:n=1	
807	6	-7.94	722 -723 -807		u=7	imp:n=1	
c							
810	6	-7.94	719 -720 -730		u=7	imp:n=1	
811	6	-7.94	719 -720 -731		u=7	imp:n=1	
812	6	-7.94	719 -720 -732		u=7	imp:n=1	
813	6	-7.94	719 -720 -733		u=7	imp:n=1	



```

814 6 -7.94 719 -720 -734 u=7 imp:n=1
815 6 -7.94 719 -720 -735 u=7 imp:n=1
816 6 -7.94 719 -720 -736 u=7 imp:n=1
817 6 -7.94 719 -720 -737 u=7 imp:n=1
818 6 -7.94 719 -720 -738 u=7 imp:n=1
819 6 -7.94 719 -720 -739 u=7 imp:n=1
820 6 -7.94 719 -720 -740 u=7 imp:n=1
821 6 -7.94 719 -720 -741 u=7 imp:n=1
822 6 -7.94 719 -720 -742 u=7 imp:n=1
823 6 -7.94 719 -720 -743 u=7 imp:n=1
824 6 -7.94 719 -720 -744 u=7 imp:n=1
825 6 -7.94 719 -720 -745 u=7 imp:n=1
826 6 -7.94 719 -720 -746 u=7 imp:n=1
827 6 -7.94 719 -720 -747 u=7 imp:n=1
c
c Universe 30: "box" around fuel
c
c 310 2 -2.713 -313 317 u=30 imp:n=1 $ radial left
c 311 2 -2.713 316 -310 u=30 imp:n=1 $ tangential bot
c 312 2 -2.713 314 -315 317 u=30 imp:n=1 $ radial right
c 315 2 -2.713 311 -312 316 u=30 imp:n=1 $ tangential top
316 6 -7.94 315 312 u=30 imp:n=1
317 4 -1.0 (312 -317 -315):(-316 -312) u=30 imp:n=1
c
320 4 -1.0 -315 317 -320 u=30 imp:n=1 $ radial water gap
321 21 9.2244E-02 313 -314 317 320 -321 u=30 imp:n=1 $ radial boral
322 4 -1.0 -315 317 321 -322 u=30 imp:n=1
323 21 9.2244E-02 313 -314 317 322 -323 u=30 imp:n=1
324 4 -1.0 -315 317 323 -324 u=30 imp:n=1
325 21 9.2244E-02 313 -314 317 324 -325 u=30 imp:n=1
326 4 -1.0 -315 317 325 -326 u=30 imp:n=1
327 21 9.2244E-02 313 -314 317 326 -327 u=30 imp:n=1
328 4 -1.0 -315 317 327 -328 u=30 imp:n=1
329 21 9.2244E-02 313 -314 317 328 -329 u=30 imp:n=1
330 4 -1.0 -315 317 329 -330 u=30 imp:n=1
331 21 9.2244E-02 313 -314 317 330 -331 u=30 imp:n=1
332 4 -1.0 -315 317 331 -332 u=30 imp:n=1
333 21 9.2244E-02 313 -314 317 332 -333 u=30 imp:n=1
334 4 -1.0 -315 317 333 u=30 imp:n=1
c
340 2 -2.713 -313 317 320 -321 u=30 imp:n=1 $ radial Al cladding
341 2 -2.713 -313 317 322 -323 u=30 imp:n=1
342 2 -2.713 -313 317 324 -325 u=30 imp:n=1
343 2 -2.713 -313 317 326 -327 u=30 imp:n=1
344 2 -2.713 -313 317 328 -329 u=30 imp:n=1
345 2 -2.713 -313 317 330 -331 u=30 imp:n=1
346 2 -2.713 -313 317 332 -333 u=30 imp:n=1
c
347 2 -2.713 314 -315 317 320 -321 u=30 imp:n=1 $ radial Al cladding
348 2 -2.713 314 -315 317 322 -323 u=30 imp:n=1
349 2 -2.713 314 -315 317 324 -325 u=30 imp:n=1
350 2 -2.713 314 -315 317 326 -327 u=30 imp:n=1
351 2 -2.713 314 -315 317 328 -329 u=30 imp:n=1
352 2 -2.713 314 -315 317 330 -331 u=30 imp:n=1
353 2 -2.713 314 -315 317 332 -333 u=30 imp:n=1
c
360 4 -1.0 -312 316 -320 u=30 imp:n=1 $ tangential water gap
361 21 9.2244E-02 310 -311 316 320 -321 u=30 imp:n=1 $ tangential boral
362 4 -1.0 -312 316 321 -322 u=30 imp:n=1
363 21 9.2244E-02 310 -311 316 322 -323 u=30 imp:n=1
364 4 -1.0 -312 316 323 -324 u=30 imp:n=1
365 21 9.2244E-02 310 -311 316 324 -325 u=30 imp:n=1
366 4 -1.0 -312 316 325 -326 u=30 imp:n=1
367 21 9.2244E-02 310 -311 316 326 -327 u=30 imp:n=1
368 4 -1.0 -312 316 327 -328 u=30 imp:n=1
369 21 9.2244E-02 310 -311 316 328 -329 u=30 imp:n=1
370 4 -1.0 -312 316 329 -330 u=30 imp:n=1
371 21 9.2244E-02 310 -311 316 330 -331 u=30 imp:n=1
372 4 -1.0 -312 316 331 -332 u=30 imp:n=1
373 21 9.2244E-02 310 -311 316 332 -333 u=30 imp:n=1
374 4 -1.0 -312 316 333 u=30 imp:n=1
c
380 2 -2.713 316 311 -312 320 -321 u=30 imp:n=1 $ horizontal Al cladding
381 2 -2.713 316 311 -312 322 -323 u=30 imp:n=1
382 2 -2.713 316 311 -312 324 -325 u=30 imp:n=1

```

```

383 2 -2.713 316 311 -312 326 -327 u=30 imp:n=1
384 2 -2.713 316 311 -312 328 -329 u=30 imp:n=1
385 2 -2.713 316 311 -312 330 -331 u=30 imp:n=1
386 2 -2.713 316 311 -312 332 -333 u=30 imp:n=1
c
387 2 -2.713 316 -310 320 -321 u=30 imp:n=1 $ horizontal Al cladding
388 2 -2.713 316 -310 322 -323 u=30 imp:n=1
389 2 -2.713 316 -310 324 -325 u=30 imp:n=1
390 2 -2.713 316 -310 326 -327 u=30 imp:n=1
391 2 -2.713 316 -310 328 -329 u=30 imp:n=1
392 2 -2.713 316 -310 330 -331 u=30 imp:n=1
393 2 -2.713 316 -310 332 -333 u=30 imp:n=1
c
c Universe 51: Dummy universe containing fuel
c
c 999 1 -10.31 -999 u=51 imp:n=1 $ for diagnostics only, not used
c 1000 1 -10.31 999 u=51 imp:n=1 $ for diagnostics only, not used
c
c *****Fuel Assembly*****
c fuel pin
1 cz 0.409575 $ fuel radius
2 cz 0.41783 $ radius inside clad
3 cz 0.47498 $ radius outside clad
4 pz 182.88 $ top of fuel
5 pz -182.88 $ bottom of fuel
6 pz 202.7555 $ top of fuel pin
7 pz -184.3405 $ bottom of fuel pin
8 pz 201.4474 $ bottom of top cap
11 px -0.6688 $ lattice definition
12 px 0.6688
13 py -0.6688
14 py 0.6688
c 200 pz -119.38
c guide tube
18 cz 0.57150
19 cz 0.61214
c perimeter of fuel assembly
21 px 10.2391 $ offset from surface 905
22 px -12.1116 $
23 py -6.6593 $ offset from surface 904
24 py -29.0113 $
25 pz 226.466
26 pz -190.95720
126 pz -193.776
c *****containment*****
61 cz 36.1950
62 cz 37.6174
63 pz -197.5866 $ 1.5" thick
64 pz -193.7766 $ 1.11" below bottom of fuel (strongback bottom not modeled)
65 pz 235.6866
66 pz 237.5916
c 67 pz -203.0222
c 68 pz -201.1172
69 pz 226.4664
70 pz 228.0666
c *****outside of water refl****
72 cz 68.0974
73 pz -228.0666 $ 1' water from 63
76 pz 268.0716 $ 1' water from 66
c
c -- "box"
c
300 py -29.7925 $ defining box in u=0
301 py -29.0114
302 px -12.8928
303 px -12.1117
304 py -7.5675
305 px 9.9672
c
310 25 py 0.04445
311 25 py 0.2604
312 25 py 0.3048
313 25 px 0.04445
314 25 px 0.2604
315 25 px 0.3048

```

A

PACTEC

MFFP Safety Analysis ReportDocket No. 71-9295
Revision 2, April 2005

316	25 px 2.54
317	25 py 2.54
c	
320	pz -171.049
321	pz -119.532
322	pz -109.758
323	pz -67.412
324	pz -57.638
325	pz -15.316
326	pz -5.542
327	pz 36.855
328	pz 46.629
329	pz 89.002
330	pz 98.776
331	pz 141.097
332	pz 150.871
333	pz 193.548
c	
c	strongback surfaces
c	
710	22 px 0
711	22 py 0
712	22 px 0.476
713	22 px 0.7808
714	22 py 0.476
715	22 py 0.7808
716	22 px -0.3114 \$ 0.43" less than surface 713
717	22 py -0.54
718	22 cz 0.7808
719	22 py 0.5205
720	22 py 0.7364
722	22 px 0.5205
723	22 px 0.7364
c	
730	22 c/y -2.7752 -189.6872 0.47625
731	22 c/y -2.7752 -179.5526 0.47625
732	22 c/y -2.7752 -172.3187 0.47625
733	22 c/y -2.7752 -118.2624 0.47625
734	22 c/y -2.7752 -111.0285 0.47625
735	22 c/y -2.7752 -66.1416 0.47625
736	22 c/y -2.7752 -58.9077 0.47625
737	22 c/y -2.7752 -14.0462 0.47625
738	22 c/y -2.7752 -6.8123 0.47625
739	22 c/y -2.7752 38.1254 0.47625
740	22 c/y -2.7752 45.3593 0.47625
741	22 c/y -2.7752 90.2716 0.47625
742	22 c/y -2.7752 97.5055 0.47625
743	22 c/y -2.7752 142.3670 0.47625
744	22 c/y -2.7752 149.6009 0.47625
745	22 c/y -2.7752 194.8180 0.47625
746	22 c/y -2.7752 202.0519 0.47625
747	22 c/y -2.7752 213.8172 0.47625
c	
750	22 c/y -16.7452 -189.6872 0.47625
751	22 c/y -16.7452 -179.5526 0.47625
752	22 c/y -16.7452 -172.3187 0.47625
753	22 c/y -16.7452 -118.2624 0.47625
754	22 c/y -16.7452 -111.0285 0.47625
755	22 c/y -16.7452 -66.1416 0.47625
756	22 c/y -16.7452 -58.9077 0.47625
757	22 c/y -16.7452 -14.0462 0.47625
758	22 c/y -16.7452 -6.8123 0.47625
759	22 c/y -16.7452 38.1254 0.47625
760	22 c/y -16.7452 45.3593 0.47625
761	22 c/y -16.7452 90.2716 0.47625
762	22 c/y -16.7452 97.5055 0.47625
763	22 c/y -16.7452 142.3670 0.47625
764	22 c/y -16.7452 149.6009 0.47625
765	22 c/y -16.7452 194.8180 0.47625
766	22 c/y -16.7452 202.0519 0.47625
767	22 c/y -16.7452 213.8172 0.47625
c	
770	22 c/x -5.9248 -189.6872 0.47625
771	22 c/x -5.9248 -179.5526 0.47625
772	22 c/x -5.9248 -172.3187 0.47625



PACTEC

MFFP Safety Analysis Report

Docket No. 71-9295
Revision 2, April 2005

773 22 c/x -5.9248 -118.2624 0.47625
 774 22 c/x -5.9248 -111.0285 0.47625
 775 22 c/x -5.9248 -66.1416 0.47625
 776 22 c/x -5.9248 -58.9077 0.47625
 777 22 c/x -5.9248 -14.0462 0.47625
 778 22 c/x -5.9248 -6.8123 0.47625
 779 22 c/x -5.9248 38.1254 0.47625
 780 22 c/x -5.9248 45.3593 0.47625
 781 22 c/x -5.9248 90.2716 0.47625
 782 22 c/x -5.9248 97.5055 0.47625
 783 22 c/x -5.9248 142.3670 0.47625
 784 22 c/x -5.9248 149.6009 0.47625
 785 22 c/x -5.9248 194.8180 0.47625
 786 22 c/x -5.9248 202.0519 0.47625
 787 22 c/x -5.9248 213.8172 0.47625

c
 790 22 c/x -16.9789 -189.6872 0.47625
 791 22 c/x -16.9789 -179.5526 0.47625
 792 22 c/x -16.9789 -172.3187 0.47625
 793 22 c/x -16.9789 -118.2624 0.47625
 794 22 c/x -16.9789 -111.0285 0.47625
 795 22 c/x -16.9789 -66.1416 0.47625
 796 22 c/x -16.9789 -58.9077 0.47625
 797 22 c/x -16.9789 -14.0462 0.47625
 798 22 c/x -16.9789 -6.8123 0.47625
 799 22 c/x -16.9789 38.1254 0.47625
 800 22 c/x -16.9789 45.3593 0.47625
 801 22 c/x -16.9789 90.2716 0.47625
 802 22 c/x -16.9789 97.5055 0.47625
 803 22 c/x -16.9789 142.3670 0.47625
 804 22 c/x -16.9789 149.6009 0.47625
 805 22 c/x -16.9789 194.8180 0.47625
 806 22 c/x -16.9789 202.0519 0.47625
 807 22 c/x -16.9789 213.8172 0.47625

c
 809 pz -188.417
 810 pz -181.331 \$ PH 1 (bottom)
 811 pz -170.541 \$ PH 1
 812 pz -120.040 \$ PH 2
 813 pz -109.250
 814 pz -67.920 \$ PH 3
 815 pz -57.130
 816 pz -15.824 \$ PH 4
 817 pz -5.034
 818 pz 36.347 \$ PH 5
 819 pz 47.137
 820 pz 88.494 \$ PH 6
 821 pz 99.284
 822 pz 140.589 \$ PH 7
 823 pz 151.379
 824 pz 193.040 \$ PH 8
 825 pz 203.830 \$ PH 8
 826 pz 212.547

c
 900 px 11.18006 \$ FIXED for strongbacks touching
 901 py -5.71956 \$ FIXED for strongbacks touching
 902 px -11.9593
 903 py -28.7574 \$ surface 901 minus 9.07"

c
 c 904 is -7.1354 and 905 is 9.7633 for nominal case (with poison holders).
 c they are shifted to cut off poison holders to allow for
 c expansion for damaged cases.

c
 c To completely "slice off" the poison holders, set
 c 904 to -6.6593 and 905 to 10.2392.

c
 904 py -6.6593 \$ tangential strongback lower bound, surface 901 minus total thickness
 905 px 10.2392 \$ radial strongback left bound, surface 901 minus total thickness
 906 pz 215.7222
 908 c/z 9.87856 -7.02106 1.3015
 909 px -9.9019
 910 py -6.35448
 911 py -7.1344 \$ fixed
 912 px 9.7653 \$ fixed

c

A
PACTEC
MFFP Safety Analysis Report

Docket No. 71-9295
Revision 2, April 2005

```

998   so 10000
999   pz 345.5565

mode  n
c     print
kcode 2000 1 30 530
ksrc   -16.08 10.4 0
        17.82  7.67 0
        0.55 -17.81 0
cut:n  j j 0 0
c
c     Materials
c
m1    92235   -0.249  $ fuel pellet
      92238   -82.615
      94239   -4.972
      94240   -0.264
      94241   -0.053
      8016    -11.847
m2    13027   1.0    $ aluminum cladding for BORAL
m4    1001     2      $ water
      8016     1
mt4   lwtr.01t
m5    6000    -0.06  $ XM-19
      7014    -0.4
      14000   -0.75
      15031   -0.04
      16032   -0.03
      23000   -0.3
      24000   -23.5
      25055   -6
      28000   -13.5
      41093   -0.3
      42000   -3
      26000   -52.12
m6    6000    -0.08  $ SS-304
      14000   -1.0
      15031   -0.045
      24000   -19.0
      25055   -2.0
      26000   -68.375
      28000   -9.5
m7    40000   -1.0  $ Cladding
c     41093   -0.030
m8    82000   1.0   $ lead
m9    6000    -25.1  $ water/steel mix, 5.8% steel by volume
      14000   -313.9
      15031   -14.1
      24000   -5964.9
      25055   -627.9
      26000   -21465.8
      28000   -2982.5
      1001    -7240.1
      8016    -57462.7
mt9   lwtr.01t
m21   5010    7.3123E-03 $ 35 mg/cm2 B-10, 75% credit
      5011    3.9244E-02
      6000    1.2248E-02
      13027   3.3439E-02
c     total 9.2244E-02
c
c     Translations
c
c     tr22 is the intersection of planes 904 and 905
c     when the poison holders are present (904 and 905 shift when it is
c     desired to "slice off" the poison holders).
c     Note that the origin of Universe 7 corresponds to the intersection
c     of these planes.
c
*tr22  9.7643 -7.1354 0.0
c
c     tr25 is the intersection of planes 300 and 302. The origin of Universe 30
c     corresponds to the intersection of these planes.
c
*tr25 -12.8928 -29.7925 0.0

```

A

PACTEC

MFFP Safety Analysis Report

Docket No. 71-9295
Revision 2, April 2005

```
c      tr30 is computed by taking the coordinates of the intersection of planes
c      22 and 24 and adding half the pitch (note: can't be exact or else planes will
c      overlap, causing program termination.)
c
*tr30  -11.6368 -28.5365 0.0
c
c      tr53 and tr54 rotate the bottom assembly to create assemblies 2 and 3
c
*tr53  0 0 0           120 30 90   150 120 90   90 90 0 $ +x+y
*tr54  0 0 0           120 150 90   30 120 90   90 90 0 $ -x-y
```



PACTEC

MFFP Safety Analysis Report

**Docket No. 71-9295
Revision 2, April 2005**

This page left intentionally blank.

REQUEST FOR ADDITIONAL INFORMATION (RAI) SUPPLEMENT

1. Explain the structural and criticality consequences when more fuel rods are axially displaced further through the top nozzle and the openings in the strongback top end plate as a result of the Fuel Control Structure (FCS) limiting the lateral displacement of the fuel assemblies in the 30-foot drop.

Response: The structural and criticality consequences of additional fuel rods being displaced through the top nozzle and the openings in the strongback top end plate are provided in Revision 2 of SAR Section 2.7, *Hypothetical Accident Conditions*, and Chapter 6.0, *Criticality Evaluation*, respectively. The revised information demonstrates that there is no effective impact on the structural or criticality safety of the package.

2. Explain the packaging responses as the result of additional weight from the FCS added to the design after the full-scale drop tests.

Response: Appendix 2.12.8, *Effect of Bounding Weight on Package Structural Responses*, has been added to Revision 2 of the SAR to address the packaging responses as a result of the additional weight of the FCS.

3. Provide the physical and nuclear parameters for the Burnable Poison Rod Assembly.

Response: Section 1.2.3, *Contents of Packaging*, has been revised to include the physical and nuclear descriptions for the Burnable Poison Rod Assemblies (BPRAs). The revised section is part of Revision 2 of the SAR.

RAI 2-11 Addendum: NRC would like more information on how the g-loads as reported in the SAR were computed.

Response: The MFFP has been qualified primarily by full-scale testing. Bounding accelerations are required only when additional calculations are warranted (e.g., demonstrating the adequacy of the FCS, analyzing the effects of the added FCS weight on the package response, etc.)

Accelerations reported in the SAR are a mixture of both estimated and measured values. Measured values were obtained during the free drop tests utilizing active accelerometers attached to the package body. The measured values bound the estimated values in all cases; therefore, all calculations utilized the bounding measured accelerations. Table 1 summarizes the certification tests performed, and the estimated and measured accelerations, as applicable. Estimated values result from calculations using high-speed video record for the applicable free drop test.

For the 80° oblique, CG-over-corner 30-foot drop, 100g was estimated (Test Series 2, Test No. 1), 120g was measured (Data Test, Test No. 11); therefore, 120g was used in all subsequent end free drop calculations. For the side drop, 140g was estimated (Test Series 1, Test No. 1), 180g was measured for the worst-case slapdown (Test Series 3, Test No. 3); therefore, 180g was used in all subsequent side free drop calculations.

Test Series 1 and 2 free drop tests did not use active accelerometers. Following the 80° oblique, CG-over-corner 30-foot drop (Test Series 2, Test No. 1), all subsequent free drop tests were performed with active accelerometers. Data Test (Test No. 11) was performed specifically to repeat Test Series 2, Test No. 1 and obtain measured accelerometer data for this free drop condition.

The estimated accelerations for Test Series 1, Test No. 1, and Test Series 2, Test No. 1 were not utilized in the evaluation of the structural response of the package because they were superseded by measured acceleration data. Any structural calculations that were performed to evaluate the effect of the added FCSs for these two orientations used only the measured values.

To provide an example of the method of determining the estimated accelerations from the video record, the photometric data for Test Series 1, Test No. 1, which is summarized in Table 2, will be used. The specific time interval data that will be used in this example is 0.0075 seconds.

Video records were taken at 400 frames per second (fps), or 1/400 (0.0025) seconds per frame. Once a reference point in the video record was established and a scale factor determined, the displacement for the package during each time increment could be estimated. With this data, the velocity, V_i , could be determined by differentiating the change in displacement with respect to time. Similarly, the acceleration, a_i , is determined by differentiating the change in velocity with respect to time (i.e., second differential of displacement with respect to time). Using the data at time interval 0.0075 seconds as an example, the velocity and acceleration are determined as follows:

$$V_i = \frac{y_i - y_{i-1}}{\Delta t} = \frac{3.38 - 2.52}{0.0025} = 344.0 \text{ in/sec}$$

$$a_i = \frac{V_i - V_{i-1}}{\Delta t} = \frac{344.0 - 481.6}{0.0025} = -55,040 \text{ in/sec}^2 = -142.4 \text{ g}$$

The value of 142.4g is approximate and is rounded to 140g in the SAR. Velocity and accelerations for the complete impact event are listed for each time interval in Table 2.

Table 1 – MFFP Certification Tests Summary

Test Series	Test No.	Test Description	Estimated Acceleration (from video frames)	Measured Acceleration (from accelerometers)
1	1	30-foot free side drop	140	N/A
2	1	80° oblique, CG-over-corner 30-foot drop	100	N/A
3	1	15° slapdown, 30-foot drop (lid end primary)	N/A	140 (primary impact) 155 (secondary impact)
3	3	15° slapdown 30-foot drop (lid end secondary)	N/A	125 (primary impact) 180 (secondary impact)
Data Test	11	80° oblique CG-over-corner, 30-foot drop	N/A	120

Table 2 – Data from MFFP Test Series 1, Test No. 1 Video

Time (sec)	Total Displacement (in)	Velocity (in/sec)	Accelerations (in/sec²)	Acceleration (g)
0	0	527.5		
0.0025	1.32	527.5	0	0.0
0.0050	2.52	481.6	-18,346	-47.5
0.0075	3.38	344.0	-55,040	-142.4
0.0100	3.96	229.3	-45,866	-118.7
0.0125	4.24	114.7	-45,866	-118.7
0.0150	4.41	68.8	-18,346	-47.5
0.0175	4.36	-22.9	-36,692	-95.0
0.0200	4.13	-91.7	-27,519	-71.2
0.0225	4.13	0	36,692	95.0
0.0250	3.96	-68.8	-27,519	-71.2
0.0275	3.67	-114.7	-18346	-47.5